Mauritius Research Council

INNOVATION FOR TECHNOLOGY

INVESTIGATING THE OUTDOOR PERFORMANCE OF THREE PV TECHNOLOGIES IN THE TROPICAL CLIMATE OF MAURITIUS

Final Report

January 2019

Mauritius Research Council

Address:

Level 6, Ebene Heights
34, Cybercity
Ebene

Telephone: (230) 465 1235
Fax: (230) 465 1239
e-mail: mrc@intnet.mu
Website: www.mrc.org.mu

This report is based on work supported by the Mauritius Research Council under award number MRC/RUN-1503. Any opinions, findings, recommendations and conclusions expressed herein are the author's and do not necessarily reflect those of the Council.

University of Mauritius

Investigating the outdoor performance of three PV technologies in the tropical climate of Mauritius

January 2019

DISCLAIMER

The information contained in this report is a collection of the authors' own research, interpretation, opinions, beliefs and personal experiences. The authors assume no liability for any loss, damage, or injury alleged to be caused directly or indirectly by the use of information provided or referenced within this report.

LIST OF CONTRIBUTORS

Principal Investigator

Dr Ramgolam Yatindra Kumar

Investigator

Mr Shamachurn Heman

Research Assistant

Mr Coret Jonathan Yannick

Contents

List of Figures

LIST OF FIGURES

LIST OF FIGURES

LIST OF FIGURES

List of Tables

ACKNOWLEDGEMENTS

The authors of the report wish to express their gratitude to all parties who have assisted them in conducting this study. The authors are very thankful to the Mauritius Research Council for funding the whole project and to the University of Mauritius for providing the administrative support in procuring the equipment and conducting interviews of Research Assistants.

ABSTRACT

The aim of the project is to carry out a performance assessment of different solar photovoltaic (PV) technologies in the climatic context of Mauritius. Currently, only two PV technologies are proposed by local PV system installers, namely the crystalline silicon (c-Si) and Copper Indium diselenide (CIS) thin film PV modules, but no performance comparison has been carried out so far to conclude about the best technology suited to the climate of Mauritius in general and to the specific location where the system will be installed. Installers simply tend to propose to their customers a system based on the peak rating only, irrespective of the technology. In addition, no study has being done to investigate the effect of the local climatic conditions on the short- and long-term performance over time. This research project has addressed the above mentioned issues and has provided highly reliable information on the performance of different PV technologies. The targeted objectives of the proposed research were to investigate the effect of climatic and environmental parameters such as temperature, relative humidity, soiling, UV level, spectral-, global and diffuse irradiance on power output of three widely used PV technologies (mono-Si, poly-Si and CIS). In order to achieve the objectives, a state of the art outdoor test facility has been developed that can perform simultaneous measurement of electrical, climatic and environmental parameters. An in-depth analysis of high resolution measurement data has been performed. A report based on the results has been produced, which can be readily used by stakeholders of the PV industry as well as decision makers to support their decision on choice of technology, design and appraisal of PV projects.

Abbreviations

CIS : Copper Indium Selenium

CIGS : Copper Indium Gallium Selenium

STC : standard test conditions

AM : air mass

W : Watts

A : Ampere

V : Volt

mV : milliVolts

K : Kelvin

kK : kiloKelvin

eV : electron Volt

PV : photovoltaic

S : Irradiance

T : temperature

V_{oc} : open circuit voltage

I_{sc} : short circuit current

I_{ph} : photocurrent of PV cell

I_s : saturation current of diode

R_s : series resistance of PV cell

R_{sh}: shunt resistance of PV cell

IV : current-voltage

kS/s/ch : kilosamples per second per channel

Chapter 1

Introduction

1.1 Overview

Our society has become conscious that a shift towards alternative sources of energy is crucial. The use of fossil fuels, a finite resource of energy, has caused excessive pollution and is known to be a main cause of global warming. Temperature rise in the Indian Ocean and increase in sea level has triggered the need for remedial measures to mitigate the effect of climate change. The government of Mauritius had signed the Kyoto Protocol and is also signatory of the Paris Agreement, and has set a target of achieving 35% of electricity production from renewable energy sources by 2025 (Ministry of Finance, 2008). It has since 2009 promoting renewable energy (RE) in our energy production mix. Photovoltaic technology is one of the main renewable energy sources which has shown great potential worldwide. Its basic principle is about converting sunlight directly to electricity. Through the introduction of a number of RE project and promotion mechanisms, Mauritian government has been encouraging the installation of photovoltaic systems. As a result of the increasing demand for solar-based electricity, the price of PV systems is continuously decreasing.

1.2 Aims and objectives

Rapid growth in technological advances has not only provided the market with a wide range of PV materials and structures, but has also introduced an intra-market competition which

has helped a reduction in the costs of PV modules. Nevertheless, reliable information on short and long-term outdoor performance of most commonly used PV material technologies is not available. This is firstly due to the fact that it requires major investment in equipment and as well requires expertise of qualified people who may perform high level research in the field. The government of Mauritius, as well as many private companies, have been promoting sustainable development through the implementation of photovoltaic systems to meet their energy requirements. Unfortunately, due to lack of information on performance of different PV technologies, local contractors have been implementing mostly mono-Si or poly-Si PV systems, with the latter a better choice quality-cost wise. Decisions on choice of material should not only be based only on efficiency of a component which has been defined at STC. Efficiency is dependent on spectral irradiance and temperature as well. Other climatic factors such as relative humidity can also influence cell efficiency and hence PV system's performance. Being in the tropical region and according to solar geometry fundamentals, Mauritius is exposed to almost two months of direct overhead Sunlight at noon. Therefore an enhanced UV exposure may be realistic. The latter is detrimental to long-term PV system's performance. Performance study of such systems is essential to estimate their energy production through the development of suitable models and simulation studies. Therefore, the I-V characteristics have to be studied by using the appropriate equipment as per established standards, with the objective of comparing the performance of different PV technologies in different weather conditions over a whole year. To achieve the goal, a system has to be designed to acquire the performance data of the different technologies and subsequently perform a detailed analysis. When searching for the most appropriate PV modules for a given PV system, the data provided by suppliers are usually those acquired under standard test conditions. However, the system will experience varying outdoor weather conditions during its lifetime. Currently, only two PV technologies are proposed by local PV system installers, namely the crystalline silicon (c-Si) and Copper Indium diselenide (CIS) thin film PV modules, but no performance comparison has been carried out so far to conclude about the best technology suited to the climate of Mauritius in general and to the specific location where the system will be installed. Installers simply tend to propose to their customers a system based on the peak rating only, irrespective of the

technology. In addition, no study has being done to investigate the effect of the local climatic conditions on the short- and long-term performance over time. The aim of the project is to carry out a performance assessment of different solar photovoltaic (PV) technologies in the climatic context of Mauritius. The proposed project addresses the above mentioned issues and provide highly reliable information on how to optimize the energy output from a PV system. Therefore, the targeted objectives of the proposed research is to investigate the effect of climatic and environmental parameters such as temperature, relative humidity, soiling, UV level, spectral-, global and diffuse irradiance on power output of three widely used PV technologies (monocrystalline Silicon, polycrystalline Silicon and CIS/CIGS). In order to achieve the objectives, a state of the art outdoor test facility will be developed that can perform simultaneous measurement of electrical, climatic and environmental parameters.

The objectives of the study are to:

• Develop and implement an outdoor state of the art test facility which will be used for the measurement of PV performance.

• Measure weather parameters.

• Evaluate the impact of various climatic factors on the performance of different PV modules in the tropical climate of Mauritius.

Chapter 2

Literature review, theoretical framework and background concept

This section elaborates on the various aspects of a photovoltaic system, its operations, and the various factors affecting its power output. Moreover, information about the current state of energy in Mauritius is also provided.

2.1 The Sun

The Sun is the star at the center of the solar system. It is a sphere of hot plasma in which nuclear fusion occurs whereby a series of reaction turns the hydrogen into helium(Woolfson, 2000).During this process tremendous amount of energy is released in the form of electromagnetic radiation. It currently fuses about 600 million tons of hydrogen into helium every second, converting 4 million tons of matter into energy every second as a result. This energy, which can take between 10,000 and 170,000 years to escape from its core, is the source of the Sun's light and heat(Wikipedia, 2018). The temperature of its core is close to 15.7 million Kelvins(K) and its surface temperature is around 5.8 kK(Hathawat, 2015).

The core is the only region in the Sun that produces an appreciable amount of thermal energy through fusion; 99% of the power is generated within 24% of the Sun's radius, and by 30% of the radius, fusion has stopped nearly entirely. The remainder of the Sun is heated by this energy as it is transferred outwards through many successive layers. The proton?proton

chain occurs around $9.2*10^{37}$ times each second in the core, converting about $3.7*10^{38}$ protons into alpha particles (helium nuclei) every second, or about $6.2*10^{11}$ kg/s. Fusing four free protons (hydrogen nuclei) into a single alpha particle, that is a helium nucleus, releases around 0.7% of the fused mass as energy, so the Sun releases energy at the mass?energy conversion rate of 4.26 million metric tons per second, for 384.6 yottawatts ($3.846*10^{26}$ W), or $9.192*10^{10}$ megatons of TNT per second(Philips and H, 1995).

The spectrum of the Sun's solar radiation is close to that of a black body(Iqbal, 1983) as shown in figure . The Sun emits EM radiation across most of the electromagnetic spectrum. Although the Sun produces gamma rays as a result of the nuclear-fusion process, internal absorption and thermalization convert these super-high-energy photons to lower-energy photons before they reach the Sun's surface and are emitted out into space. As a result, the Sun does not emit gamma rays from this process, but it does emit gamma rays from solar flares. The Sun also emits X-rays, ultraviolet, visible light, infrared, and even radio waves; the only direct signature of the nuclear process is the emission of neutrinos.

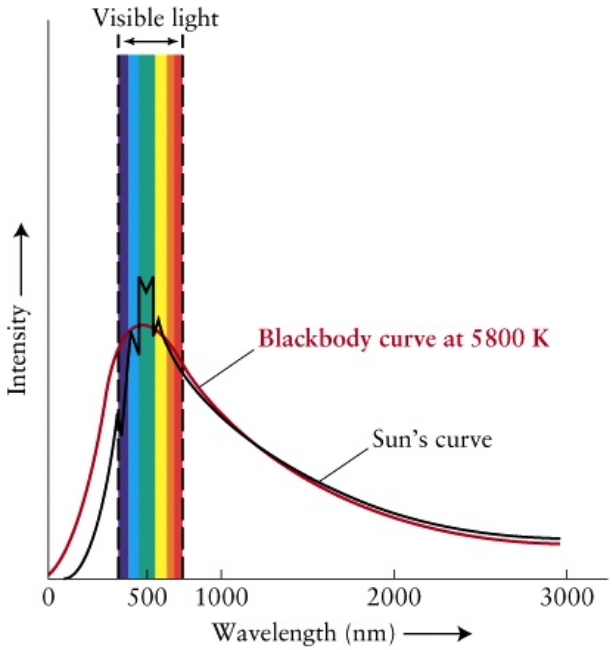

Figure 2.1: Solar spectrum(Pogosian, 2018)

The Earth is the third planet in the solar system. It orbits the Sun at an average distance of 149.60 million km and one complete orbit takes 365.256 days(Sshekhtman and Thompson,

2018). The orbit of the Earth round the sun is an ellipse with an eccentricity of 0.0167 as shown in figure 2.2 (which is almost a circle; the latter has eccentricity 0)(Australian Space Academy, 2018).

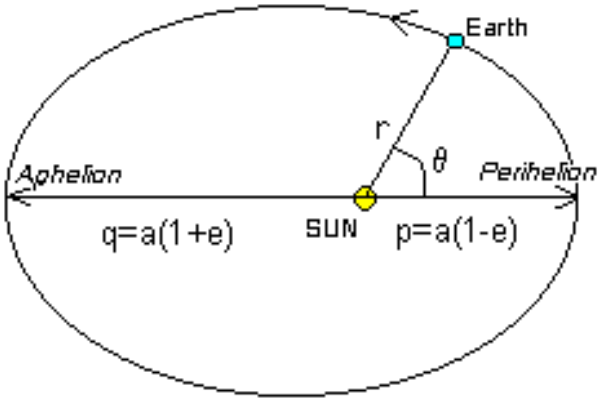

Figure 2.2: Earth orbit representation(not to scale)(Australian Space Academy, 2018)

The Earth receives $174*10^{15}$W of incoming solar radiation (insolation) at the upper atmosphere in which approximately 30% is reflected back to space while the rest is absorbed by clouds, oceans and land masses(Smil, 1991). The amount of energy received by the Earth from the Sun in an hour is enough to supply the Earth's demand for a whole year(Morton, 2006).

2.2 Seasons on Earth

As demonstrated in figure 2.2 the distance between the Earth and the Sun does not vary by much. The farthest away Earth is from the Sun during its orbit is $1.52*10^{11}$ m and the closest is $1.47*10^{11}$ (Stine and Geyer, 2018). Though less energy is received when the Earth is farther away, the main reason which cause seasons on Earth is the fact that the Earth's axis of rotation is not perpendicular with the ecliptic plane(the plane in which it orbits the Sun). Rather it is at an angle of 23.5 ° as shown in figure 2.3. Thus it causes the path of the Sun in the Earth's sky, that is the ecliptic, to change throughout the year. Hence the rays from the Sun reaches the Earth's atmosphere at different angle throughout the year.

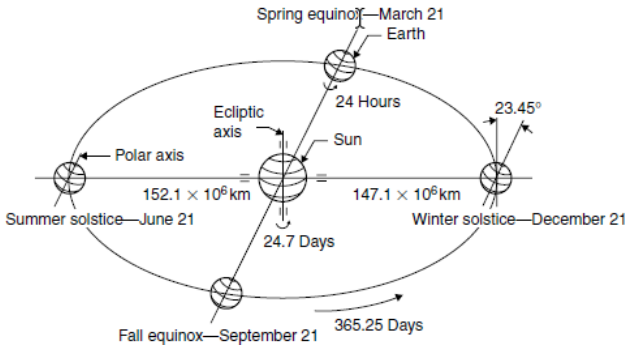

Figure 2.3: Earth orbit and axial tilt(not to scale)(Kalogirou, 2009)

The declination of the ecliptic varies throughout the year as illustrated in figure 2.4.

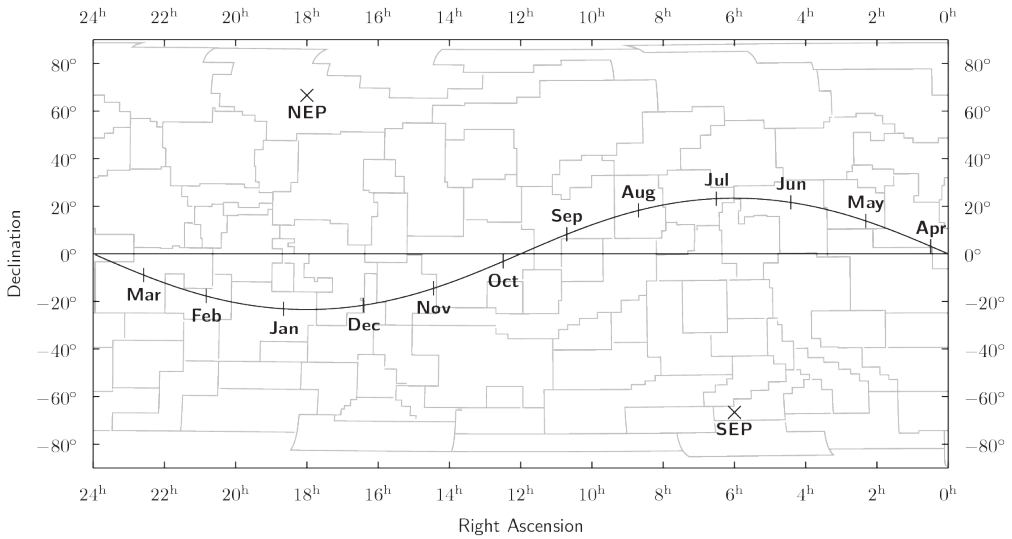

Figure 2.4: Declination of ecliptic(Ford, 2011)

2.3 Atmospheric attenuation

As mentioned previously, not all energy incident from the Sun reaches Earth's surface, when entering the Earth's atmosphere some are reflected back and part is refracted, the amount which passes through depends on the angle of the rays at which they penetrate the Earth's atmosphere. This angle is dependent upon the declination of the Sun. After penetrating the Earth's atmosphere some specific frequencies of the electromagnetic radiation are absorbed by elements present in the atmosphere. Thus only specific wavelength of EM wave reaches

the surface. This is illustrated in figure 2.5

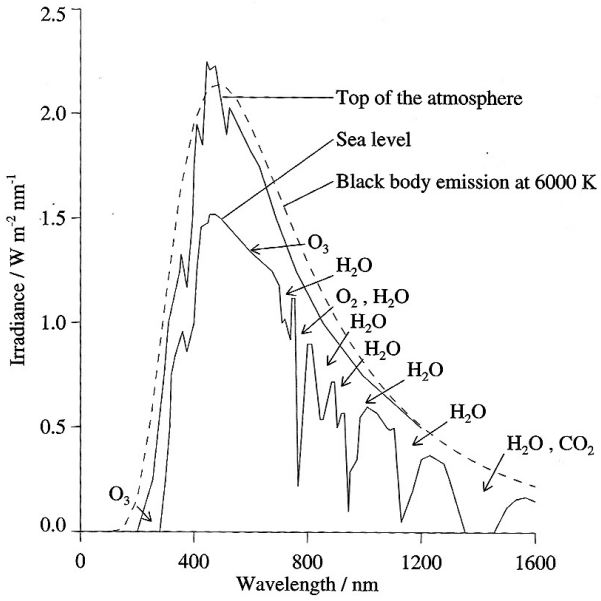

Figure 2.5: atmospheric absorption Spectrum (Goody and Walker, 1972)

The longer distance the Sun rays have to travel to reach Earth's surface the more they are attenuated by absorption and scattering. To be able to define the extent to which the rays are attenuated the air mass is defined as the path length for light rays from a celestial source to pass through the atmosphere, expressed as a ratio relative to the path length vertically upwards, that is the Zenith.

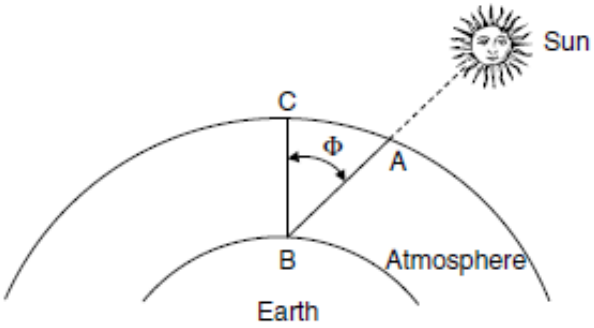

Figure 2.6: Air mass definition(Kalogirou, 2009)

From figure 2.6, air mass, m, is defined as

$$m = \frac{AB}{BC} = \frac{1}{\phi}$$

Thus the lower the Sun is in the sky the higher will be the air mass and this relates to a lower performance of PV panels.

2.4 Photoelectric effect

During the 19th century, experiments carried out by Hertz showed that light incident on certain metallic surfaces caused the emission of electrons from the surfaces. Today this phenomenon is known as the photoelectric effect and the emitted electrons are referred to as photoelectrons(Serway *et al.*, 1983). In 1905 Einstein published 3 papers in which one explaining the photoelectric effect. He was awarded a nobel prize as a result of this publication for his discovery of the law of photoelectric effect(The Nobel Foundation, 2018). Based on this materials which generate a voltage potential and thus allow a current to flow in a given closed circuit was developed.

2.5 Semiconductors

Materials are generally classified in three groups, namely conductors, insulators and semiconductors. The main attribute used to separate them is their conductivity, which is a macroscopic property but this phenomenon can only be explained through the microscopic behaviour of the electrons. Electrons are usually bonded to a nucleus and if all electrons in a nucleus are bonded then none is available to conduct electricity and the material is an insulator. There are region referred as conduction bands in which electrons may reside, in such band they are no more bounded to a nucleus thus can conduct electricity. Usually energy is needed to move from the valence band, that is the region they are in when bounded to a nucleus, to the conduction band. This energy is referred to as the energy gap and is used to define conductors, insulators and semiconductors. For a conductor this value is very small and sometimes the conduction band and the valence band overlap, for an insulator it is greater than 10 eV and for a conductor it is of the order of 1 eV(Serway *et al.*, 2005). Figure 2.7 shows a depiction of the different bands.

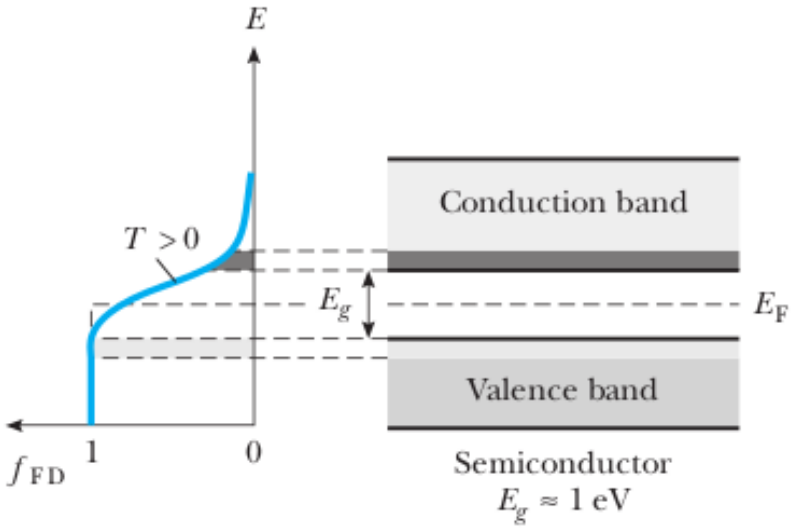

Figure 2.7: The band structure of a semiconductor at ordinary temperatures(T ≈ 300 K)(Serway *et al.*, 2005)

Classification of semiconductors

Semiconductors are classified as intrinsic and extrinsic. Intrinsic semiconductors are pure conductors which does not contain impurity atoms and are insulator at 0K. Extrinsic semiconductors contain impurity atoms, known as dopants which creates a disbalance in the number of electrons to number of holes (that is vacant electron place). There are two type of impurities used:

•Donors - creating n-type semiconductors with more electrons than holes,

•Acceptors - creating p-type semiconductors with less electrons than holes.

2.6 The p-n junction

When a p-type and n-type semiconductor is brought together as shown in figure 2.8 diffusion of electrons and holes occur. Electrons and holes near the boundary are attracted towards each other, recombine and hence leave behind ionised donors and acceptors. Hence, a depletion region is formed with an internal electric field which stops any further diffusion.

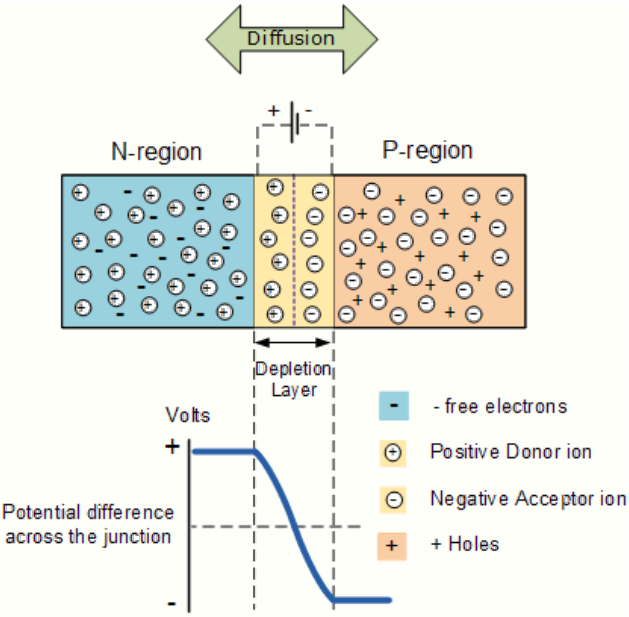

Figure 2.8: Structure of PN junction with potential illustration(ElectronicsTutorials, 2018)

2.7 The photovoltaic effect

When electromagnetic wave is incident on such a pn junction, if the photon has enough energy(ie energy bandgap) to supply to the electrons move to the conduction band and leave behind a hole in the valence band. The net increase in positive charges at the p side and the ned increase in the negative charge at the n side causes a potential difference to appear across the pn junction. This generation of photo-voltage is known as as photovoltaic effect and if the pn junction is completed with a circuit a photocurrent in the circuit is delivered. thus a photovoltaic cell can simply be regarded as a pn junction.

2.8 The PV cell

A photovoltaic cell can simply be regarded as a pn junction which allow the conversion of solar energy, that is electromagnetic wave, into electrical energy. The behaviour of the cell is illustrated through an IV curve and an example is shown in figure 2.9 below, where I_{sc} is defined as the short circuit current, V_{oc} is the open circuit voltage and P_m is the maximum

power point.

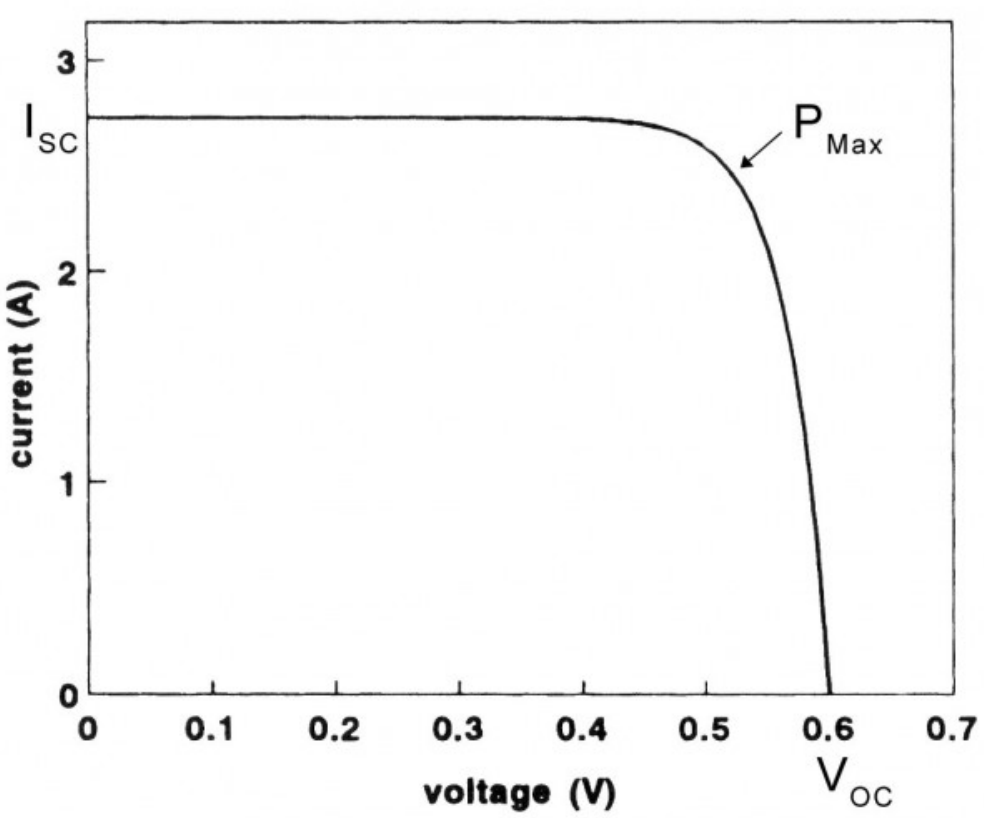

Figure 2.9: A typical I-V curve for a silicon photovoltaic cell.(ITACA, 2018)

There are various factors which affect the IV characteristics of a specific PV cell. This include irradiance, temperature and soiling.

2.8.1 Dependencies of output of PV cell

a. Effect of irradiance

According to Firdaus and Daniyal (2013) modelling of a PV module shows that with increase in irradiance both I_{sc} and V_{oc} increases as illustrated in figure 2.10. This gives rise to an overall increase in output power. Hosseini *et al.* (2018) discussed about the responses of various technologies to different wavelength of light. Depending of climatic conditions, different PV technologies would have better response under different AM causing more or less production in output power. Thus spectral response of the technology is a key criteria

when choosing the most adequate one. For instance crystalline Si has a better response than amorphous silicon at higher AM, making it more advantageous to use in cloudy conditions.

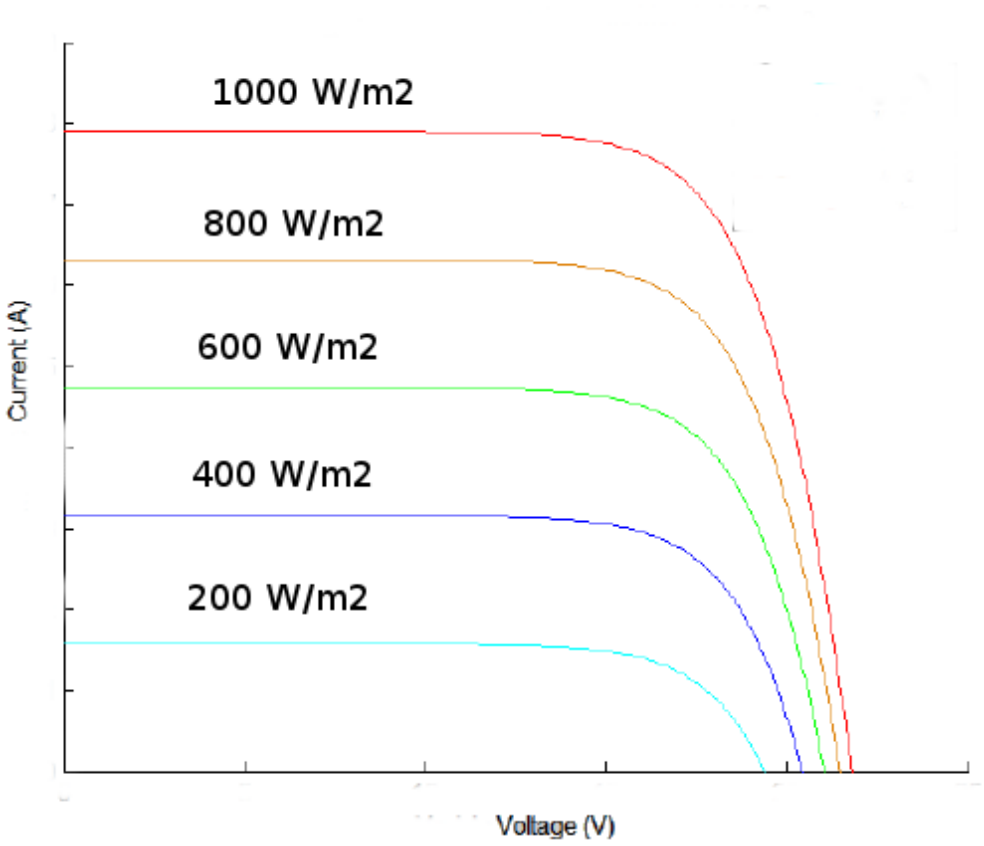

Figure 2.10: Effect of irradiance on IV curve.

Hosseini *et al.* (2018) studied the behaviour of various modules in outdoor conditions and the results obtained corresponds to theory. Experimental results show the same variation as in figure 2.10 with change in irradiance.

b. Effect of temperature

Tsuno *et al.* (2005) carried out experiments to study the change in the IV curve with changing temperature, they noticed that there is a decrease in both I_{sc} and V_{oc} with increasing temperature, but I_{sc} decreases very slowly and can be considered negligible whereas V_{oc} decreases faster. Thus with increase in temperature there is a decrease in efficiency. Arjyadhara *et al.* (2013) and Hüttl *et al.* (2019) studied the effect of irradiance and temperature

on the IV curve of certain given panels and the experimental graphs obtained showed good correspondence with theoretical one as per figure 2.11. A net decrease in output power as temperature increases is expected for the various types of technologies tested.

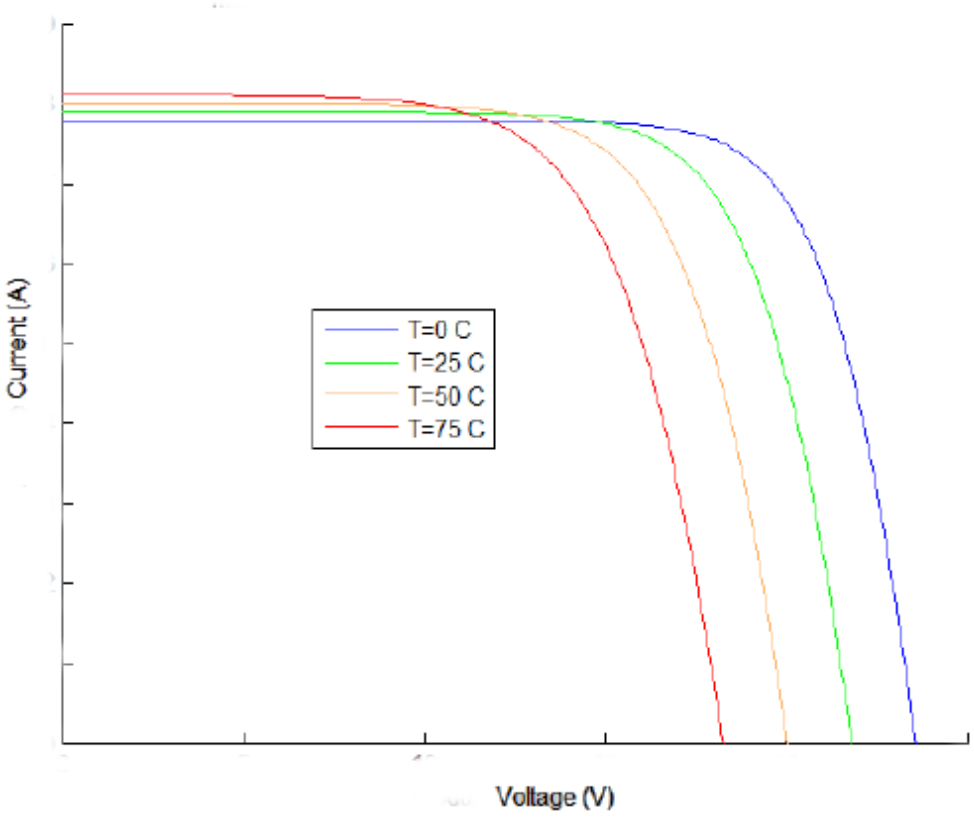

Figure 2.11: Effect of temperature on IV curve.

c. Effect of soiling

Soiling is the process during which fine particles deposit on the PV module thus affecting its performance. Soiling is usually expressed as the percentage energy loss in presence of soiling compared to when there is no soiling and is given by the following equation:

$$\text{Soiling loss} = \left(1 - \frac{\text{Incident irradiance in presence of soiling}}{\text{Incident irradiance in absence of soiling}}\right) * 100\% \qquad (2.1)$$

Maghami *et al.* (2016) did a review of various environmental factors which affect energy yield of system, and came to the conclusion that the location itself, without any regard to the amount of sunlight it receives is of great importance.

Mejia and Kleissl (2013) and Kimber (2013) studies showed that there is a decrease in output when PV panels are left unattended and are not cleaned on a regular basis. This occurs as the particles block some of the light incident on the panel. Their studies showed that soiling affects system where rain is not frequent. Soiling is much dependent on the location under study as it depends on the speed of wind, the frequency of rainfall and how polluted the surrounding air is.

Appels *et al.* (2013) a study to analyse the effect of soiling and frequency of rainfall on output of PV systems. They came to the conclusion that the more frequent rainfall is the less soiling is observed but also that the size of the dust particles in the location affects soiling greatly as they affect the transmissivity of the glass.

Miller and Jackson (2009) study showed that urban region has a greater soiling percentage than rural region in most of the case. However this depends on the soil and dust in the region itself.

2.9 Measurement techniques of PV characteristic curve

Before performing any analysis on the behaviour of the PV cells in different condition, first the IV curves themselves need to be collected. Various methods have been developed throughout the years. An extensive list of the various methods available is elaborated in the work of Duran *et al.* (2008) and Shenawy *et al.* (2014).

Amiry *et al.* (2018) designed a low cost system with an arduino as the brain of the system. Its main characteristics are that it has a fast sampling rate and resolution such that the IV curve of the panel can be reconstructed from the obtained data. Also it combines two different PV characteristic curve measurement techniques, namely resistor as load and electronic load, the resistor provides a way to vary the current and the mosfet used allows for rapid switching thus explaining its characteristics. The main disadvantage is the number of mosfets and resistors required to be able to swipe over all the IV curve. Drouiche et al. developed an algorithm to study the aging of PV module using the one diode model. It requires only experimental data, for instance the IV characteristics at open, short circuit and at maximum power, no further information from the manufacturer is required. It makes

use of empirical formula to express the 5 parameters in terms of the known values and uses the Newton Raphson method to find an approximation to the parameters, thus a system of 5 non linear algebraic equations need to be solved simultaneously which leads to much computational time and also increases the possibility of divergence.

A. Willoughby and O. Osinowo (2018) developed an I-V curve tracer based around a mosfet and an arduino to record the IV curve of two panels, a clean one and a dusty one to study the effect of soiling on the performance of the panel. The mosfet is fed with a pwm signal of 8 bits resolution and 488 Hz at its gate. The main issue with this setup is because of the 8 bit resolution the coordinates are scattered over the graph thus the exact location of the maximum power point is not determined accurately enough. But using curve fitting the data was successfully used to deduce that soiling has much impact on current than voltage and causes a decrease in output power.

Variable resistor as load

The simplest way to measure the I-V curve of a module is to use a variable resistor R as it is shown in figure 2.12. The value of R will be varied in steps from zero to infinity in order to capture the points of the I-V curve from short circuit to open circuit, by measuring the voltage and the current in each step. This method is only applicable to low-power modules since resistors for higher power are hardly available. Load resistors are not recommended for photovoltaic module characterization because I_{sc} is never exactly reached and the reverse bias characteristics cannot be determined. Further the load resistor is increased manually in steps. Thus it is a time consuming process and can only be used when all other variables such as temperature and irradiance are controlled.

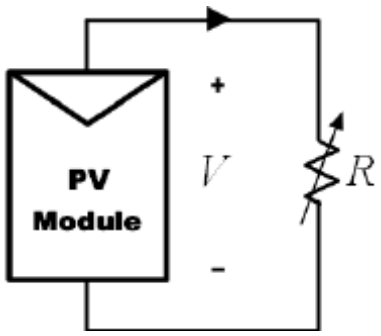

Figure 2.12: Variable resistor scheme(Duran *et al.*, 2008).

Electronic load

The electronic load method, as shown in figure 2.13 uses a transistor (usually a MOSFET) as load; the resistance between drain and source is modulated through the gate-source voltage, and consequently the flow of current supplied by the module. When this method is used to trace the I-V curve of the module, the MOSFET must operate in its three modes of operation (cut-off, active and ohmic region). As a result, most of the power delivered by the module will have to be dissipated by this device, which limits its application to medium power. Its advantage is the fast variation of the equivalent load resistance of the MOSFET. The linear MOSFET is driven by a low frequency scan signal with a large enough amplitude to cover the complete range of panel characteristic. This was the adopted method for the study.

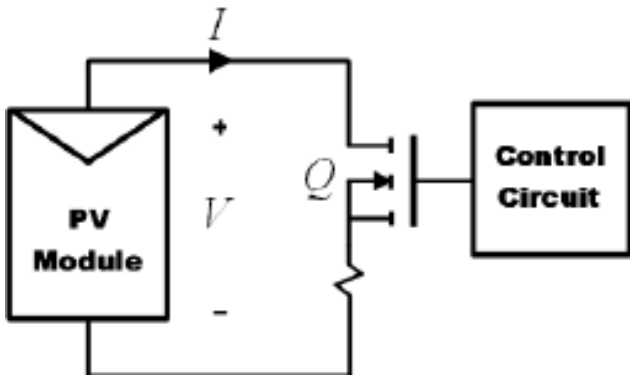

Figure 2.13: Mosfet used as a dc load(Duran *et al.*, 2008).

2.10 Modelling of PV module

The most often used models for describing the IV characteristic of a PV cell are the one diode model(Senturk, 2018)(gang Wang *et al.*, 2017)(Boutana *et al.*, 2018) and the two diode model(Kashif Ishaque, 2011).

One diode model

Figure 2.14 shows a schematic of the model. It is mathematically described by equation through the five parameters I_{ph}, I_s, R_s, R_{sh} and n.

$$I = I_{ph} - I_s \left[exp\left(\frac{V + IR_s}{nV_{th}}\right) - 1 \right] - \frac{V + IR_s}{R_{sh}} \tag{2.2}$$

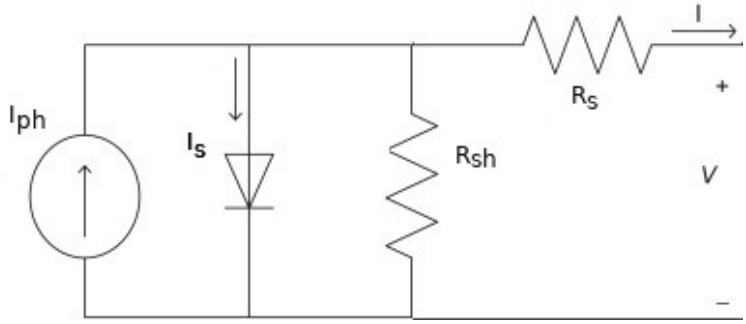

Figure 2.14: Schematic of the one diode model

Drouiche *et al.* (2018) developed an algorithm to study the aging of PV module using the one diode model. It requires only experimental data, for instance the IV characteristics at open, short circuit and at maximum power, no further information from the manufacturer is required. It makes use of empirical formula to express the 5 parameters in terms of the known values and uses the Newton Raphson method to find an approximation to the parameters, thus a system of 5 non linear algebraic equations need to be solved simultaneously which leads to much computational time and also increases the possibility of divergence.

Two diode model

Figure 2.15 shows a schematic of the model. It is mathematically described by equation through the seven parameters $I_{ph}, I_{s1}, I_{s2}, R_s, R_{sh}$,$n_1$ and n_2.

$$I = I_{ph} - I_{s1} \left[exp\left(\frac{V + IR_s}{n_1 V_{th1}}\right) - 1 \right] - I_{s2} \left[exp\left(\frac{V + IR_s}{n_2 V_{th2}}\right) - 1 \right] - \frac{V + IR_s}{R_{sh}} \tag{2.3}$$

Where V_{thi} is thermal voltage of respective diode.

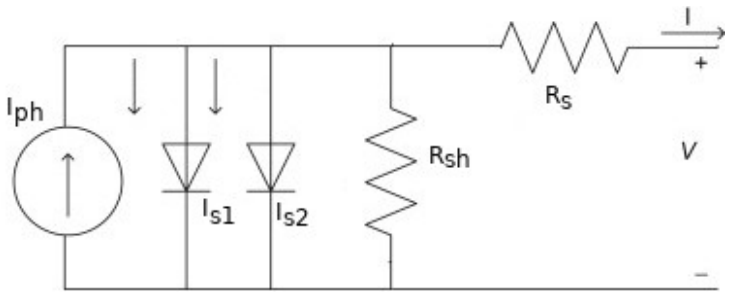

Figure 2.15: Schematic of the two diode model

2.11 Suitability of location for photovoltaic

A discussed in the previous sections, factors such as temperature and irradiance have great impact on the energy yield of different PV technologies. Preliminary studies of the various climatic conditions for a given site are important to choose the most suited technology ensuring a larger energy yield. Below is a non exhaustive list of a few factors to be considered.

2.11.1 Insolation and cloud coverage

Daily insolation is the amount of amount of solar energy received per unit area daily. It is obtained from irradiance using the following equation:

$$\text{Daily insolation} = \int_{day} \text{Irradiance } dt \tag{2.4}$$

The larger the value of insolation the better is the location for solar farming. Regions which are sunny throughout the year is more desirable than one which will encounter lot of cloud coverage since a cloudy weather imply a lower irradiance thus less energy hitting that location. But intermittent rainfall is beneficial to the PV panels as it washed away any dust deposited on them. Doorga *et al.* (2018) investigates the potential sites for solar farming over Mauritius using GIS tools combined with multi-criteria decision making tools applying weight to a large array of factors making a site more suitable for solar farming. Premalatha and Rahim (2017) investigates the performance of three PV technologies under sunny and cloudy conditions and concluded that for cloudy conditions thin film technology yields better

output than crystalline technology and better insight is given on choosing the best technology with respect to weather condition. McCormick and Suehrcke (2018) analysed the effect of intermittent solar radiation due to passing by clouds on the output power of PV systems and also on battery lifespan. It was concluded that intermettency in solar radiation has a negative impact of batteries and as far as possible batteries should be avoided if on-grid systems is an option.

2.11.2 Topology and shading

A flat land is preferred over one with much slope as it is easier to install and maintain the panels on a flat one. But Mauritius is a small island and solar farming involves the use of large surface area. Thus much effort must be placed in choosing the best location and alternatives to land are to be considered. Al-Chalabi (2015) discuss about the feasibility of placing solar panels on skyscrapers. The area around building are merely used for anything and using them for solar farming would imply decreasing the carbon footprint of the buildings and also flat land which would otherwise be used for solar farming will be available for other uses.Shading on a site where solar farming is to be conducted is undesirable as this will imply that less solar energy is hitting the solar panels. Thus region with electrical poles, trees or mountains causing shading is to be avoided. Shading occurs when only a few cells in a panel are blocked from the direct sunlight, this may arise due to presence of trees of electrical poles. Fadhel *et al.* (2019) studied the effect of shading on the IV curve of panels and conclude that there is a decrease of about 65% in the output and on the long term shading may cause failure of a complete panel due to burnt cell in a string rendering the complete string useless. Baka *et al.* (2019) discussed the financial benefits of a good shading analysis and numerates various topology to increase energy yield when all panels are not alligned in a particular direction increasing feasibility of solar farming on uneven terrain.

2.12 Energy situation in Mauritius

Mauritius is a small volcanic island, and is considered to be a young island. As such it does not have natural resources of fossil fuels but rely heavily of of them for its energy needs,

all of which are imported. A publication by the Statistic Mauritius (2018) stated that the total primary energy requirement for year 2017 was 1,603 thousand tonnes of oil equivalent, increasing by 3.1% from 1,555 in 2016. Imported fuels comprising of 57% petroleum products and 29% coal made up 86% of the total primary energy requirement in 2017. The remaining 14% consisted of locally available sources namely bagasse, hydro, wind, landfill gas, photovoltaic and fuelwood.

The government of Mauritius is committed to decrease our dependency on fossil fuel. A forecast by the Ministry of Energy and Public Utilities (2009) is shown in table 2.1 below:

t

Table 2.1: Forecasted energy mix for the period 2009-2025(Ministry of Energy and Public Utilities, 2009)

Fuel Source		Percentage of Total Electricity Generations			
		2010	2015	2020	2025
Renewable	Bagasse	16%	13%	14%	17%
	Hydro	4%	3%	3%	2%
	Waste to water	0%	5%	4%	4%
	Wind	0%	2%	6%	8%
	Solar PV	0%	1%	1%	2%
	Geothermal	0%	0%	0%	2%
	Sub-total	20%	24%	28%	35%
Non-Renewable	Fuel Oil	37%	31%	28%	25%
	Coal	43%	45%	44%	40%
	Sub-total	80%	76%	72%	65%
TOTAL		100 %	100 %	100 %	100 %

The main obstacle to use more of PV technology is its intermittent nature. To use photovoltaic efficiently and economically, much of the power delivered during the peak production hours must be used. The effect of temperature and irradiance on output power must be understood in order to design large systems properly.

2.13 Initiative by the Government

The Mauritian government has been encouraging independent to rely on PV technologies for their energy needs. Several schemes has been set to allow the connection of PV systems to the grid. A Small-Scale Distributed Generation (SSDG) project was launched in December 2010. Households can produce their own energy during daytime while injecting their excess in the grid and at night use energy from the grid, also independent energy producers can produce and sell energy which is directly inputted into the grid.

For the SSDG project to be feasible, a Grid Code has been established to permit the integration of photovoltaic, wind turbine, and mini-hydro technologies within the CEB grid. The maximum permissible installed capacity of the above-mentioned technologies for the SSDG Feed-in Tariff Project has been set to 50 kW per customer. The maximum projected capacity (2 Megawatt) has been attained and the CEB will no longer accept any new application from potential producers.

Table 2.2: Feed-in Tariffs(CEB, 2015)

Feed-in tariff for 15 years	Wind Rs/kWh	Hydro Rs/kWh	PV Rs/kWh
Micro (up to 2.5 kW)	20	15	25
Mini (2.5 kW to 10 kW)	15	15	20
Small (10 to 50 kW)	10	10	15

Table 2.3: Greenfield Tariffs(CEB, 2015)

Greenfield tariff for 15 years	Wind Rs/kWh	Hydro Rs/kWh	PV Rs/kWh
Micro (up to 2.5 kW)	17	12.75	21.25
Mini (2.5 kW to 10 kW)	12.75	12.75	17
Small (10 to 50 kW)	8.50	8.50	12.75

The most recent solar project by the Mauritian government is the home solar project which inaugurated on the 17 May 2018. This project, being implemented by the CEB and

CEB (Green Energy) Co. Ltd ams at installing solar PV systems on the rooftops of 10000 households in Social category tariff 110A as port of the Government's efforts to alleviate poverty whilst contributing to the national target of achieving 35% of renewable electricity in the energy mix by 2025(Government Information Service,, 2018).

2.14 Solar plants in Mauritius

The solar park located at Bambou was the first solar park to be built at Mauritius. It was a project of sarako (2012) and the project was started on February 2013 and connected to the grid February 2014, a mere one year from start to completion. Up to 15.2 megawatts of solar power is produced at this 34-hectare site and fed into the local grid. The summary was written by the Ministry of Social Security, National Solidarity, and Environment and Sustainable Development (2012).

The company Synnove Energy Ltd has constructed and commissioned two 2 MW solar farms namely at Esperance Moka and at Petite Retraite, which the electricity output was then sold to the CEB. n an effort to shift towards more sustainable energy sources, the CEB called for bids from Independent Power Producers through an Open Advertised Bidding for the production and supply of electricity from photovoltaic (PV) farms of 10 to 15 MW. An agreement was made by Synnove Energy Ltd and the CEB for the setting up of a 8.64MW solar farm at Petite retraite which is an extension of the existing farm. The farm was commissioned in 2016(Ministry of Social Security, National Solidarity, and Environment and Sustainable Development, 2016).

To reach its target of 35% of renewable electricity in the energy mix by 2025 the government of Mauritius has initiated the construction of a 2 MW solar farm at Henrietta. The Solar PV farm is a project of the Central Electricity Board (Green Energy) Co. Ltd and estimates suggest that iw will produce approximately 3 GWh of renewable energy annually, thus avoiding the equivalent emission of 3,000 tons of carbon dioxide into the atmosphere. The solar farm should be operational by the end of November 2018(Mbogo, 2018).

One of the latest solar farm project is the Henrietta 17MW solar farm initiated by Medine and Akuo Energy (2018) after winning the call for tender from the Central Electricity Board

(CEB) in 2016. Apart from solar energy harvesting, livestock grazing and beekeeping will be performed on the site.

In order to make even larger solar farms which must be efficient and deliver their expected rating throughout sunshine hours, it is important to understand the behaviour of the PV cells themselves. Thus in the next chapter, the methods employed to acquire the various data needed for the analysis are described.

Chapter 3

Research methodology

In this chapter, the experimental setup is discussed. Hardwares and softwares used to acquire the IV curves of the various panels are elaborated and processing of the data is also stated.

3.1 Development of experimental setup

Figure 3.1 shows an overview of the different hardwares used to acquire the different IV curves. The system is implemented in the following steps:

• The different PV modules being assessed,

• The electronic components comprising of the temperature sensors, pyranometers, current and voltage sensors on the printed circuit board,

• The various daq devices for data acquisition

• A server running labview to run the labview VI and store the data.

From the server data can be retrieved to perform analysis.

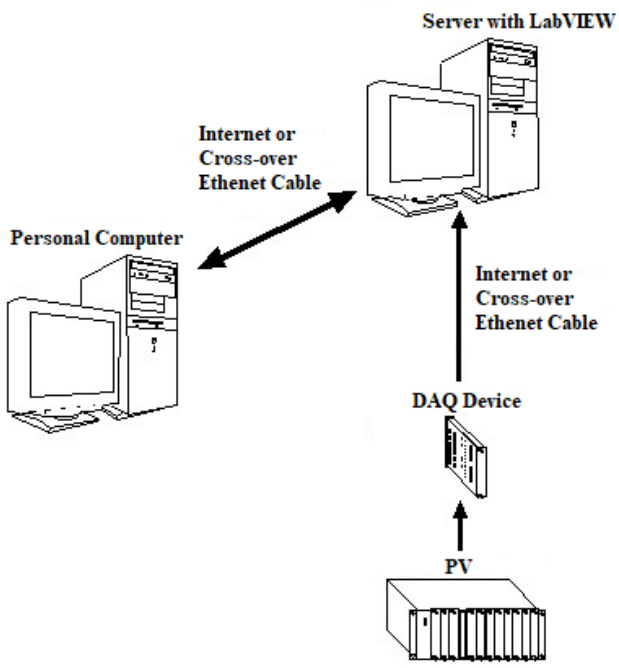

Figure 3.1: Data acquisition system(NATIONAL INSTRUMENTS, 2016)

3.2 PV modules used

Three different PV technologies was investigated, namely CIS/CIGS, polycrystalline silicon and monocrystalline silicon. The various module characteristics are displayed in the table 3.1 below. All values are given for standard test condition (STC).

Technology	CIS/CIGS	polycrystalline	monocrystalline
Maximum power/W	12	20	20
V_m/V	15.8	18.6	17.2
I_m/A	0.76	1.08	1.16
V_{oc}/V	23	22.14	21.6
I_{sc}/A	0.9	1.16	1.26

Table 3.1: Module characteristics

3.3 Sensors and calibration

3.3.1 Pyranometer

2 SolData pyranometers were calibrated against the already calibrated SolData Pyranometer no. 912spc with a sensitivity of 156 mV/(kw/m^2). These pyranometers were chosen due to their linearity in voltage with change in irradiance.

The procedure was as followed. The three pyranometers were connected on three different channels of a HOBO U12-008 data logger and the contraction was placed on a flat surface in sunlight with no object in the vicinity which would cause any sort of shading. All three pyranometers should be as closed to each other to prevent them from having different irradiance to be incident on them. After being thoroughly cleaned the data logger was started and left to acquire data for a period of one day with a frequency of 30 s. Plotting irradiance against voltage of the pyranometers allows to obtain the calibration graph. The irradiance is obtained from the SolData Pyranometer no. 912spc. The graphs obtained are shown in figures 3.2 and 3.3.

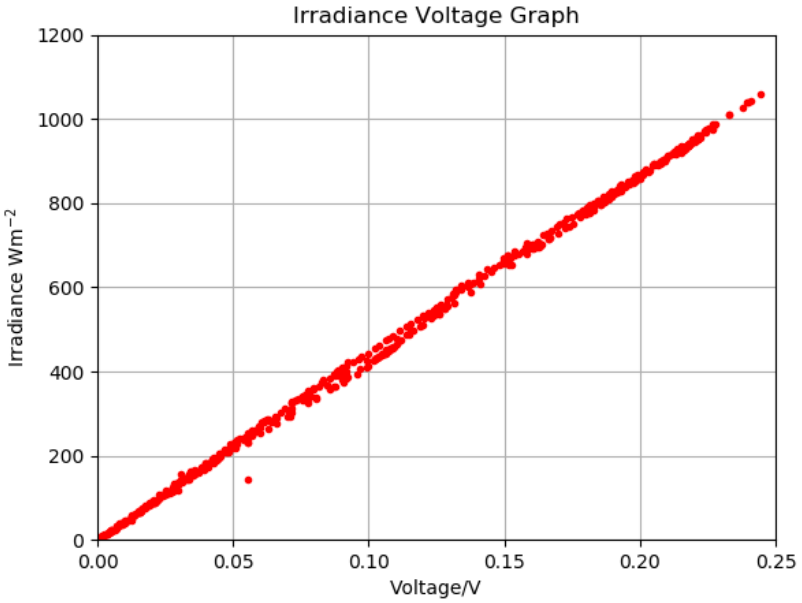

Figure 3.2: Pyranometer 1 calibration graph

3.3 Sensors and calibration

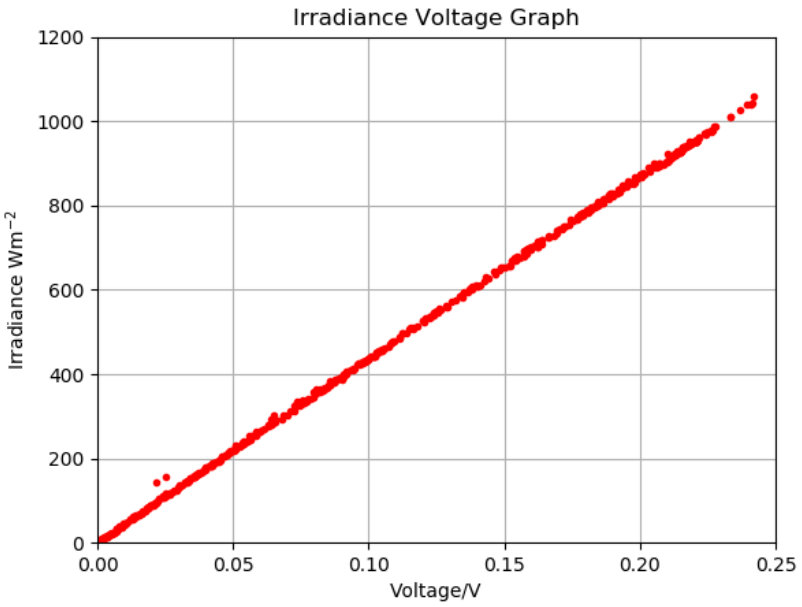

Figure 3.3: Pyranometer 2 calibration graph

The equation of the lines were obtained using the least square method and thus the calibration curves are:

$y=4.3261x+0.0009$, with $R^2=0.996$, for pyranometer 1,

$y=4.3416x+0.0009$, with $R^2=0.996$, for pyranometer 2.

where y is irradiance and x is voltage in mV.

Figure 3.4 shows the two pyranometers used in the final setup. They are placed as closed as possible to each other such that the same amount of sunlight will be incident on them. Further to study the soiling percentage of the test location one is to be kept clean, with weekly cleaning and the other is left untouched in weather conditions.

Figure 3.4: Pyranometers in final setup

3.3.2 Temperature sensor

The ic lm35 from Texas Instrument is used to acquire ambient temperature and temperature of the different board. It was chosen because of its linear temperature calibration in Degrees Celsius. Though it is already calibrated when manufactured a calibration process was performed to obtain a more accurate value. The lm35 is an active component thus requires power. The circuit used to power it is shown in figure 3.5 and the 5V is supplied by a 7805

ic.

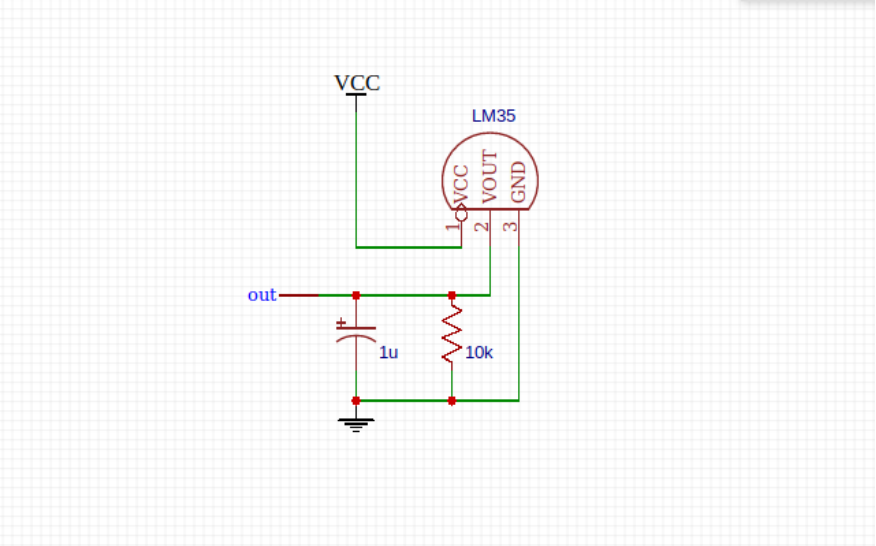

Figure 3.5: Lm35 circuit

For the calibration of the lm35 used, a HOBO U12-008 data logger with a TMC20-HD were used. The various sensors were mounted on a piece of metal sheet, using thermal paste to ensure good thermal conductivity, and the metal sheet in turn stuck to a metal flask. Hot water was poured in the flask and allowed to cool. The outputs of the various sensors were recorded using the data logger at a frequency of 10s. The TMC20-HD was already callibrated to Degree Celsius and thus the relationship between the output of the lm35 and the temperature being measured could be obtained.

Four lm35 were used, one for each three boards and one for ambient temperature and the calibration graph obtained was:

$y=98.575x+0.5231$, with $R^2=0.994$, for lm32 1,

$y=102.62x+0.0786$, with $R^2=0.996$, for lm32 2,

$y=111.64x-2.0789$, with $R^2=0.994$, for lm32 3,

$y=91.533x-1.5302$, with $R^2=0.994$, for lm32 4,

where y is temperature and x is voltage in mV.

Figure 3.6 shows how the lm35 are mounted at the back of the panels. Thermal paiste was used to ensure good heat transfer between the panel and the sensors thus obtaining the most accurate value. Also the measurement is taken at the centre of the board.

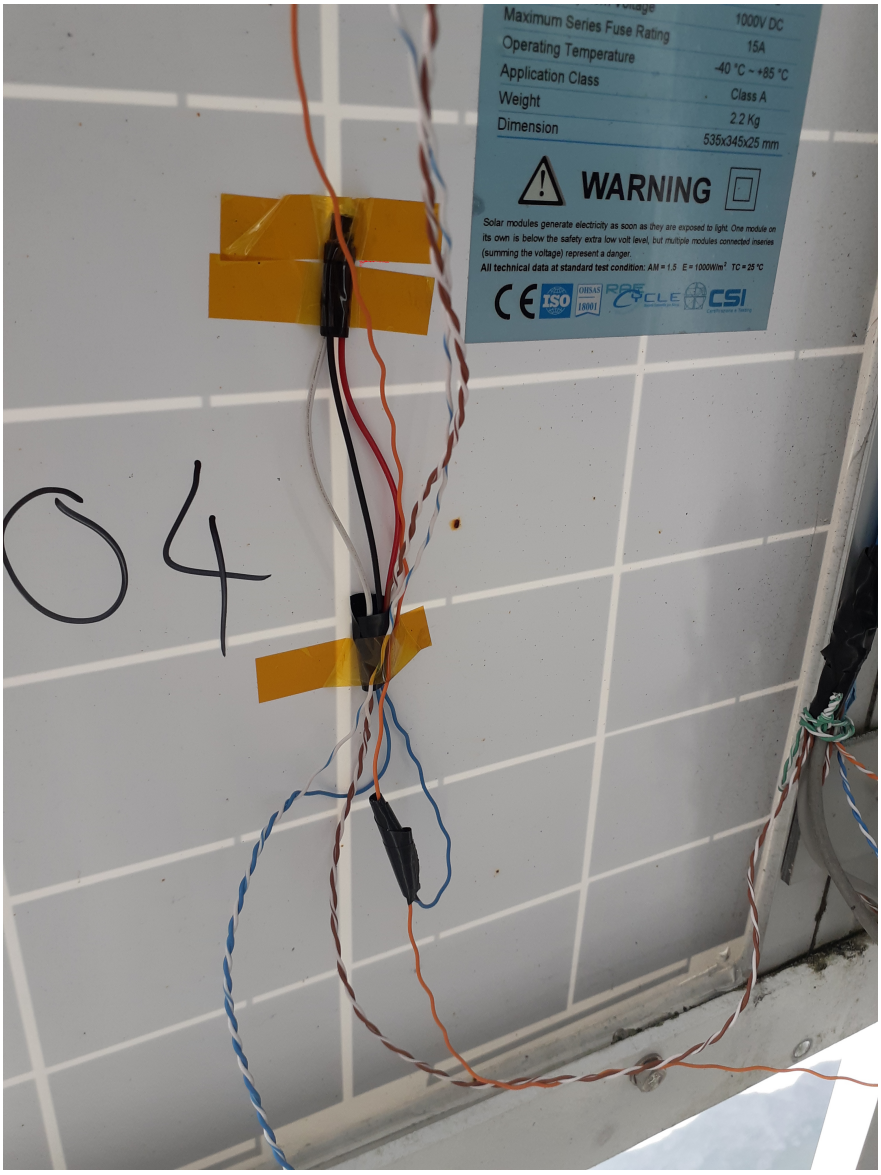

Figure 3.6: Lm35 mounted on back on PV panel

3.3.3 Voltage sensor

The voltage sensor used was the LEM LV25-P since it allows to measure a large range of Voltage. The sensors were calibrated using the circuit shown in figure 3.7.

3.3 Sensors and calibration

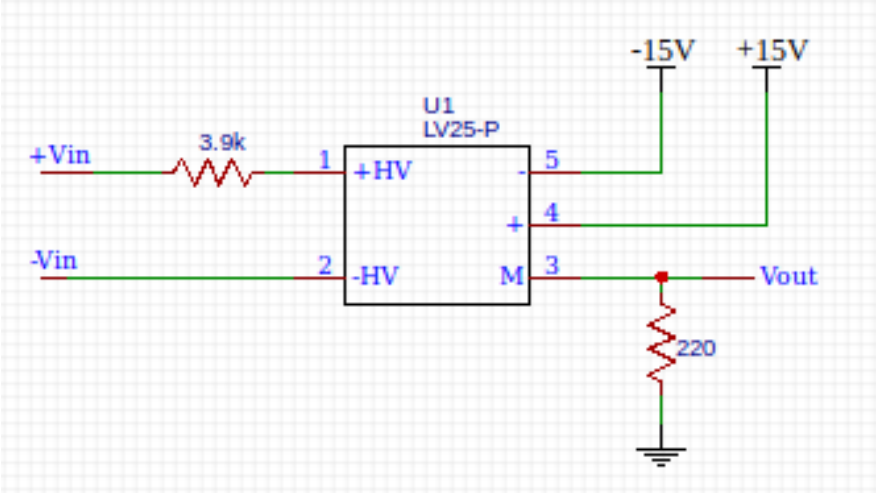

Figure 3.7: LV25-P circuit

A known voltage was applied across Vin using a lab bench power supply. The applied voltage was varied and the resulting output voltage written down. Graphs of applied voltage against output voltage were plotted to obtain the calibration graph. Calibration graph of one board is shown in figure 3.8. The equation of best fit is the calibration graph.

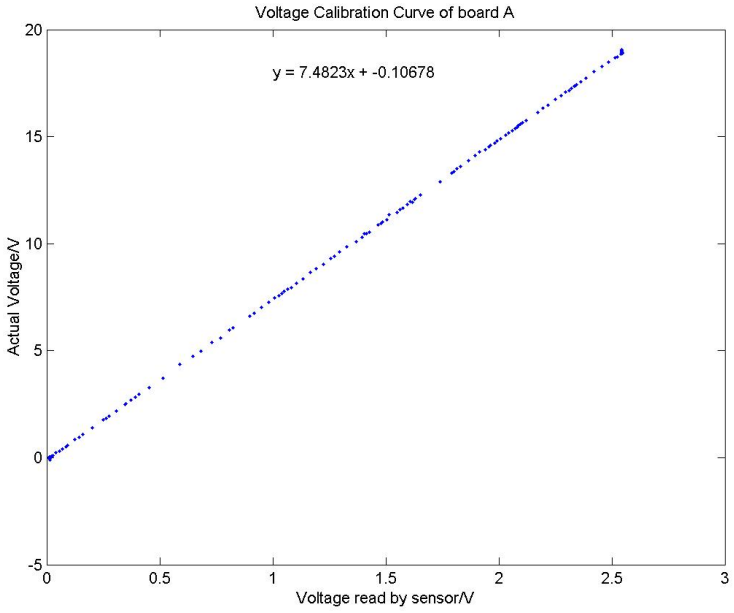

Figure 3.8: applied voltage against output voltage graph

3.3.4 Current sensor

The current sensor LV 5P was used since it uses a hall effect sensor instead of a shunt thus has virtually zero resistance and also it allows for a maximum current reading of 5A which is twice the maximum expected value. The circuit used to calibrate it is shown in figure 3.9.

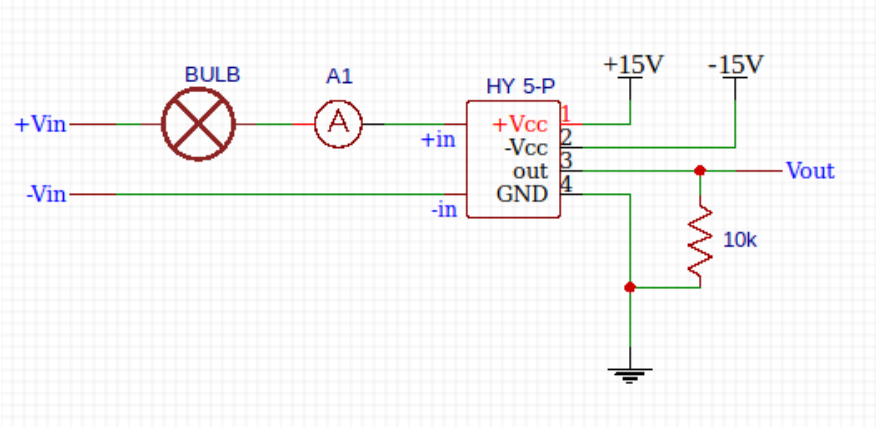

Figure 3.9: HY-5P circuit

Using a lab bench power supply, a voltage is applied across +Vin and -Vin and the corresponding current through the bulb is recorded using the ammeter.

For the given current the output voltage of the sensor is measured with ground being the reference value.

This procedure is repeated for several values of applied voltage and a graph of current against output voltage is plotted to obtain the corresponding calibration graph. Figure 3.10 shows such a graph with its equation.

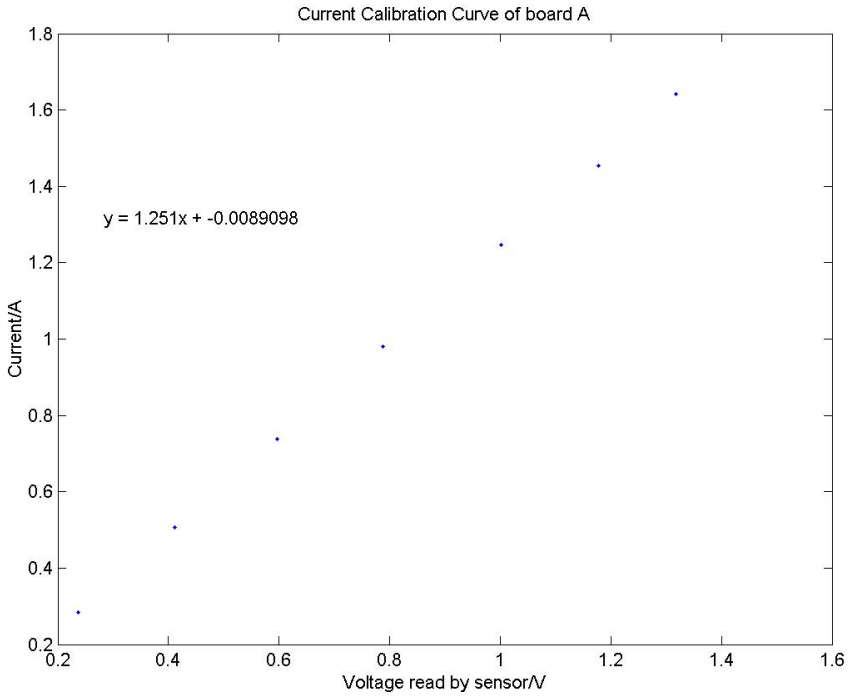

Figure 3.10: Calibration graph of current sensor

3.3.5 DC load

The APT5010JN n channel enhancement mode power mosfet was used as a dc load as it has a small internal resistance of 0.10 Ω and that it can withstand the high short circuit current from the panels.

3.4 Final circuit used

The final circuit used is as shown in figure 3.11. The dual power supply is provided by two 12V lead acid battery connected in series as in figure 3.12.

3.4 Final circuit used

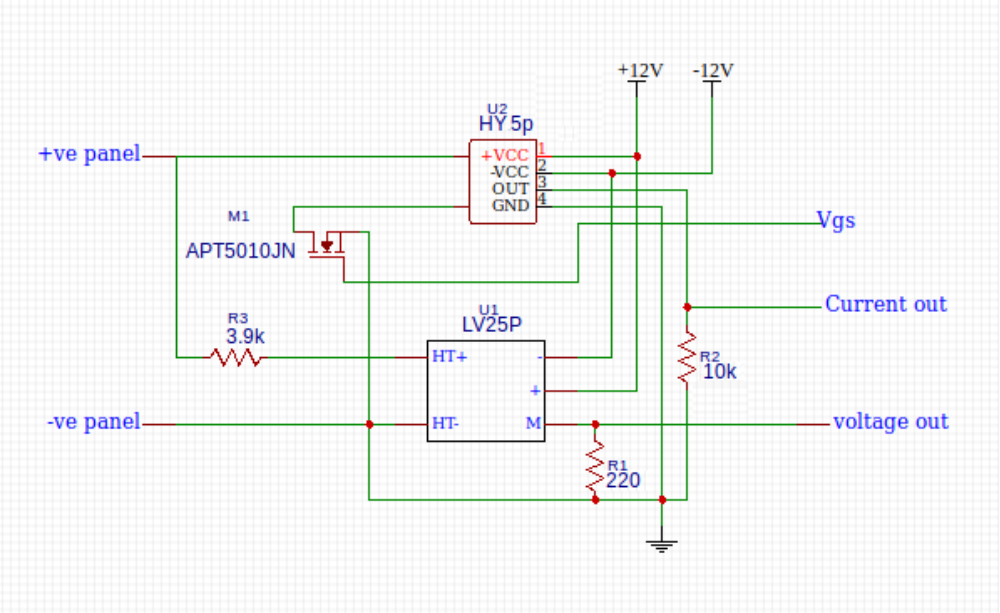

Figure 3.11: Circuit schematic

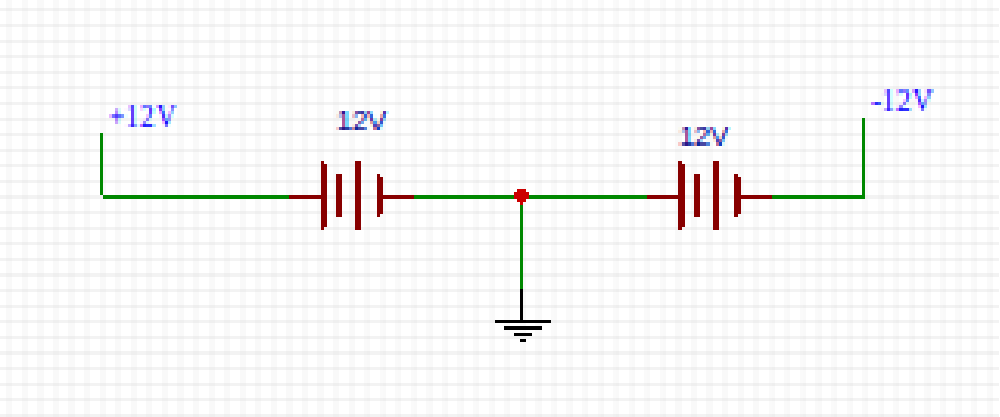

Figure 3.12: Battery configuration

The final board is as shown in figure 3.13. Three of these were made and connected to the three different PV panel technologies.

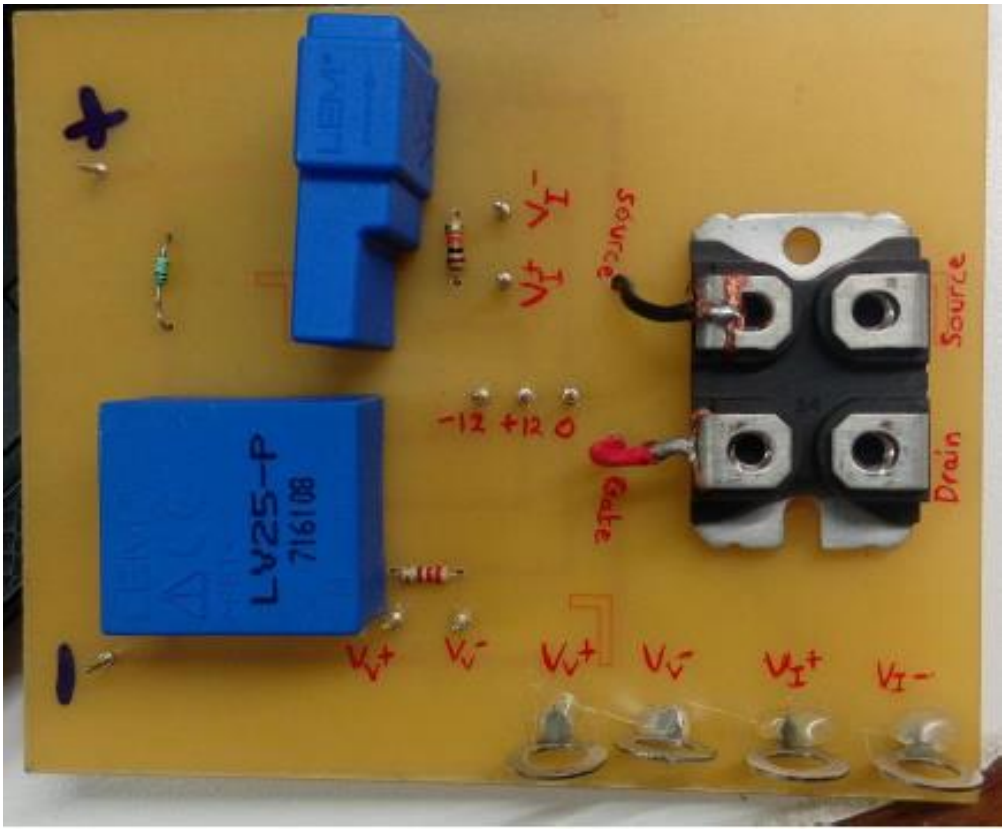

Figure 3.13: Picture of actual board

3.5 Hardwares

In order to apply and acquire the appropriate voltages NI daq devices were used. Three modules were used, one to generate voltage in the form of an analog output, one to acquire voltage, that is an analog input and a chassis to connect the two other modules and to allow communication with a computer.

3.5.1 NI-9184 Ethernet chassis

Figure 3.14 shows the chassis used. It is connected to the local server of the University via ethernet and allow communication with any computer connected to the same server. Using labview it is flashed with an appropriate code which then perform the data acquisition and communication.

Figure 3.14: Picture NI-9184 Ethernet chassis

3.5.2 NI modules

Figure 3.15 shows the NI-9263. It is an analog output module with four analog output with a range og ±10 V and a resolution of 16 bits. It has a maximum sampling rate of 100kS/s/ch. Figure 3.16 shows the NI-9205. It is a 16 channels analog input module with 16 bit resolution and a maximum sampling rate of 250kS/s/ch and allow to collect several inputs using a single module. They were chosen due to their fast sampling rate allowing to acquire the IV curve for a specific irradiance and temperature and because of their high resolution.

Figure 3.15: Picture of NI-9263 module

Figure 3.16: Picture of NI-9205 module

3.5.3 Complete setup

Figure 3.17 shows all the hardwares used for the data acquisition. Apart from the 3 PV panels being tested, 2 more panels are used to charge the batteries through the the charge controllers thus the system does not need a socket as it generates and stores its own power in the batteries. All of these sensitive electronics are well protected from weather conditions in a waterproof box.

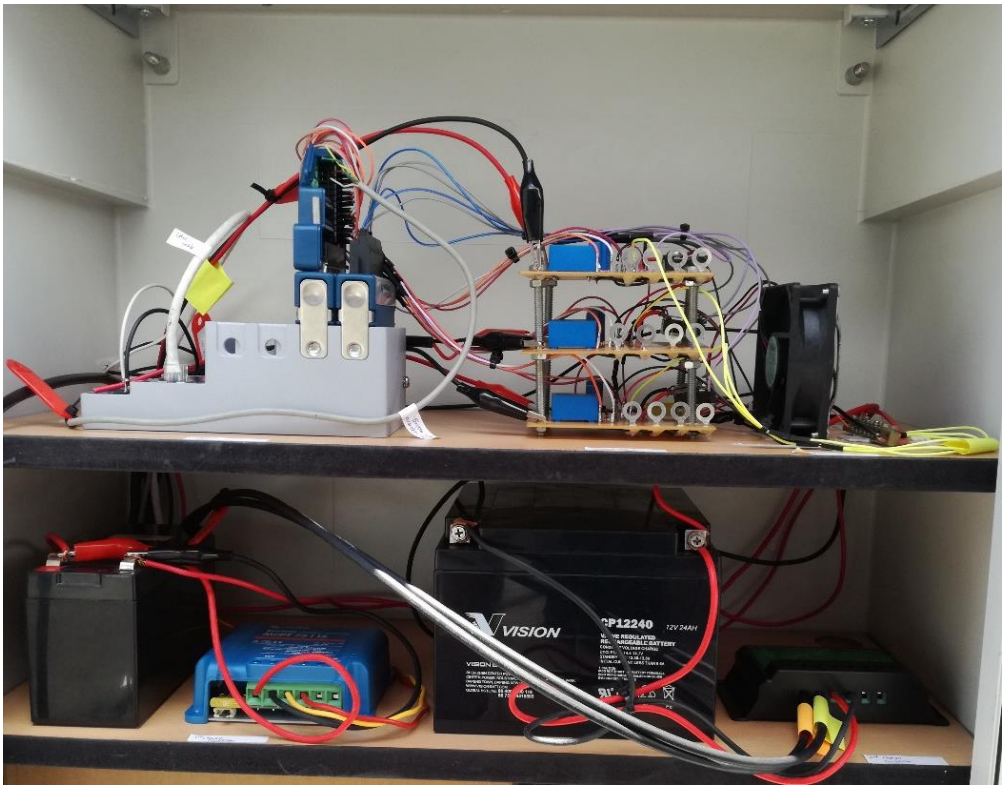

Figure 3.17: Hardware setup

The panels and all the necessary equipments are mounted on a metal frame as shown below in figure 3.18. The test rig, and thus all PV panels and pyranometers, is inclined at 20° for optimum incident radiation from sun.

Figure 3.18: Outdoor setup

3.6 Softwares

The final element of the system is the software which will give the different modules used the proper instructions for data acquisition and to perform the data transfer to the host pc since the NI modules do not have built in memory. A VI was developed using Labview and flashed to the chassis. Figure 3.19 and 3.20 show the full VI.

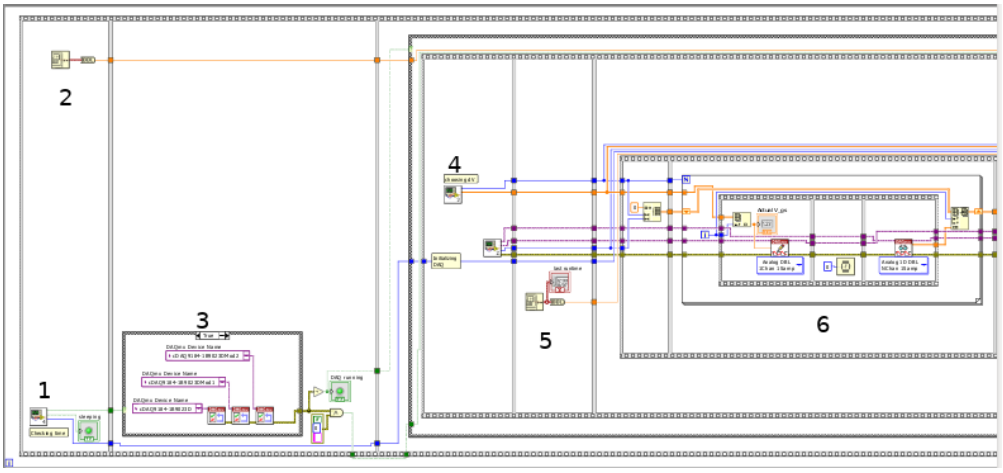

Figure 3.19: Block diagram of the VI(part 1)

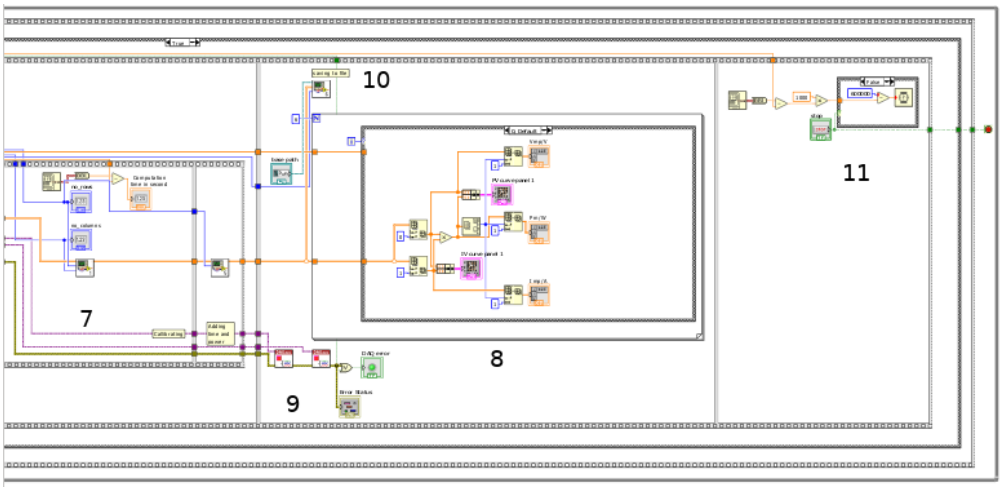

Figure 3.20: Block diagram of the VI(part 2)

The VI was designed such that it runs from 5:00 to 19:00 taking a set of data every 10 minutes. For ease of explanation several parts of the VI were labelled from 1 to 11.

Part 1 and 2 of the VI are used to obtain actual time of run. The role of part one is to check whether the actual time is in the wanted range, if yes the program continues to part 3, else it moves directly to part 11. Part 2 is used to ensure that the program will wait 10 minutes between each data acquisition

Part 3 is used to check presence and availability of the several NI modules. In case there is a connectivity issue with the module an error message will be displayed, else the program

will continue to run normally.

Part 4 is used to generate the different value of voltages to be applied to the gate of the mosfet.

Part 5 displays the last runtime.

Part 6 is the section which performs the actual data acquisition whereby a voltage is applied to the mosfets and the output of the several sensors are recorded.

Part 7 adds the actual time of the data acquisition to the data set.

Part 8 includes all the different graphs and displays in the front panel.

Part 9 is the error checking routine and display.

Part 10 saves the obtained data by concatenating it into the specific file.

Part 11 is the part which causes the program to wait 10 minutes.

On running this code the host pc is able to communicate with the NI modules and data is then stored and displayed to the host pc on the front panel

3.7 Computing parameters of PV cell

The one diode model is often used for its simplicity and relative ease to solve when compared to the two diode model. In this work the one diode model was used to obtain the various parameters of the module at cell level.

Knowing the three main points of the I-V curve, namely the coordinates at open circuit, closed circuit and at the maximum power point, equations 3.1 to 3.5 may be derived(Ramgolam, 2017). can be used to find the five parameters.

At short circuit, V=0 and I=I_{sc}:

$$I_{sc} = I_{ph} - I_s \left[exp\left(\frac{I_{sc}R_s}{nV_{th}}\right) - 1 \right] - \frac{I_{sc}R_s}{R_{sh}} \tag{3.1}$$

At open circuit, V=V_{oc} and I=I_{sc}:

$$0 = I_{ph} - I_s \left[exp\left(\frac{V_{oc}}{nV_{th}}\right) - 1 \right] - \frac{V_{oc}}{R_{sh}} \tag{3.2}$$

At maximum power point, V=V_m and I=I_m:

$$I_m = I_{ph} - I_s \left[exp\left(\frac{V_m + I_m R_s}{nV_{th}}\right) - 1 \right] - \frac{V_m + I_m R_s}{R_{sh}} \tag{3.3}$$

At maximum power point, $\frac{dP}{dV} = 0$:

$$\frac{dP}{dV} = \frac{I_{ph} - \frac{I_s}{nV_t h}(V_m - I_m R_s - nV_{th}) exp\left(\frac{V_m + I_m R_s}{nV_{th}}\right)}{1 + \frac{I_s R_s}{nV_{th}} exp\left(\frac{V_m + I_m R_s}{nV_{th}}\right) + \frac{R_s}{R_{sh}}} = 0$$

(3.4)

At maximum power point, $\frac{dI}{dV} = -\frac{I_m}{V_m}$:

$$\frac{dI}{dV} = \frac{-\frac{I_s}{nV_{th}} exp\left(\frac{V + IR_s}{nV_{th}}\right) - \frac{1}{R_{sh}}}{1 + \frac{I_s R_s}{nV_{th}} exp\left(\frac{V + IR_s}{nV_{th}}\right) + \frac{R_s}{R_{sh}}} = -\frac{I_m}{V_m} \tag{3.5}$$

Using equations 3.1 to 3.5 is put in the form of a system of five dimensional non linear algebraic equations as described by Drouiche *et al.* (2018) and is then fed to python and solved. An initial guess of the parameters is required and the guess is adjusted such that the model gives good correlation with experimental data.

Chapter 4

Results, Analysis and Discussions

This chapter presents the results obtained from the data acquisition. Analysis are then performed and several deductions are made

4.1 Front panel display

Figure 4.1 shows the all the different graphs and indicators on the front panel. Starting from the left the indicators are as follows:

• the temperature of the last runtime,

• irradiance measured using a pyranometer cleaned frequently,

• irradiance measured using a pyranometer left to environmental conditions and without any cleaning,

• last runtime,

• computation time of last run and

• actual voltage being applied of the gates of the mosfets.

The first led indicates whether the NI modules are available and running, the second one indicates whether the actual time is out of the range of 5:00 to 19:00 and the last one indicates an error.

The several graphs displayed represent data about last run time. Each column represent information about a specific technology whereby the first column is the CIS/CIGS technology,

the second the polycrystalline silicon technology and the last one the monocrystalline silicon technology. The first row is the IV graph that is the raw data being collected. The second row is the Power Voltage graph. Along with the various graphs, on top of the IV graph the temperature of board is displayed. On top of the PV curve the power, voltage and current at maximum power point is displayed.

On the rightmost is the stop button to stop the program after the next run and also an error dialog box to indicate error if any.

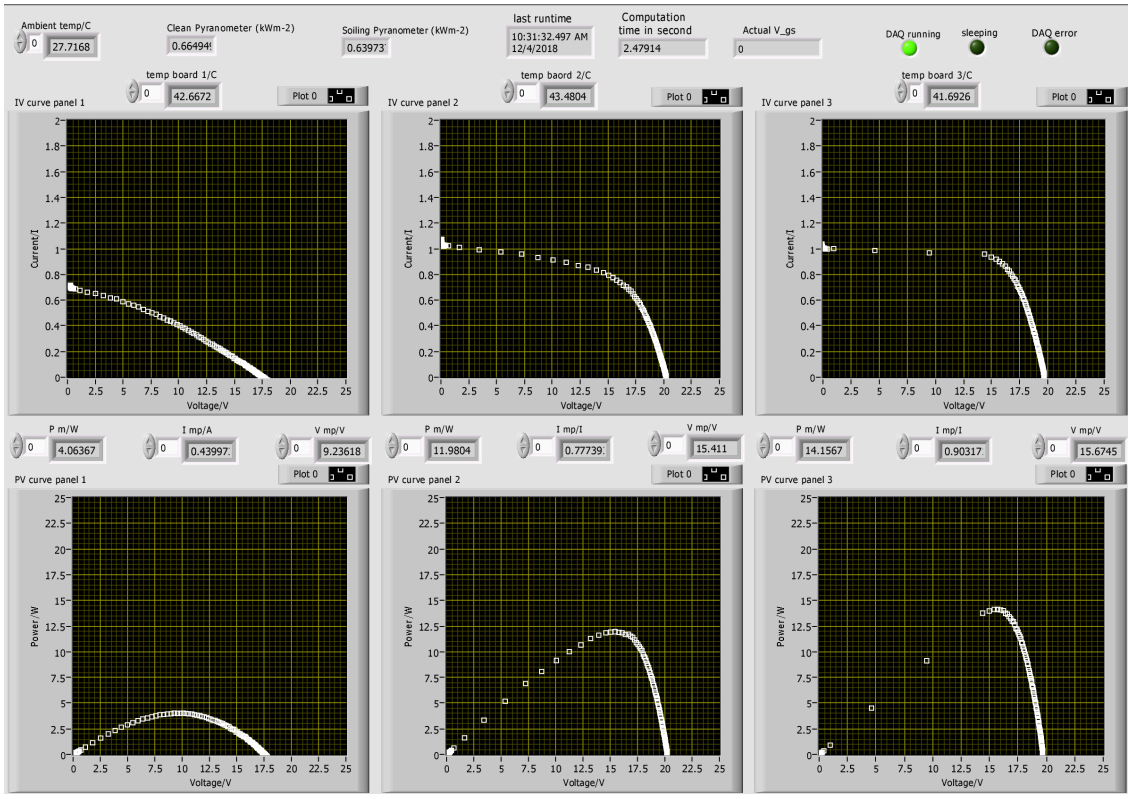

Figure 4.1: Display of the VI

4.2 Temporal variation of ambient temperature and panel temperatures

The variation of the various recorded temperatures were plotted against time, as shown in figure 4.2 and good correspondence was observed. By plotting panel temperatures against ambient temperature a linear relationship for low temperature is observed and as temperature

increases, the panel temperature increases more rapidly than ambient temperature. The behaviour tallies with literature.

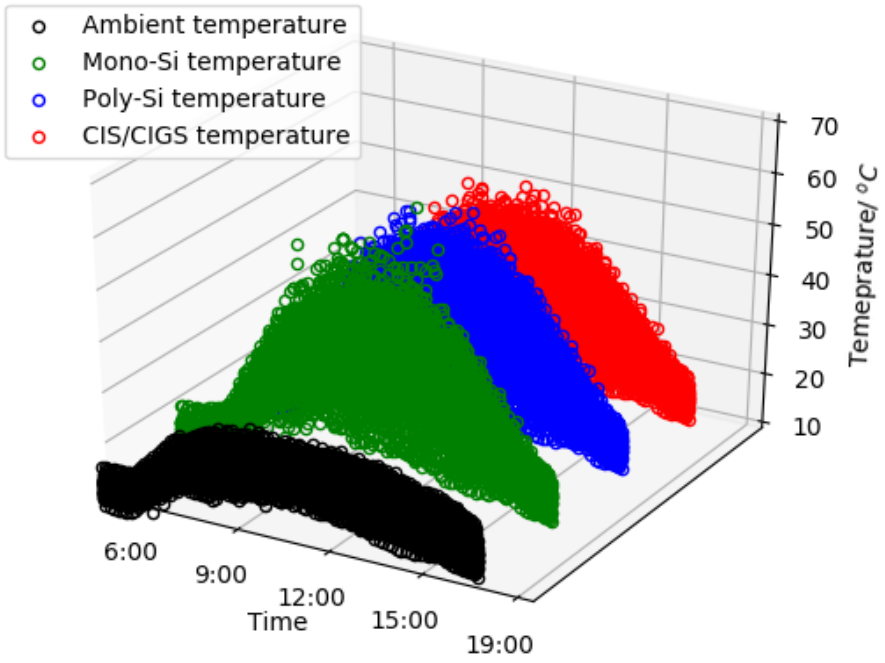

Figure 4.2: Temporal variation of temperature

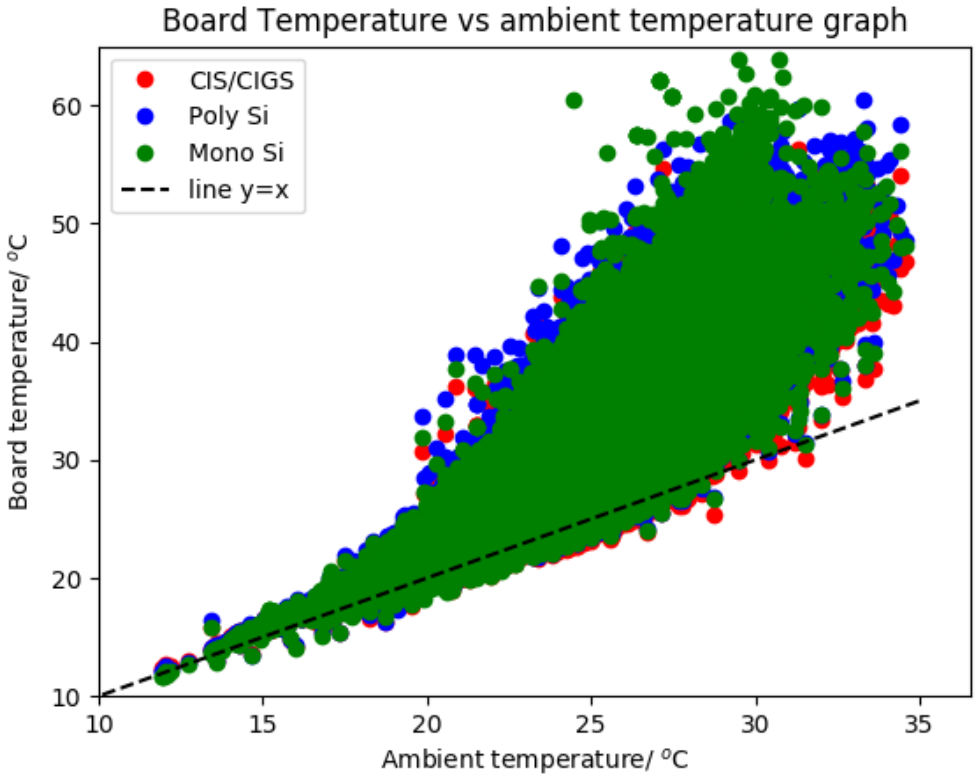

Figure 4.3: Variation of panel temperatures against ambient temperature

4.3 Variation of currents with temperature for fixed irradiance

From the collected data, the maximum power point current and short circuit current for each technology was extracted. Knowing the temperature of the boards, the data was sorted with respected to irradiance whereby a specific set of of current was plotted against temperature for a given irradiance S with a range of $\pm$ 10 Wm^{-2} about S. Figure 4.4 to figure 4.14 show several different graphs obtained:

4.3 Variation of currents with temperature for fixed irradiance

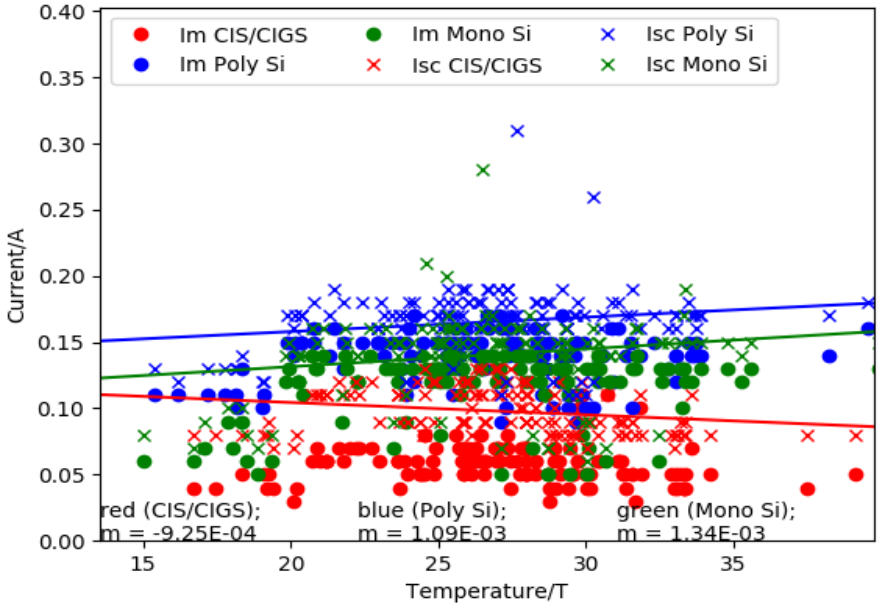

Figure 4.4: Current temperature graph at S=100W m^{-2}

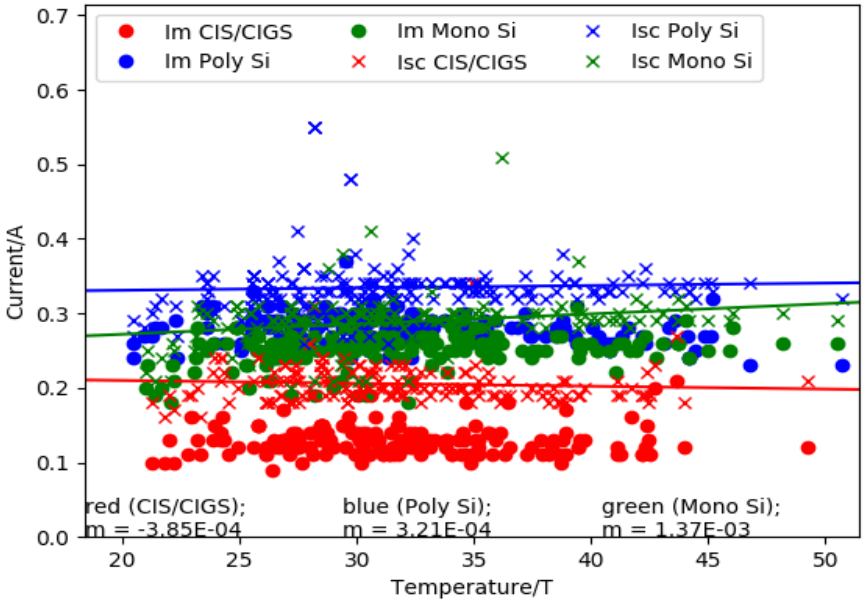

Figure 4.5: Current temperature graph at S=200W m^{-2}

4.3 Variation of currents with temperature for fixed irradiance

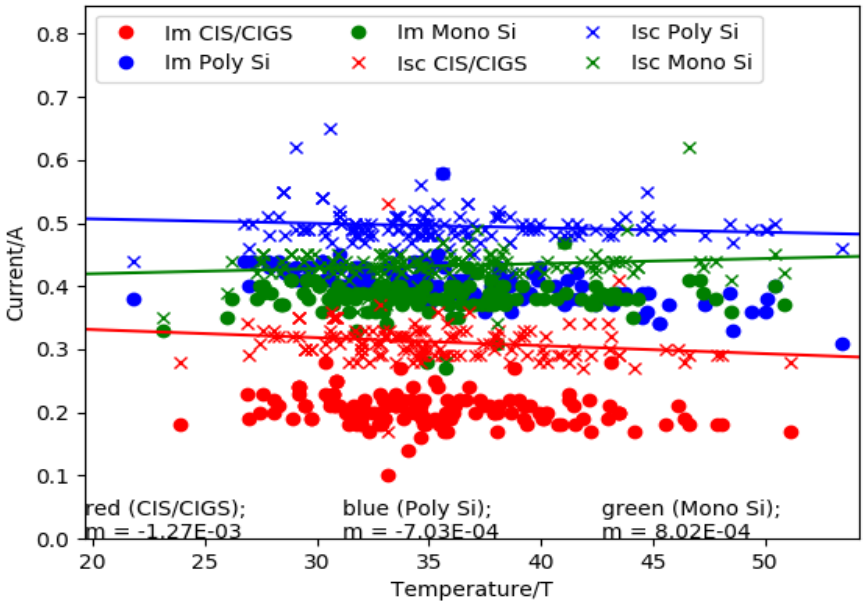

Figure 4.6: Current temperature graph at S=300W m^{-2}

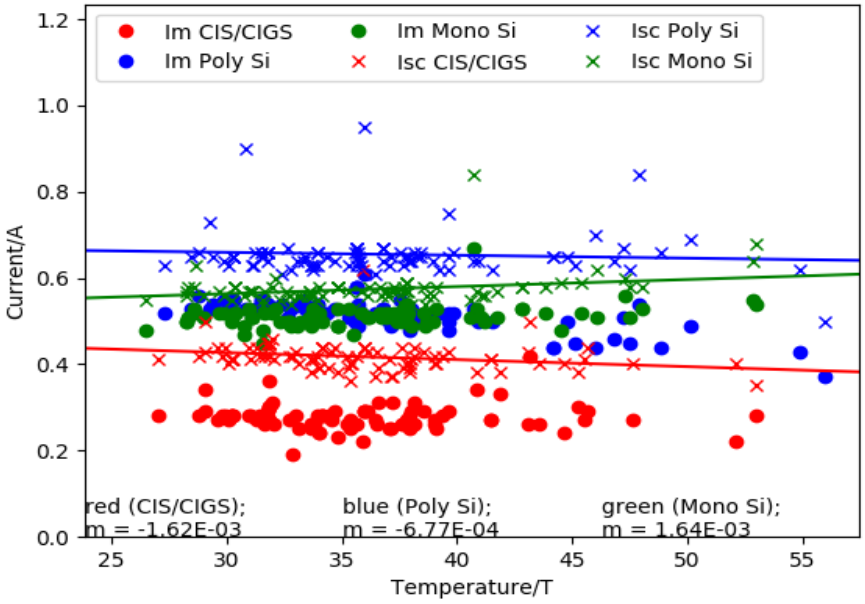

Figure 4.7: Current temperature graph at S=400W m^{-2}

4.3 Variation of currents with temperature for fixed irradiance

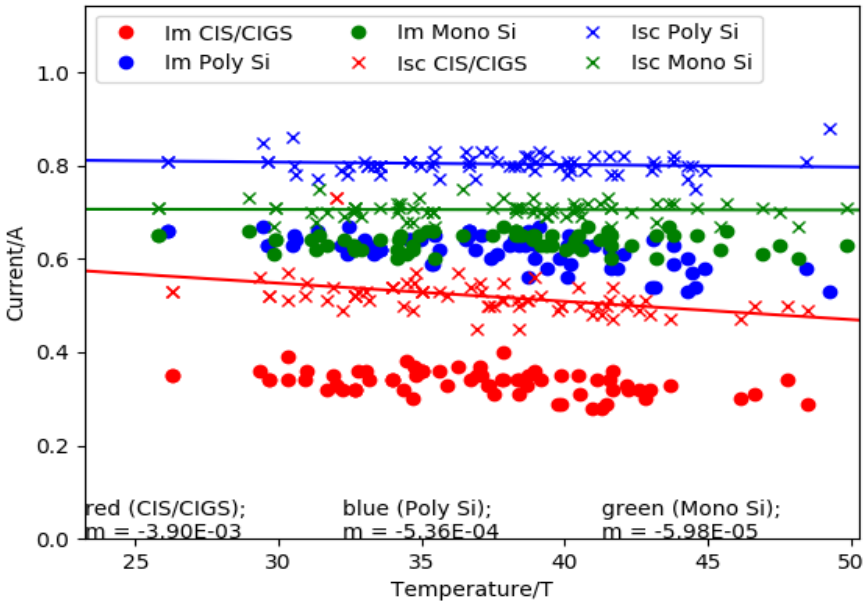

Figure 4.8: Current temperature graph at S=500W m^{-2}

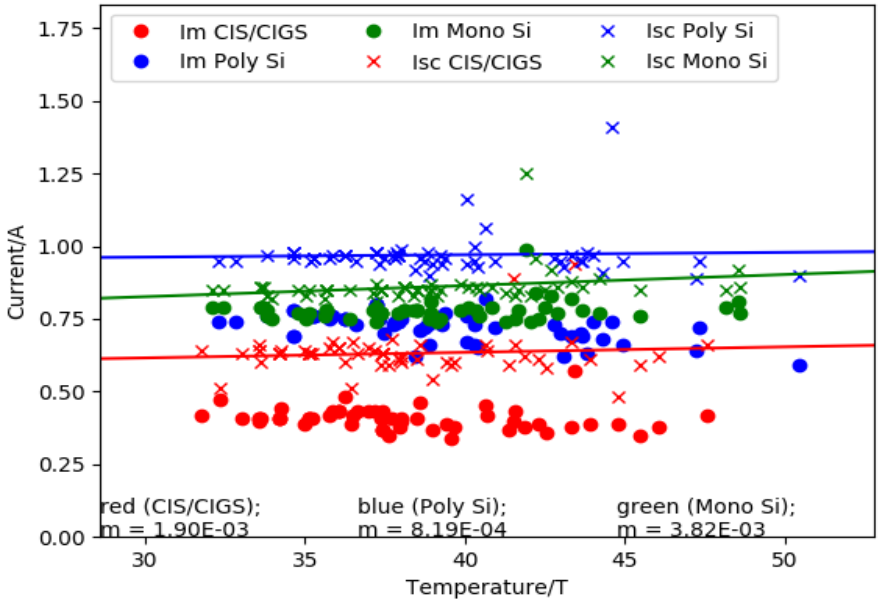

Figure 4.9: Current temperature graph at S=600W m^{-2}

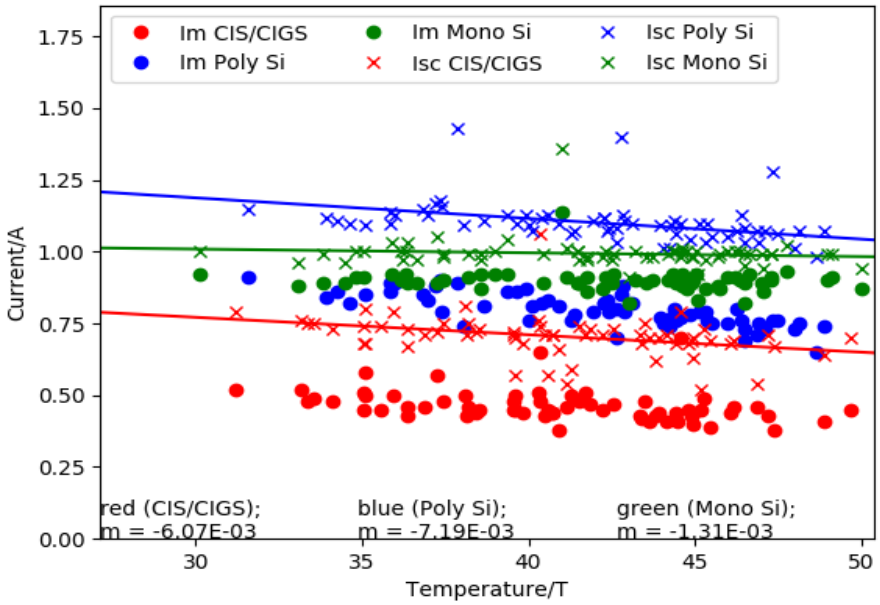

Figure 4.10: Current temperature graph at S=700W m^{-2}

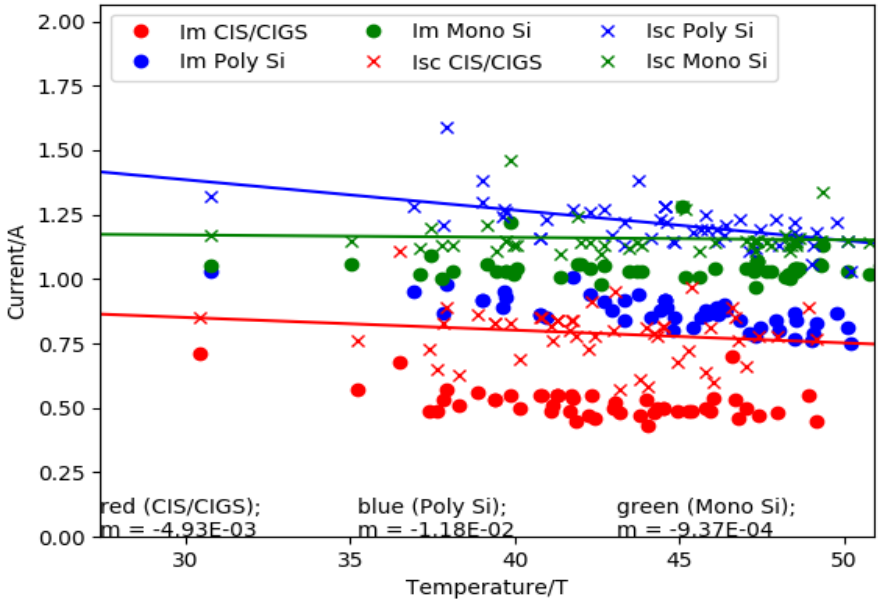

Figure 4.11: Current temperature graph at S=800W m^{-2}

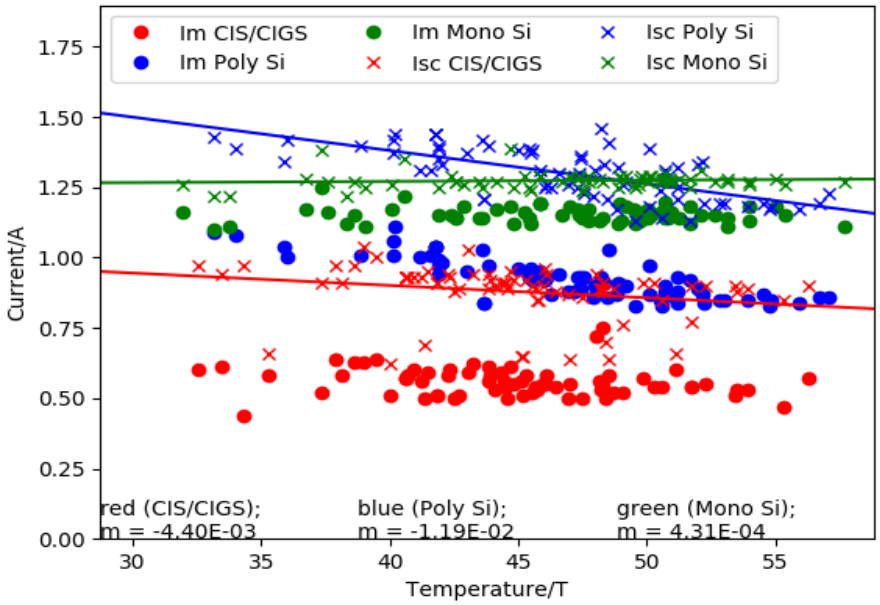

Figure 4.12: Current temperature graph at S=900W m^{-2}

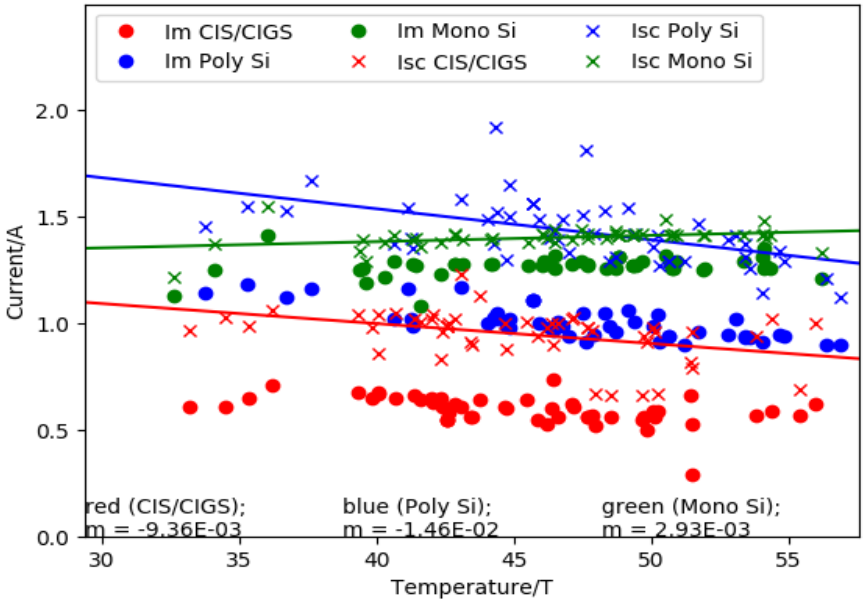

Figure 4.13: Current temperature graph at S=1000W m^{-2}

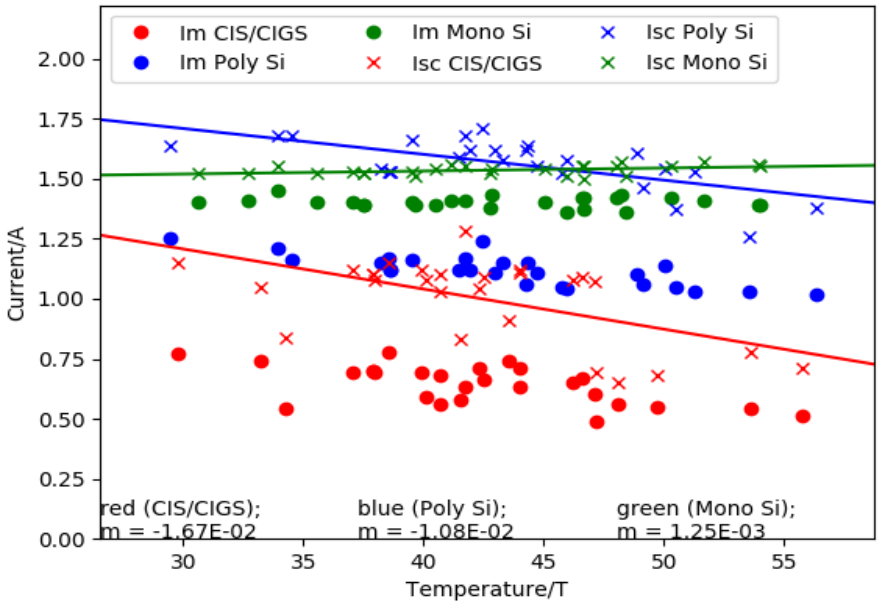

Figure 4.14: Current temperature graph at S=1100W m^{-2}

There exist a linear relationship between current and temperature. Thus the gradient of the current temperature graph is defined as temperature coefficient of current, $T_k(I)$, at the mentioned irradiance. A graph of temperature coefficient of current, $T_k(I)$, against irradiance was plotted to study its variation. The result is shown below in figure 4.15.

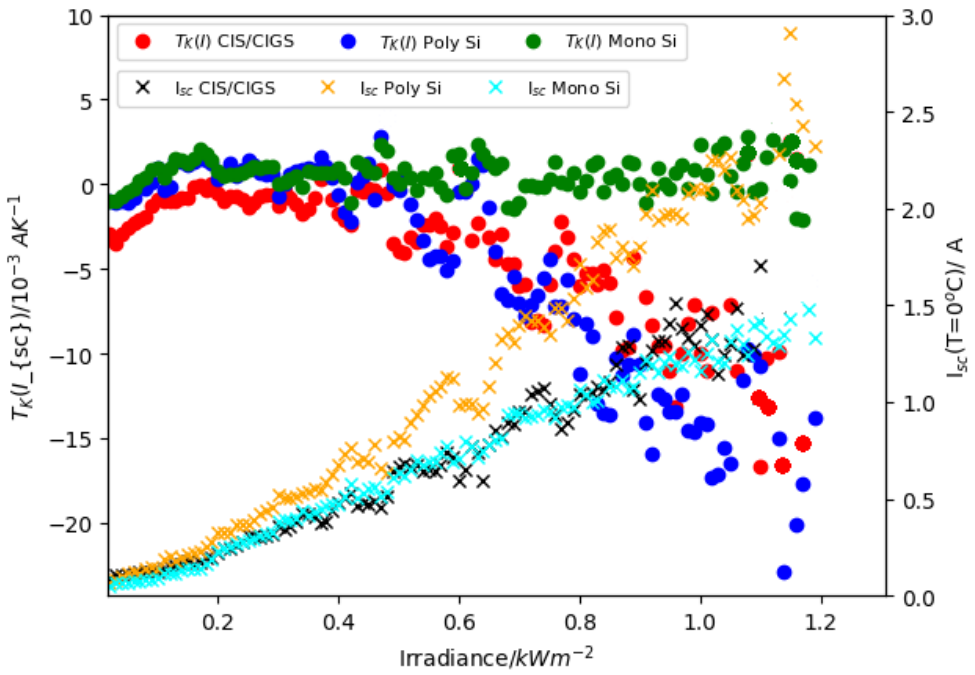

Figure 4.15: temperature coefficient of current, $T_k(I)$, irradiance graph

Studying figure 4.15 it is observed that $T_k(I)$ takes both positive and negative values for different value of irradiance. A positive value of $T_k(I)$ implies that for an increase in temperature there will be a increase in output current and a negative value implies that for an increase in temperature there will be a decrease in output current. All three technologies have positive $T_k(I)$ for 0 Wm^{-2} < S < 400 Wm^{-2}. Beyond this range the polycrystalline PV cells show the steepest decrease in $T_k(I)$ thus there will be a greater decrease in current with increase in temperature compared to the two other technologies. The monocrystalline PV cells show the greatest stability at high irradiance though a small decrease in $T_k(I)$ is observed, making it negative. The CIS/CIGS technology behaves slightly worse than the monocrystalline technology.

4.4 Variation of voltages with temperature for fixed irradiance

From the collected data, the maximum power point voltage and open circuit voltage for each technology was extracted. Knowing the temperature of the boards, the data was sorted with respected to irradiance whereby a specific set of of current was plotted against temperature for a given irradiance S with a range of $\pm$ 10 Wm^{-2} about S. Figure 4.16 to figure 4.26 show several different graphs obtained:

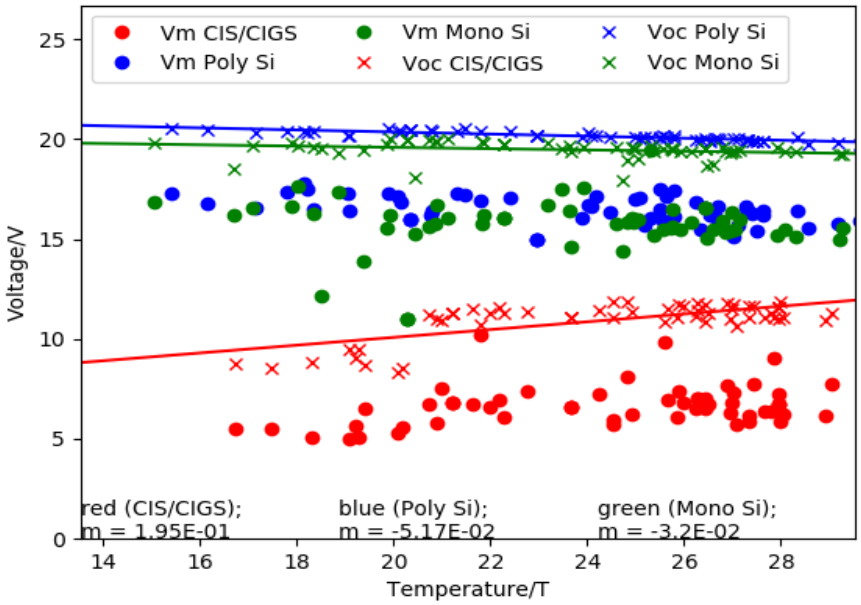

Figure 4.16: Voltage temperature graph at S=100W m^{-2}

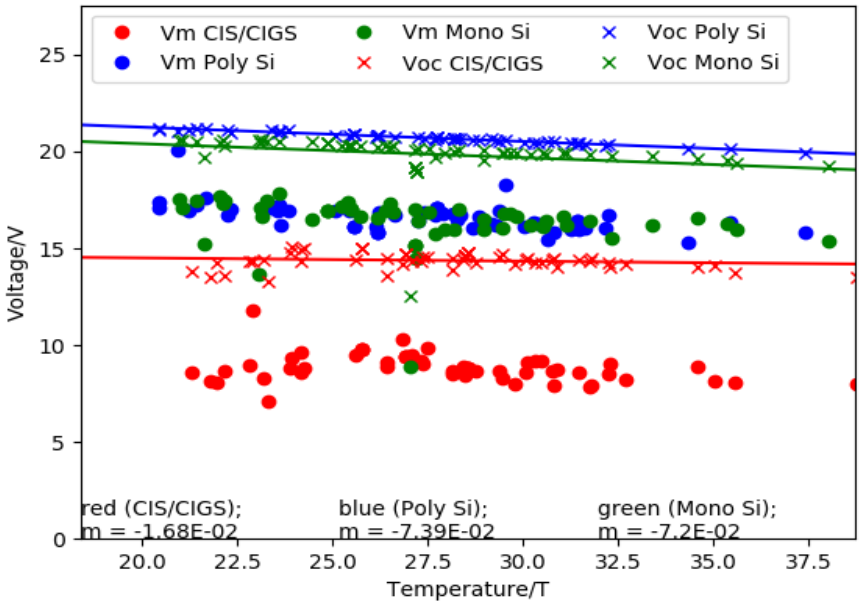

Figure 4.17: Voltage temperature graph at S=200W m^{-2}

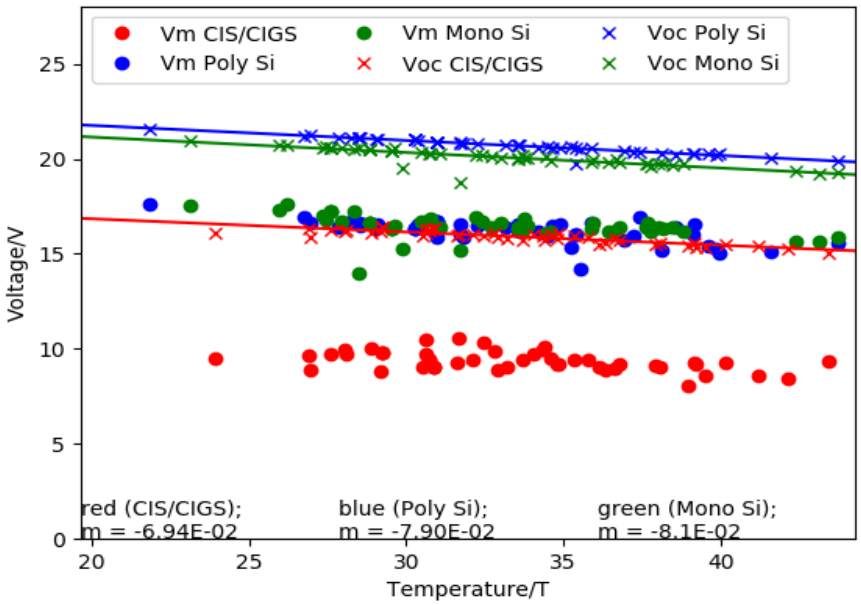

Figure 4.18: Voltage temperature graph at S=300W m^{-2}

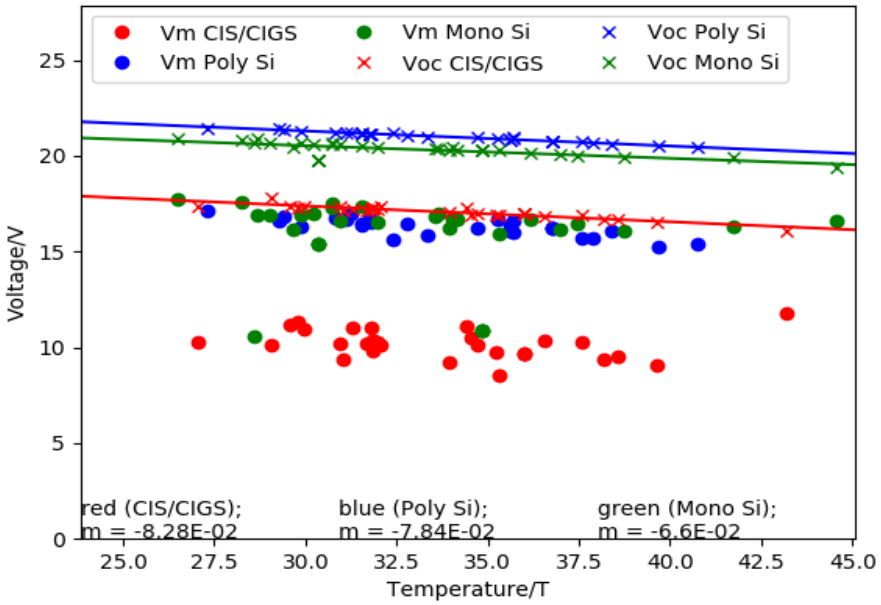

Figure 4.19: Voltage temperature graph at S=400W m^{-2}

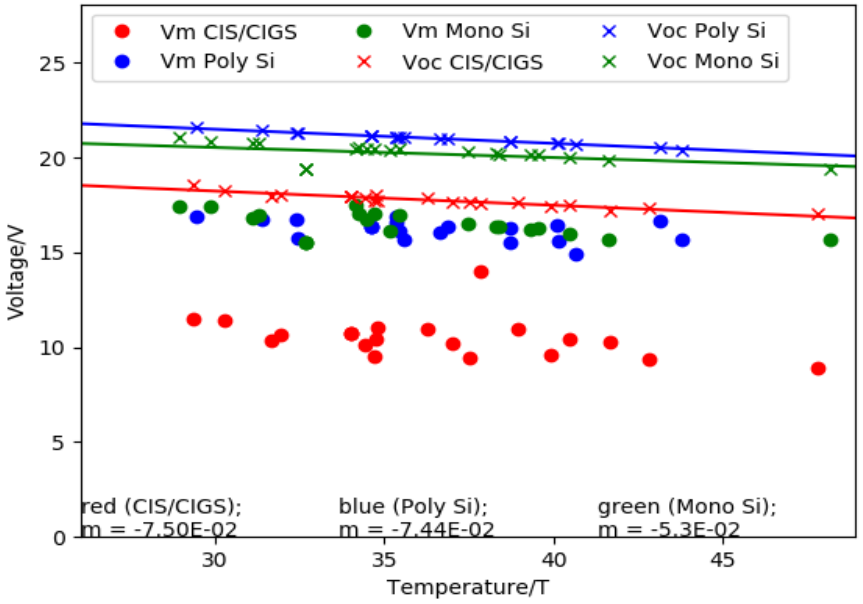

Figure 4.20: Voltage temperature graph at S=500W m^{-2}

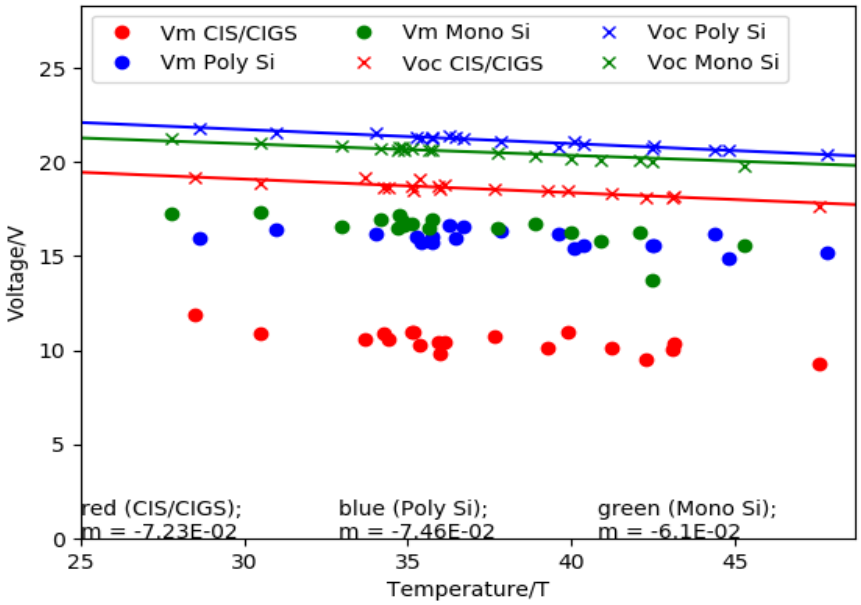

Figure 4.21: Voltage temperature graph at S=620W m^{-2}

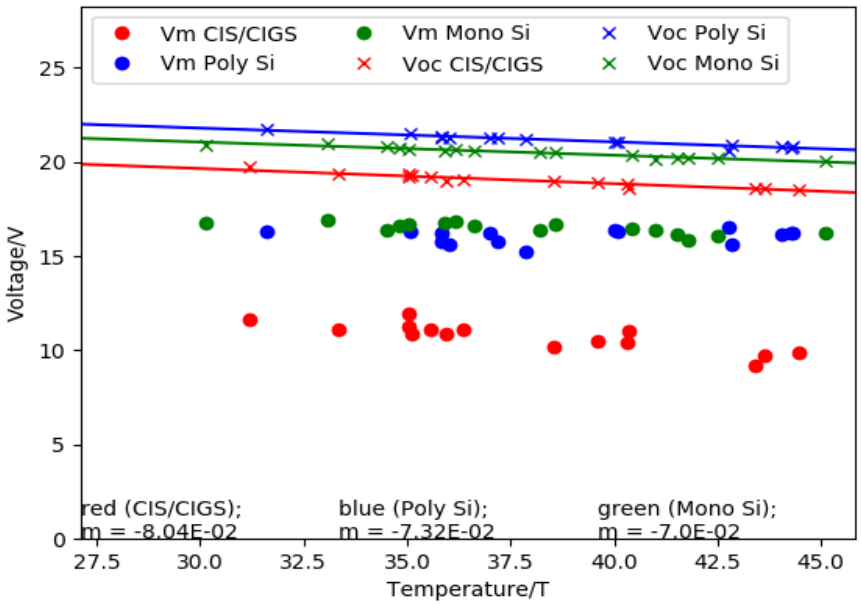

Figure 4.22: Voltage temperature graph at S=700W m^{-2}

4.4 Variation of voltages with temperature for fixed irradiance

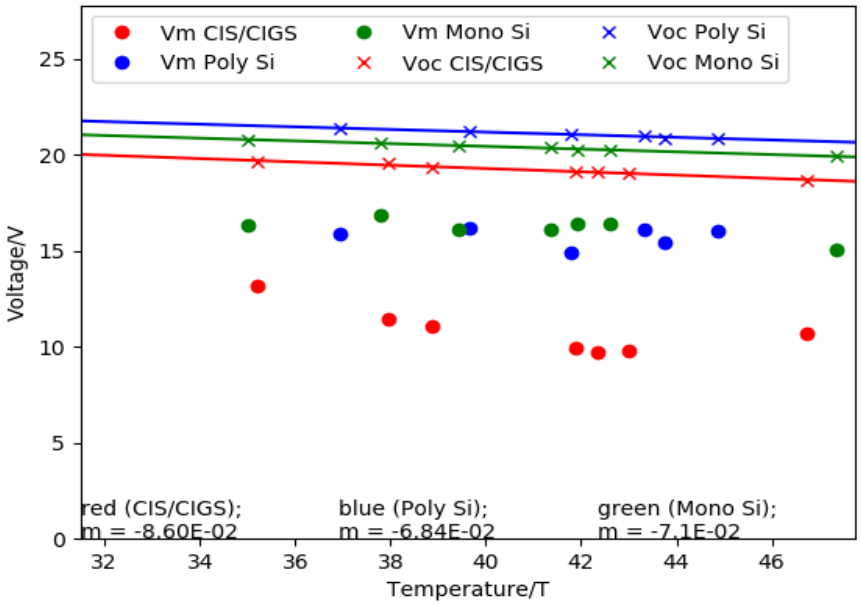

Figure 4.23: Voltage temperature graph at S=800W m^{-2}

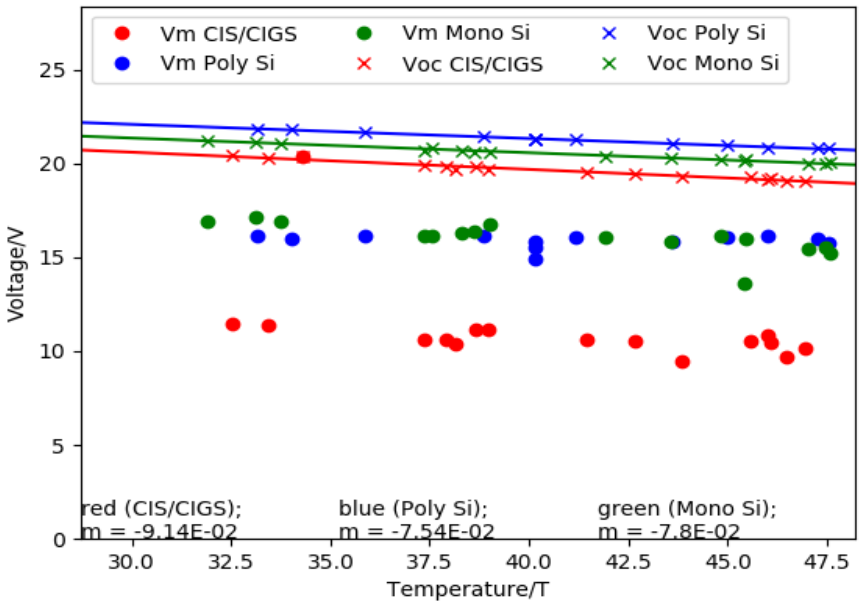

Figure 4.24: Voltage temperature graph at S=900W m^{-2}

4.4 Variation of voltages with temperature for fixed irradiance

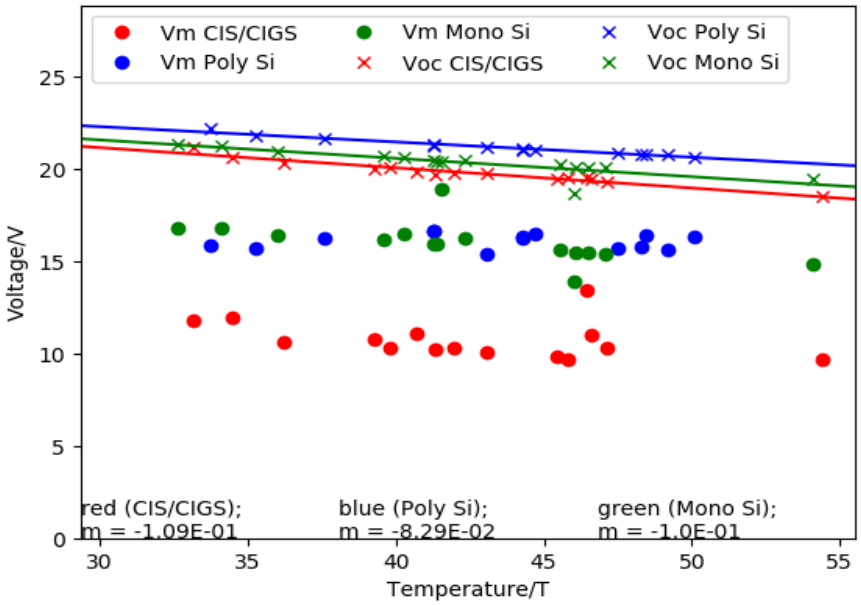

Figure 4.25: Voltage temperature graph at S=1000W m^{-2}

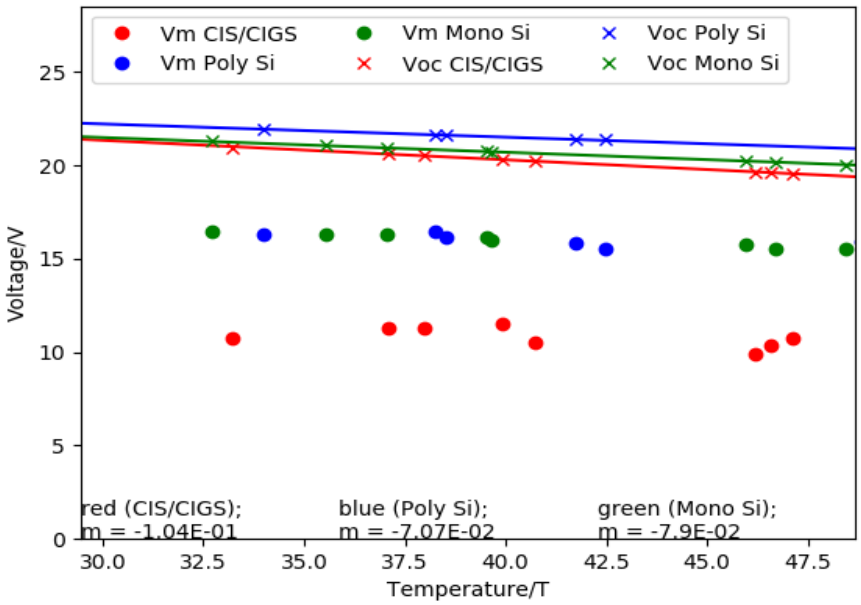

Figure 4.26: Voltage temperature graph at S=1100W m^{-2}

There exist a linear relationship between voltage and temperature. Thus the gradient of

the current temperature graph is defined as the temperature coefficient of voltage, $T_k(V)$, at the mentioned irradiance. A graph of temperature coefficient of voltage, $T_k(V)$, against irradiance was plotted to study its variation. The result is shown below in figure 4.27.

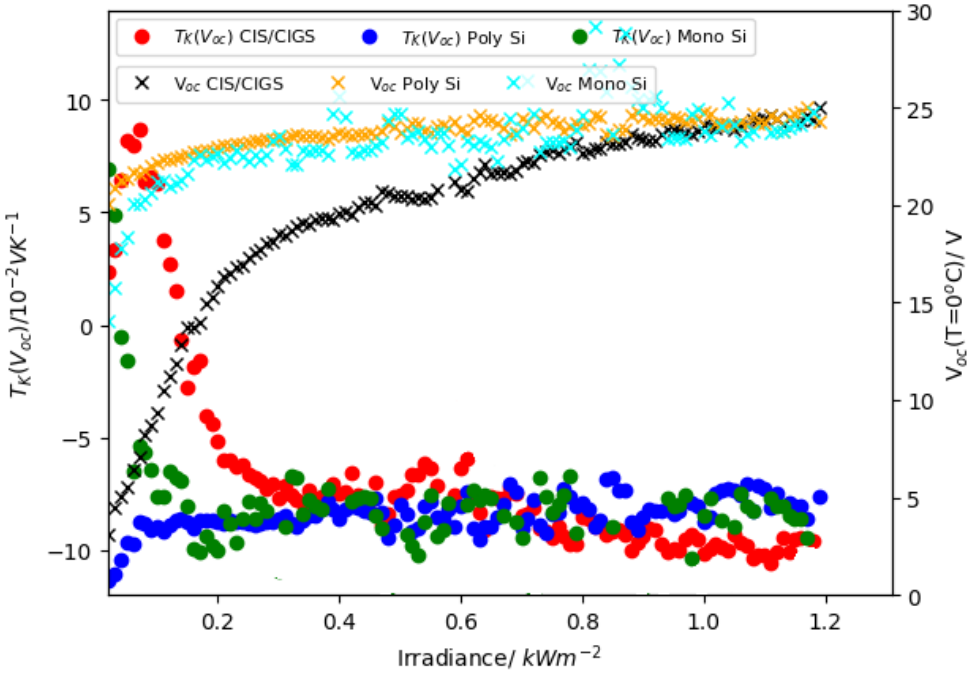

Figure 4.27: temperature coefficient of voltage, $T_k(V)$, irradiance graph

A positive value of $T_k(V)$ implies that for an increase in temperature there will be a increase in output current and a negative value implies that for an increase in temperature there will be a decrease in output current. Studying figure 4.27: CIS/CIGS has a large range of irradiance (S $<$ 200 Wm^{-2}) for which $T_k(V)$ is positive, monocrystalline technology has a much smaller range (S $<$ 80 Wm^{-2}) and $T_k(V)$ of polycrystalline technology is always negative. At high irradiance $|T_k(V)_{polycrystalline}| < |T_k(V)_{monocrystalline}| < |T_k(V)_{GIS/CIGS}|$ implying that there will be a larger decrease in Voltage for increase in temperature for CIS/CIGS and the polycrystalline shows the smallest decrease.

4.5 Variation of powers with temperature for fixed irradiance

From the collected data, the maximum power and ideal maximum power(=short circuit current * open circuit voltage) for each technology was extracted. Knowing the temperature of the boards, the data was sorted with respected to irradiance whereby a specific set of of current was plotted against temperature for a given irradiance S with a range of $\pm$ 10 Wm^{-2} about S. Figure 4.28 to figure 4.38 show several different graphs obtained:

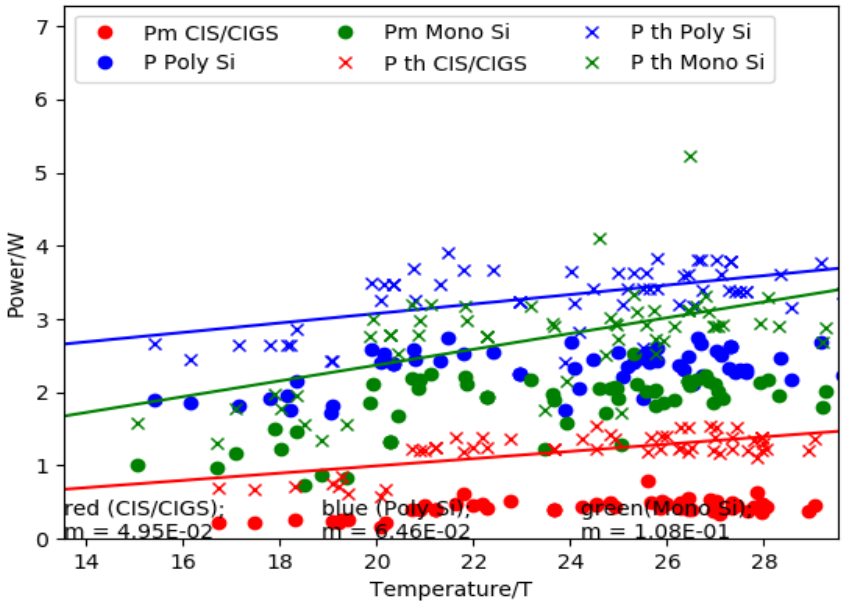

Figure 4.28: Power temperature graph at S=100W m^{-2}

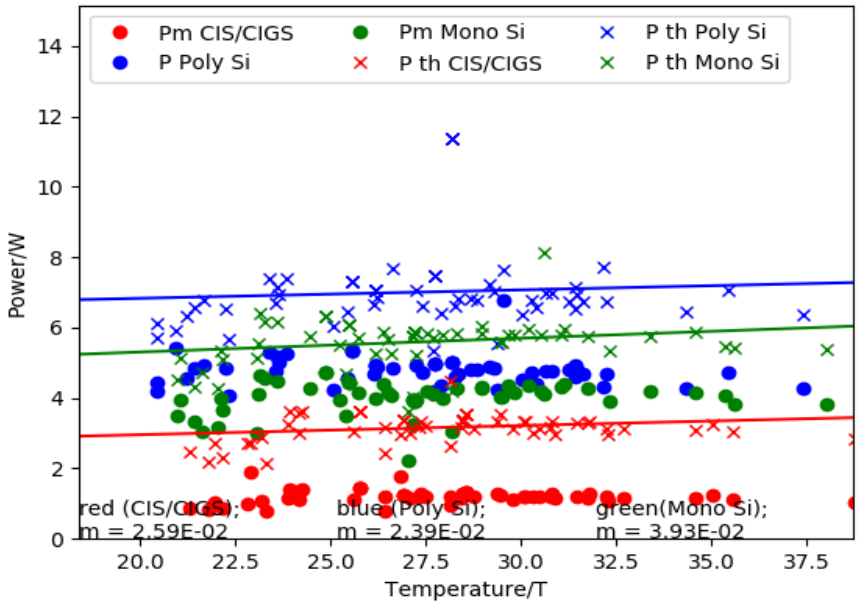

Figure 4.29: Power temperature graph at S=200W m^{-2}

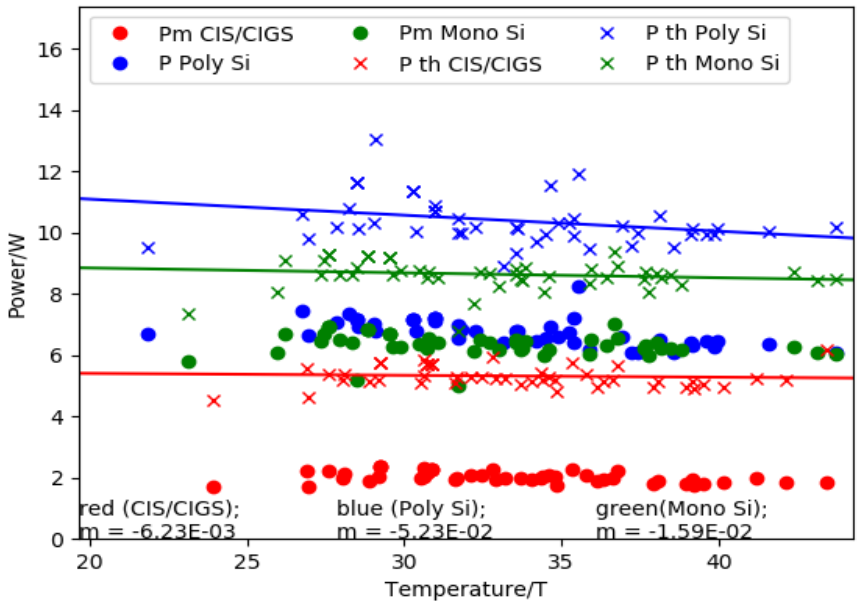

Figure 4.30: Power temperature graph at S=300W m^{-2}

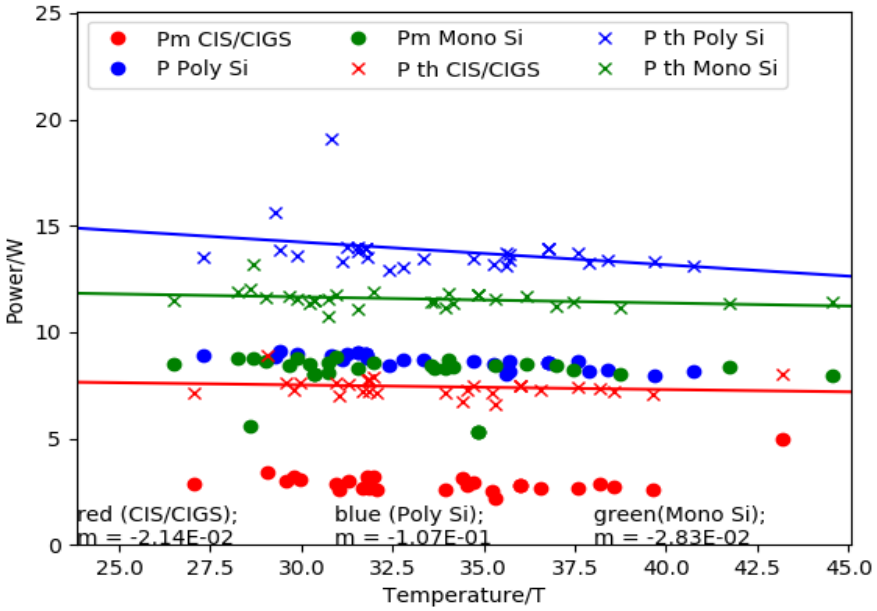

Figure 4.31: Power temperature graph at S=400W m^{-2}

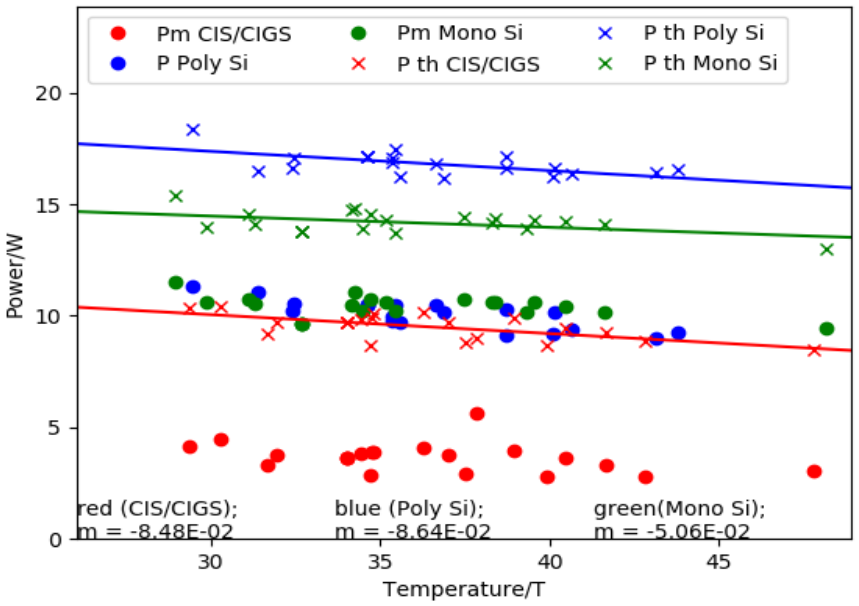

Figure 4.32: Power temperature graph at S=500W m^{-2}

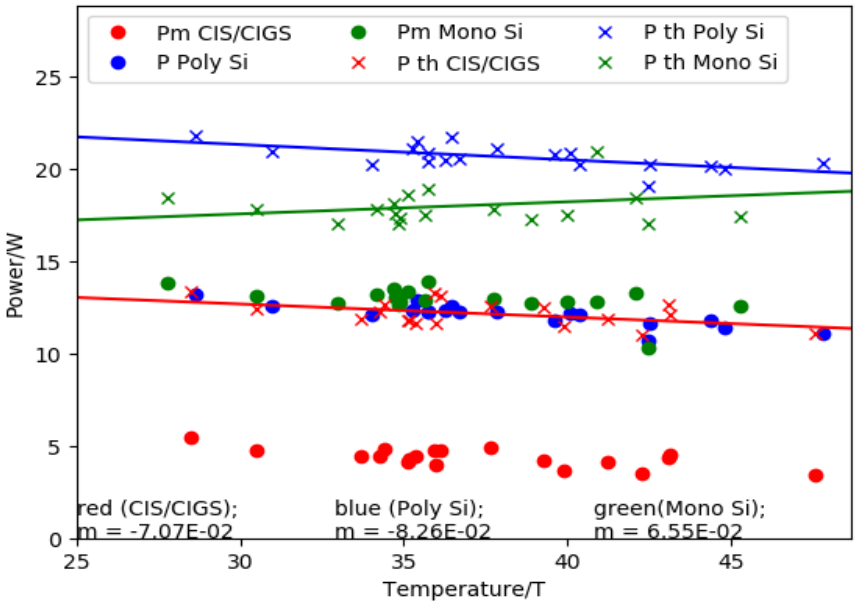

Figure 4.33: Power temperature graph at S=620W m^{-2}

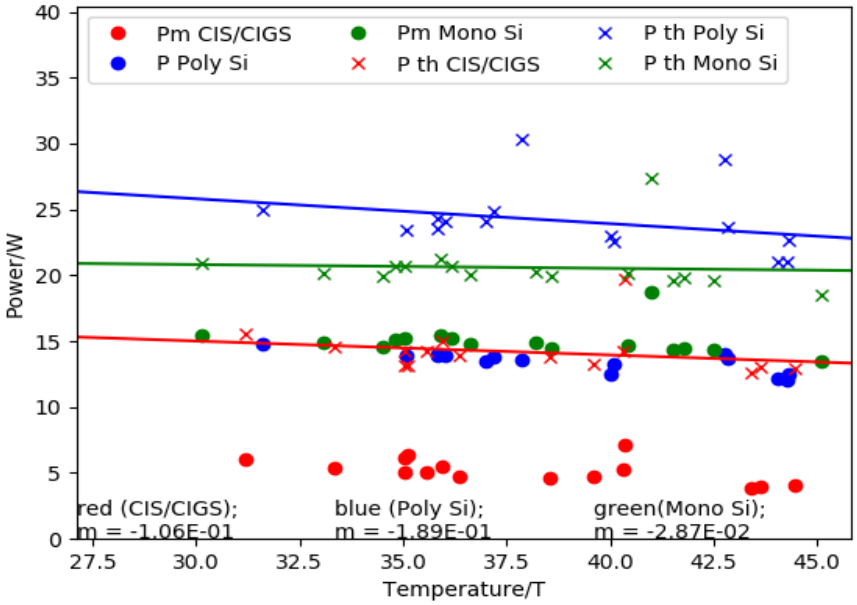

Figure 4.34: Power temperature graph at S=700W m^{-2}

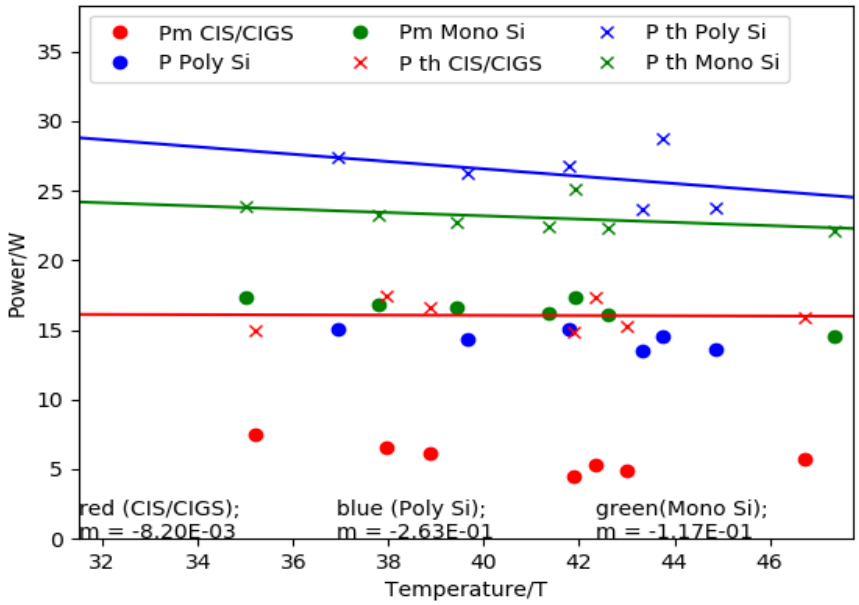

Figure 4.35: Power temperature graph at S=800W m^{-2}

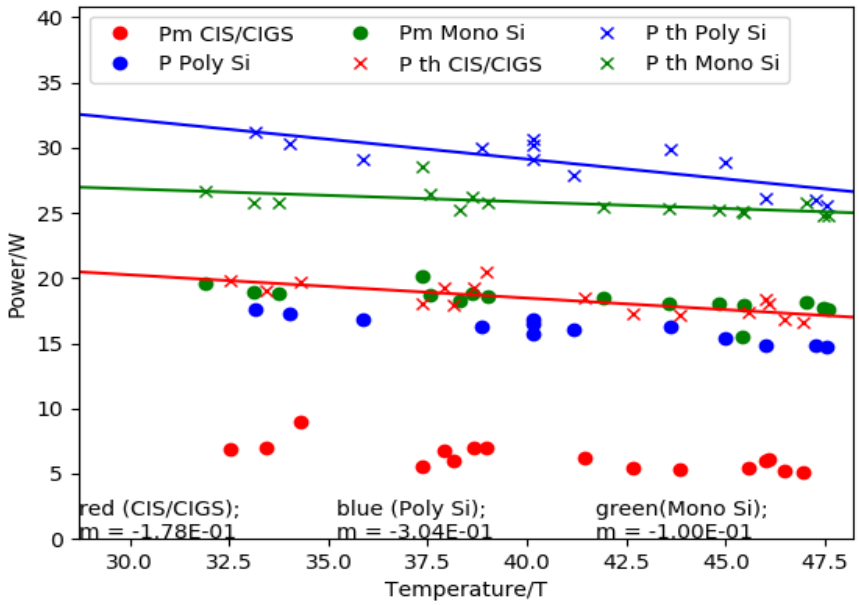

Figure 4.36: Power temperature graph at S=900W m^{-2}

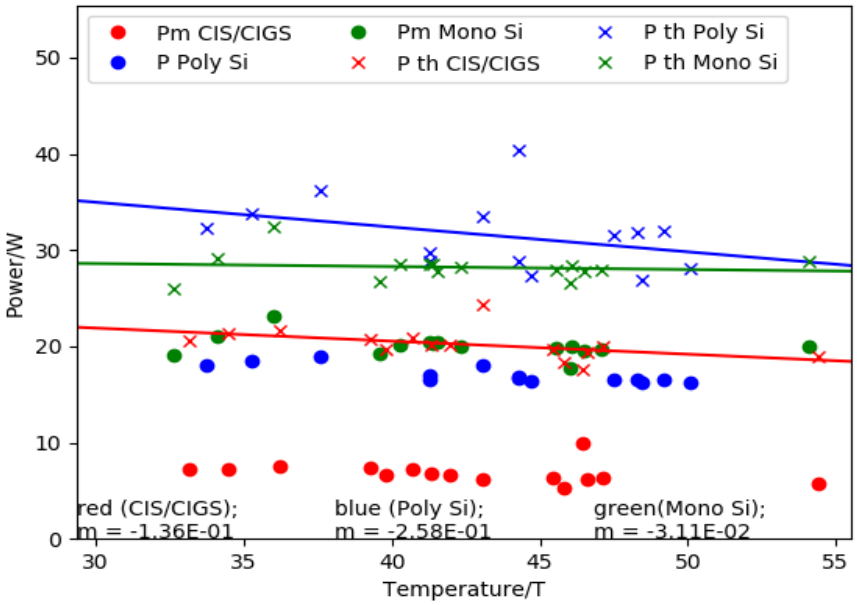

Figure 4.37: Power temperature graph at S=1000W m^{-2}

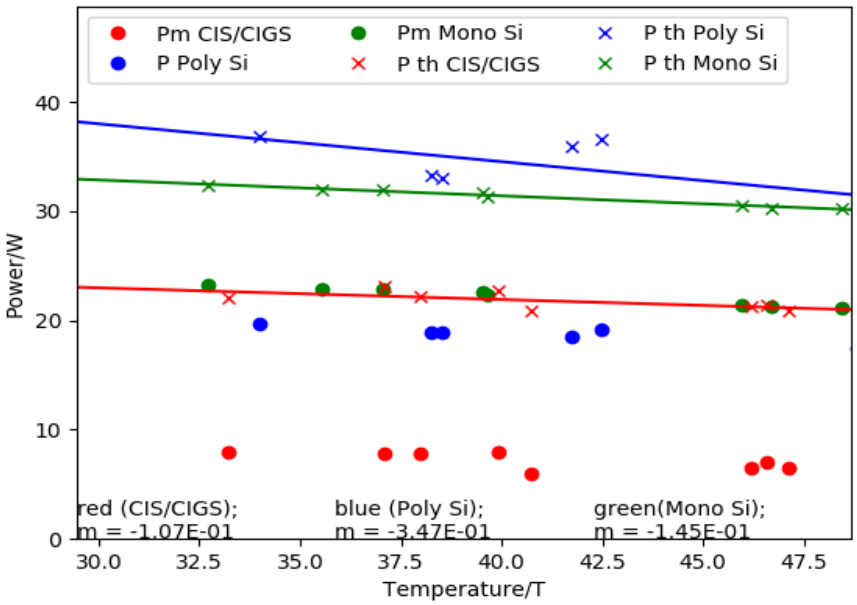

Figure 4.38: Power temperature graph at S=1100W m^{-2}

There exist a linear relationship between power and temperature. Thus the gradient of

the current temperature graph is defined as the temperature coefficient of power, $T_k(P)$, at the mentioned irradiance. A graph of temperature coefficient of power, $T_k(P)$, against irradiance was plotted to study its variation. The result is shown below in figure 4.39.

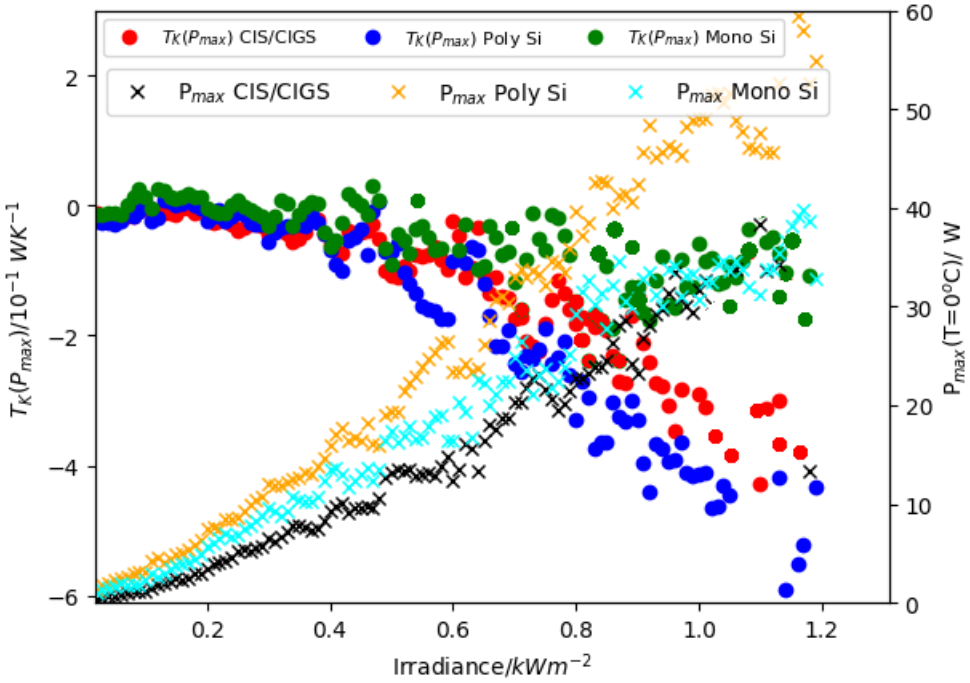

Figure 4.39: temperature coefficient of power, $T_k(P)$, irradiance graph

The behaviour of $T_k(P)$ for the three technologies is very similar to that of $T_k(I)$ with the only difference of$T_k(P)$ being three order of magnitude greater.

To get a better understanding of the effect of temperature at a fixed irradiance, the best fit lines at several irradiances were plotted and are shown in the figures 4.40 to 4.42 below.

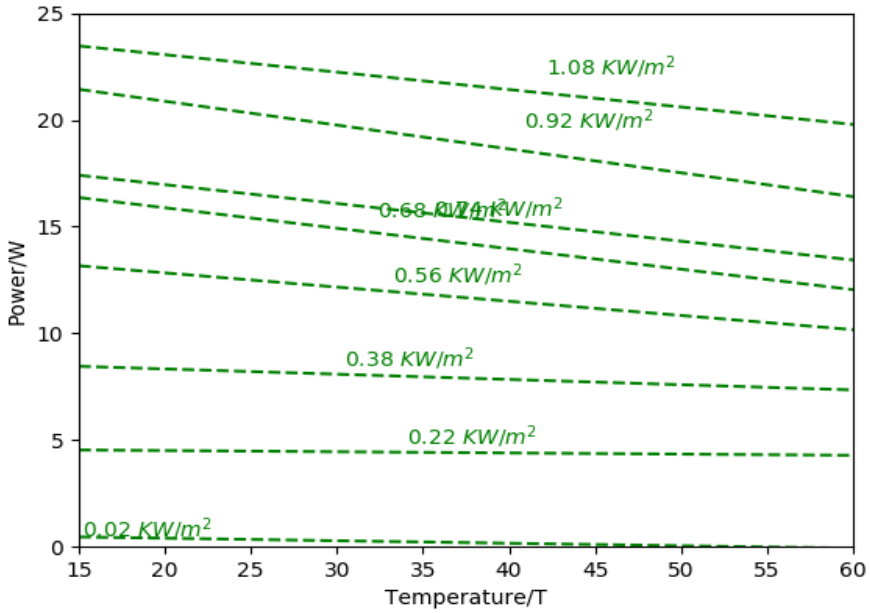

Figure 4.40: Effect of temperature on Mono-Si PV at various irradiance

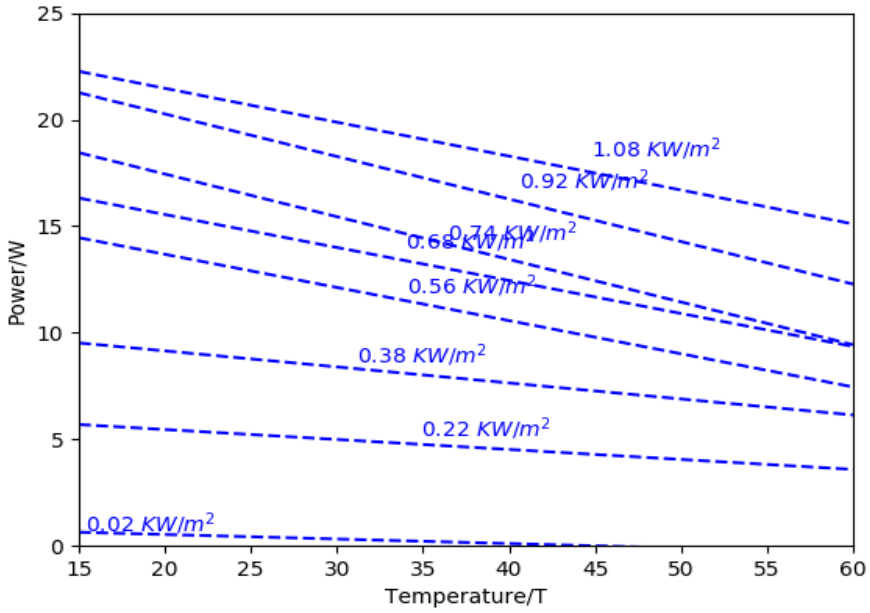

Figure 4.41: Effect of temperature on Poly-Si PV at various irradiance

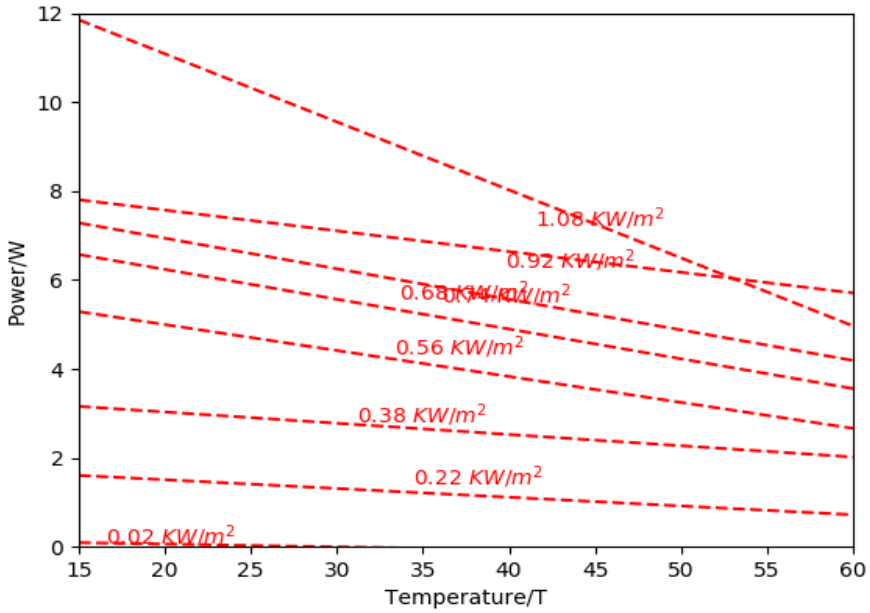

Figure 4.42: Effect of temperature on CIS/CIGS PV at various irradiance

Describing the power as a linear equation of the form Power=$T_k(S)$S+c(S), as expected, when irradiance increases output power also increases due to the constant c being a function of S and it increases rapidly with increase in S.

4.6 Variation of currents with irradiance for fixed temperature

Sorting the data with respect to the board temperatures, the maximum power point current and short circuit current were plotted against irradiance for a specific value of temperature T with a range of $\pm$ 0.5°C.Figure 4.43 to figure 4.49 show several different graphs obtained:

4.6 Variation of currents with irradiance for fixed temperature

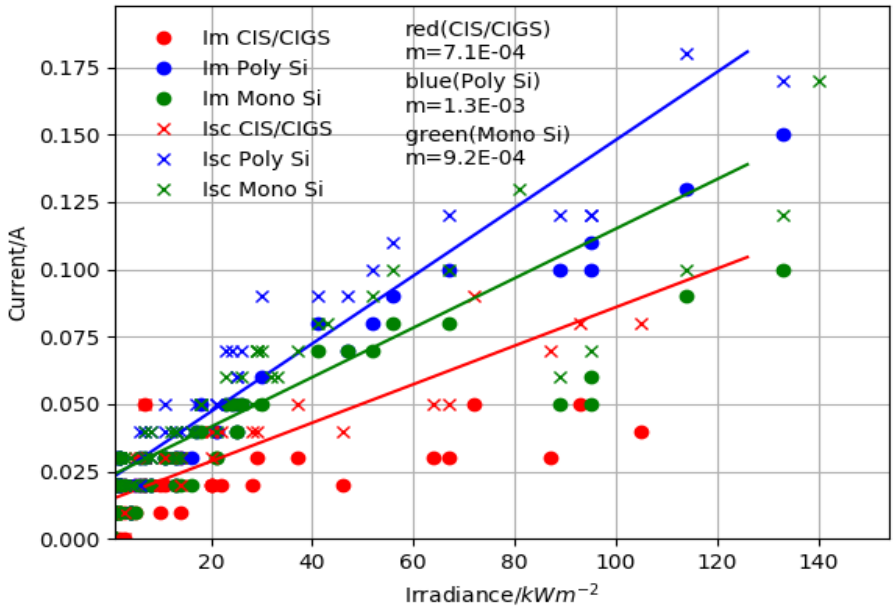

Figure 4.43: Current irradiance graph at T=20.1 $°C$

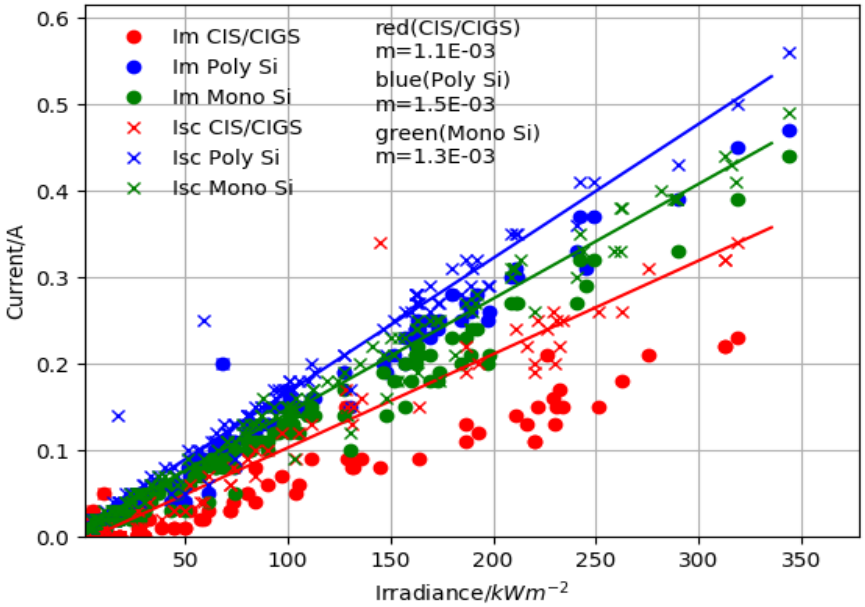

Figure 4.44: Current irradiance graph at T=25 $°C$

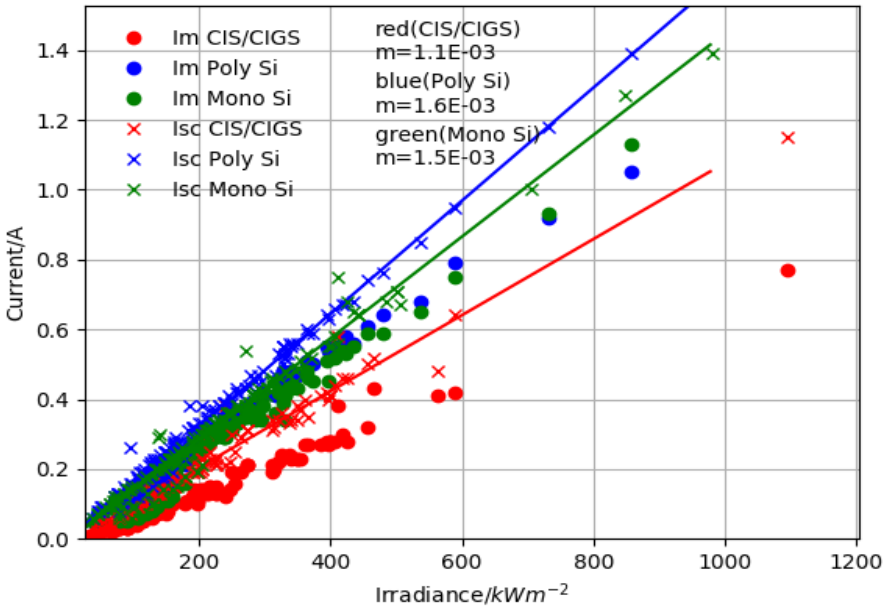

Figure 4.45: Current irradiance graph at T=30 $°C$

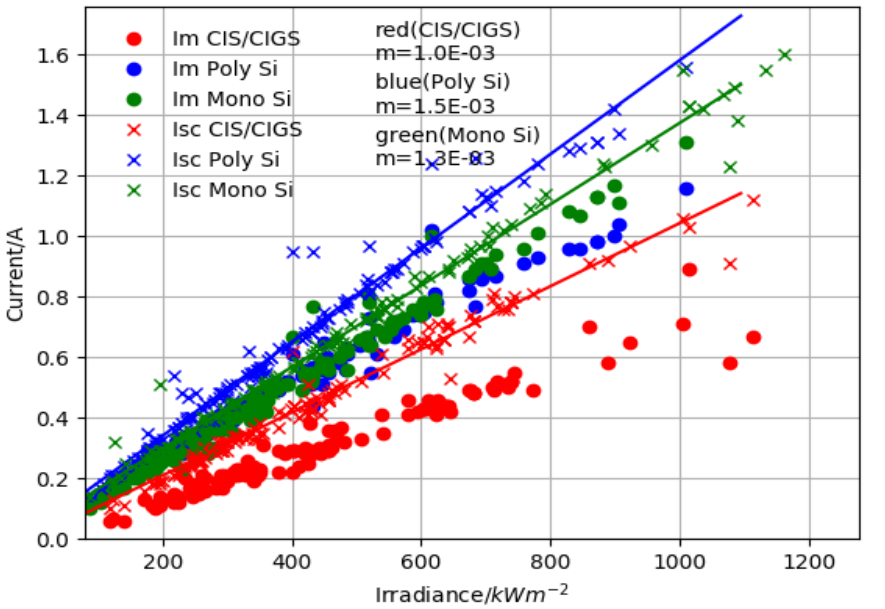

Figure 4.46: Current irradiance graph at T=35 $°C$

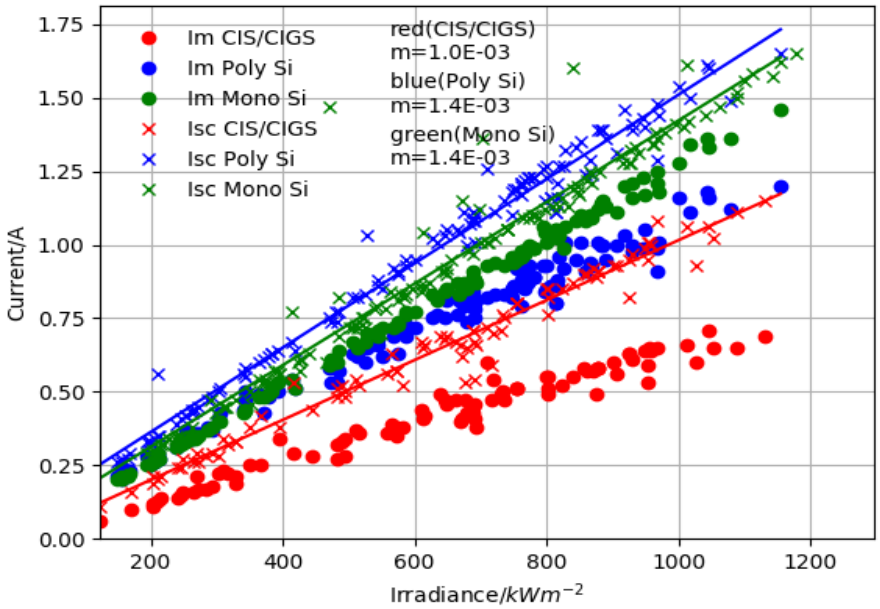

Figure 4.47: Current irradiance graph at T=40 $°C$

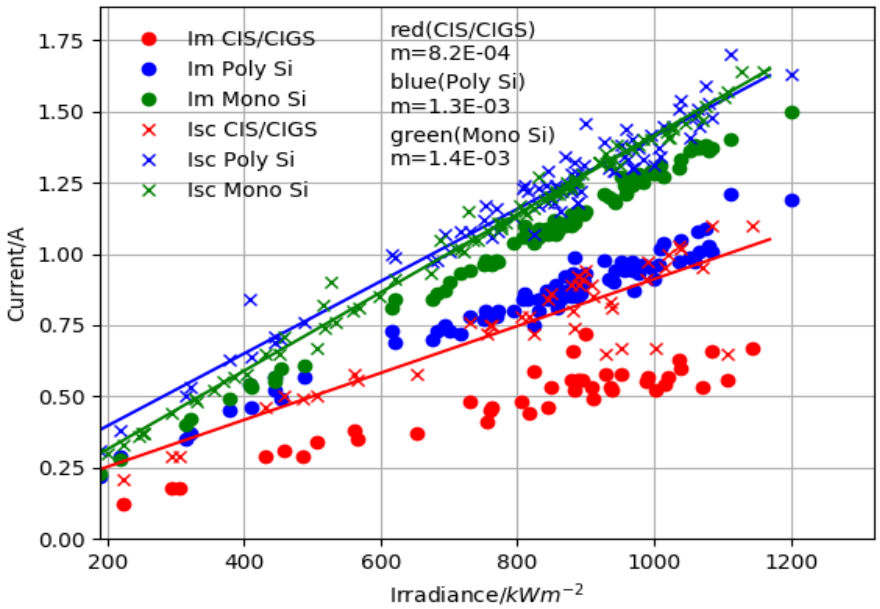

Figure 4.48: Current irradiance graph at T=45 $°C$

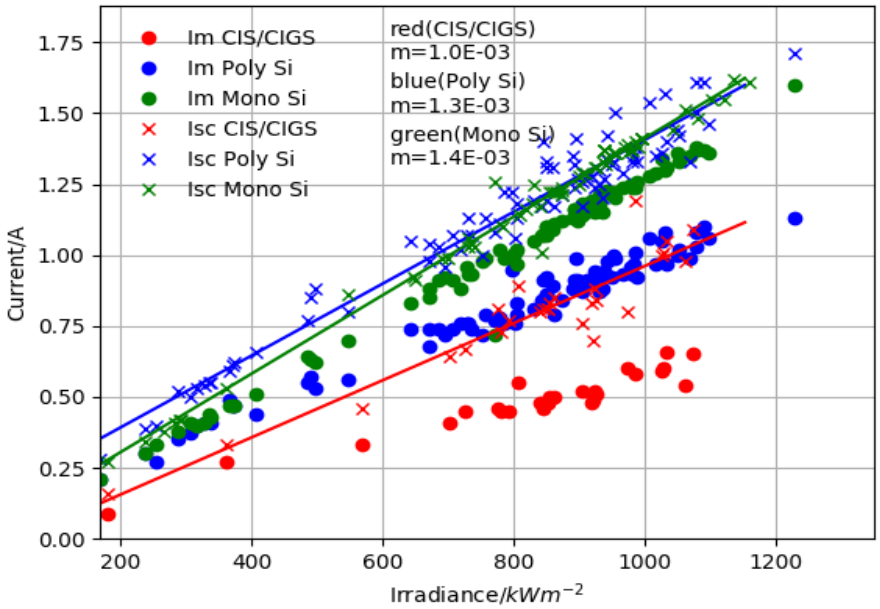

Figure 4.49: Current irradiance graph at T=50 $°C$

There exist a linear relationship between current and irradiance. Thus the gradient of the current irradiance graph is defined as the irradiance coefficient of current, $S_k(I)$, at the mentioned irradiance. A graph of irradiance coefficient of current, $S_k(I)$, against temperature was plotted to study its variation. The result is shown below in figure 4.50.

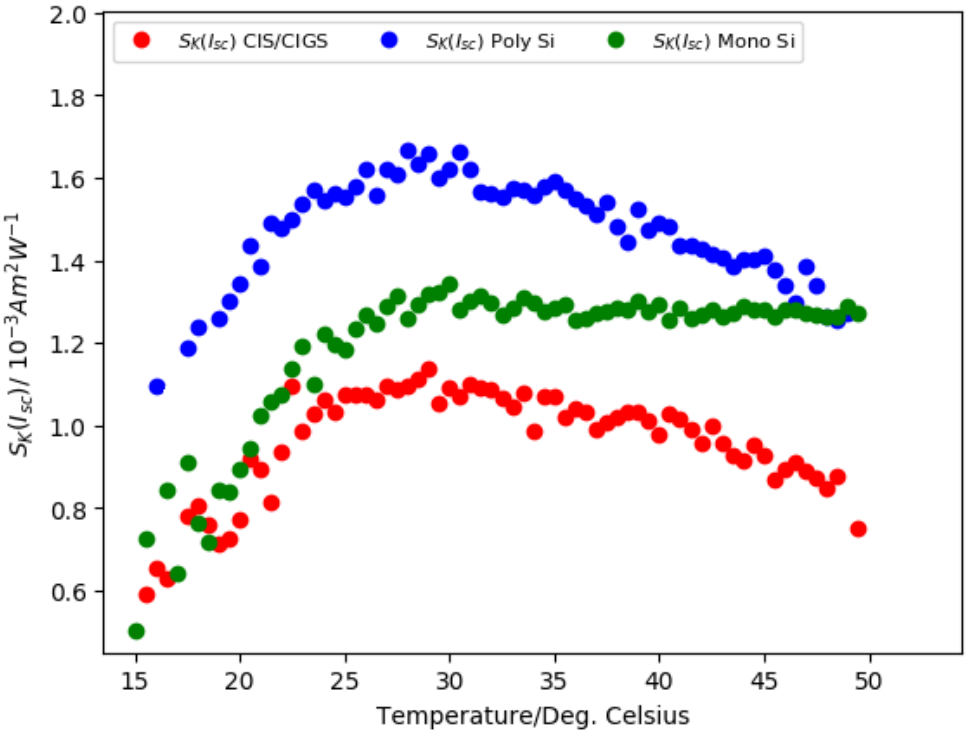

Figure 4.50: Irradiance coefficient of current, $S_k(I)$, temperature graph

The irradiance coefficient denotes the rate at which the studied property will change with a change in irradiance. A positive one implies that the property increases with an increase in irradiance coefficient and a negative one implies a decrease with an increase in irradiance coefficient. As expected $S_k(I)$ is always positive. For all three technologies at low temperature, as temperature is increased so does $S_k(I)$. And above a certain temperature (around 30 $°C4$) for monocrystalline PV cells $S_k(I)$ is almost constant whereas polycrystalline and CIS/CIGS there is a decrease in $S_k(I)$. Over the range of temperatures for which $S_k(I)$ is available $S_k(I)_{polycrystalline} > S_k(I)_{monocrystalline} > S_k(I)_{CIS/CIGS}$ implying that polycrystalline technology will exhibit a larger increase in current for a change in irradiance at a specific temperature as compared to the two other technologies.

4.7 Variation of voltages with irradiance for fixed temperature

Sorting the data with respect to the board temperatures, the maximum power point voltage and open circuit voltage for each technology were plotted against irradiance for a specific value of temperature T with a range of $\pm$ 0.5°C.Figure 4.51 to figure 4.57 show several different graphs obtained:

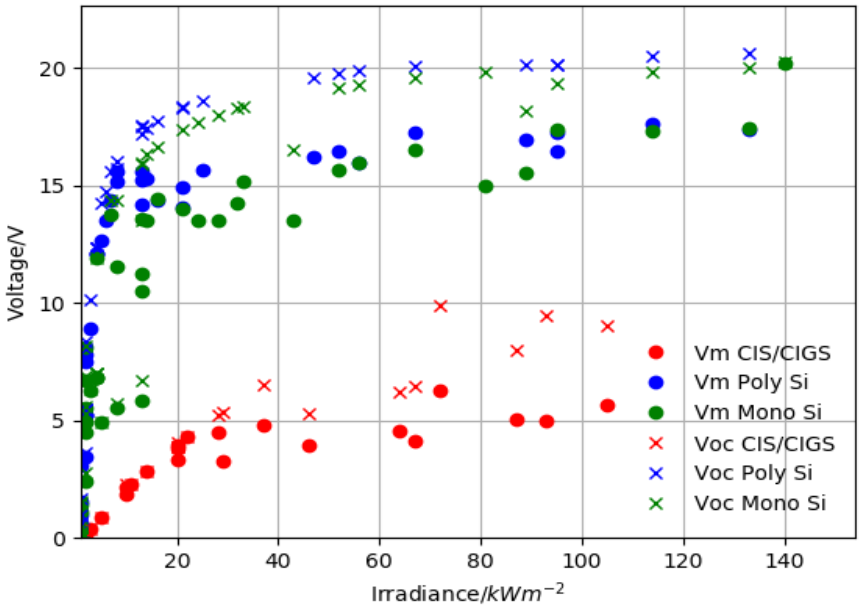

Figure 4.51: Voltage irradiance graph at T=20.1 °C

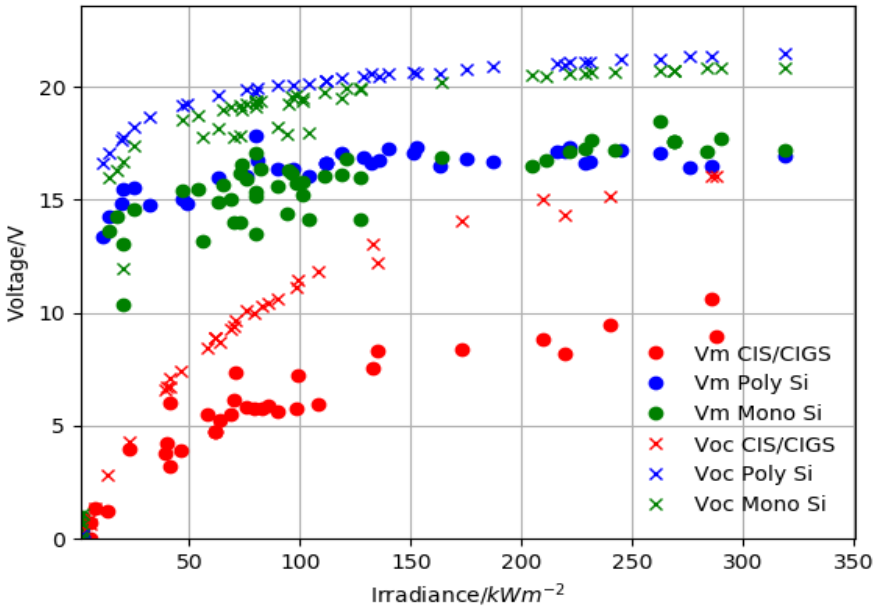

Figure 4.52: Voltage irradiance graph at T=25 $°C$

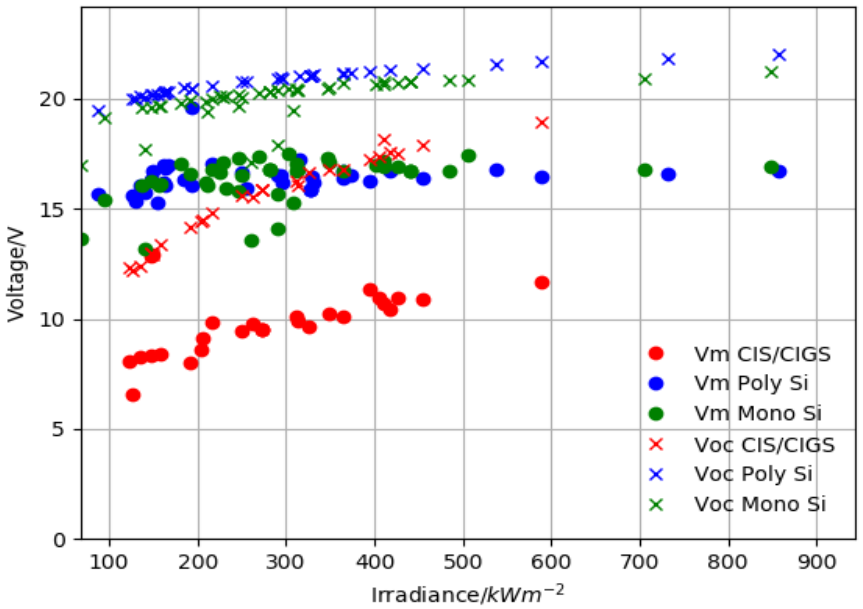

Figure 4.53: Voltage irradiance graph at T=30 $°C$

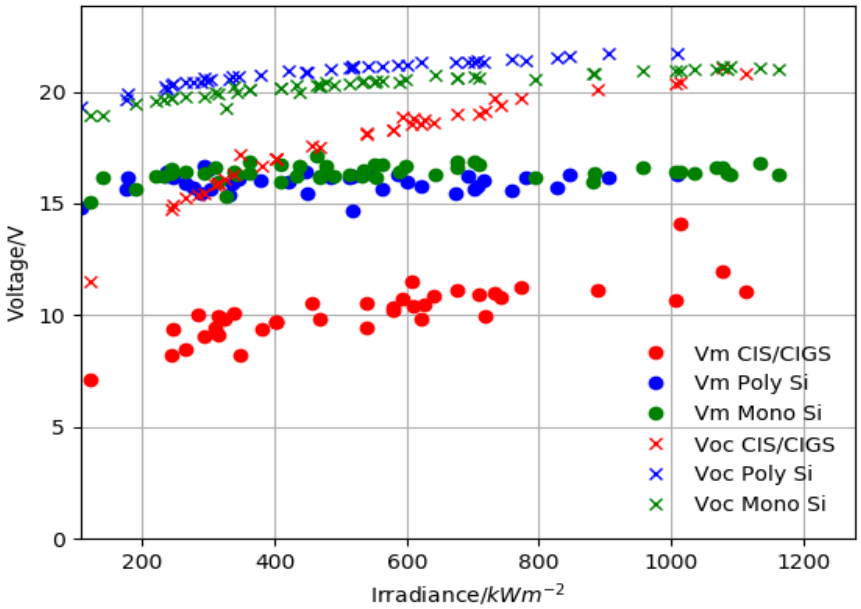

Figure 4.54: Voltage irradiance graph at T=35 $°C$

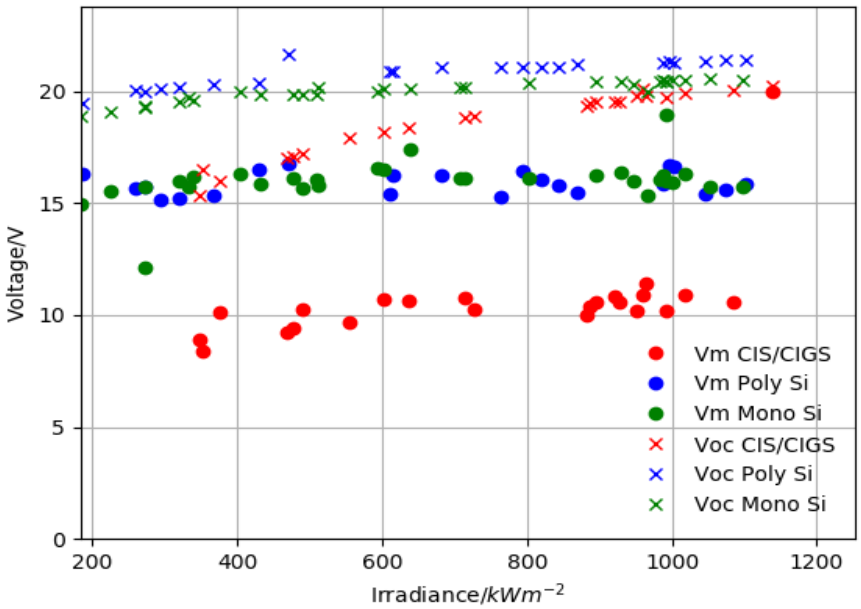

Figure 4.55: Voltage irradiance graph at T=40 $°C$

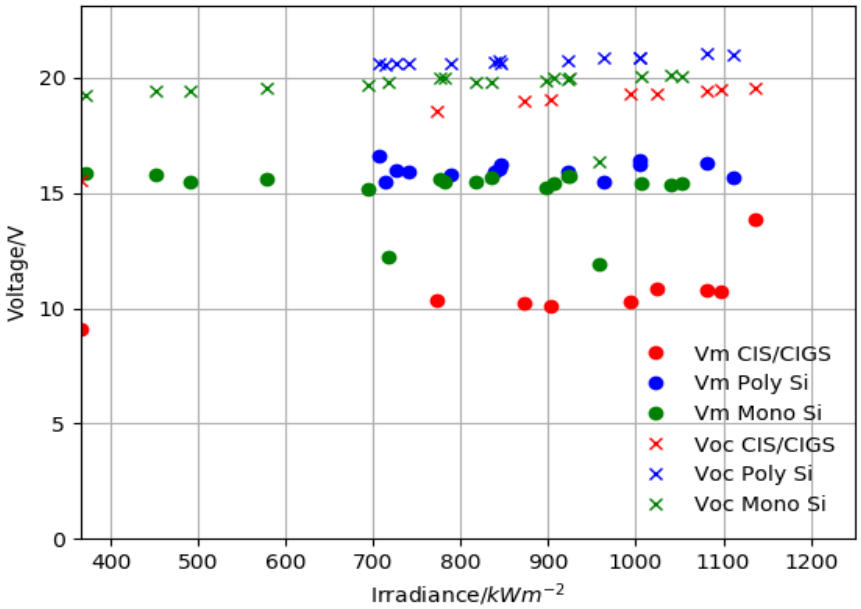

Figure 4.56: Voltage irradiance graph at T=45 $°C$

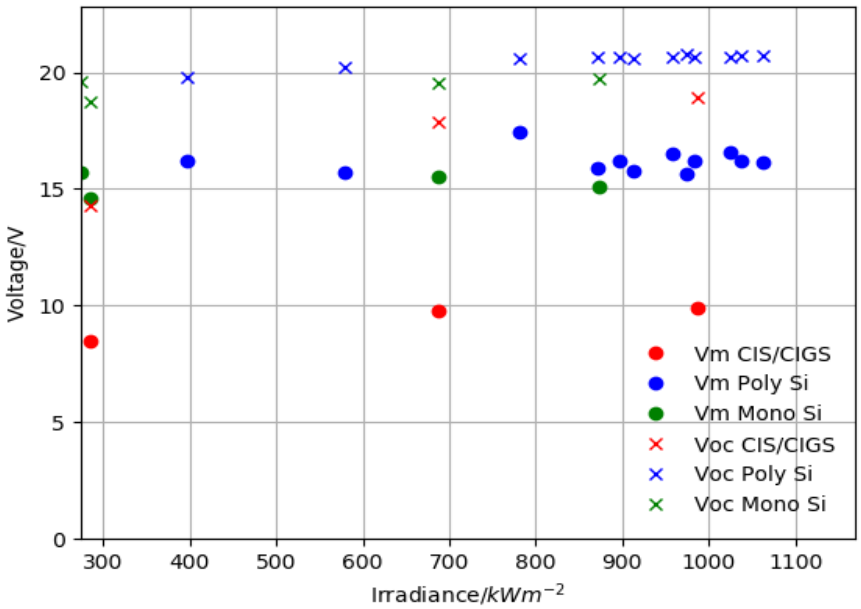

Figure 4.57: Voltage irradiance graph at T=50 $°C$

There does not exist a linear relationship between voltage and irradiance at a specific

temperature. Thus irradiance coefficient of voltage is not defined because at a given temperature it will not have a single value but will rather be a function of irradiance.

For a given temperature, at very low irradiance there is a rapid increase of voltage with an increase in irradiance then the rate of increase of voltage with irradiance at high irradiance is much smaller. This is an expected behaviour as small irradiance can lead to high open circuit voltages, for instance during the full moon the open circuit voltage of large PV systems is potentially lethal.

4.8 Variation of power with irradiance for fixed temperature

The maximum power and ideal maximum power(=short circuit current * open circuit voltage) for each technology were plotted against irradiance for a specific value of temperature T with a range of $\pm$ 0.5°C.Figure 4.58 to figure 4.64 show several different graphs obtained:

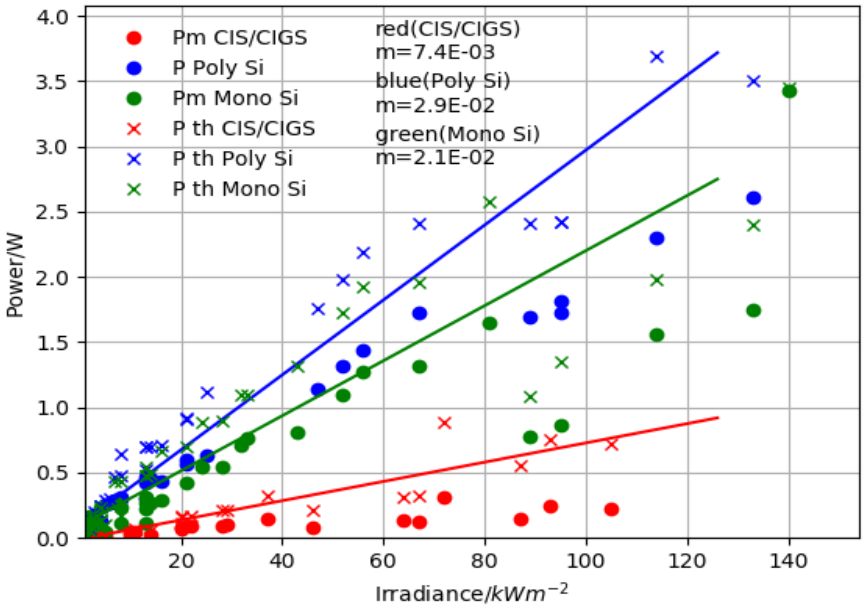

Figure 4.58: Current irradiance graph at T=20.1 °C

4.8 Variation of power with irradiance for fixed temperature

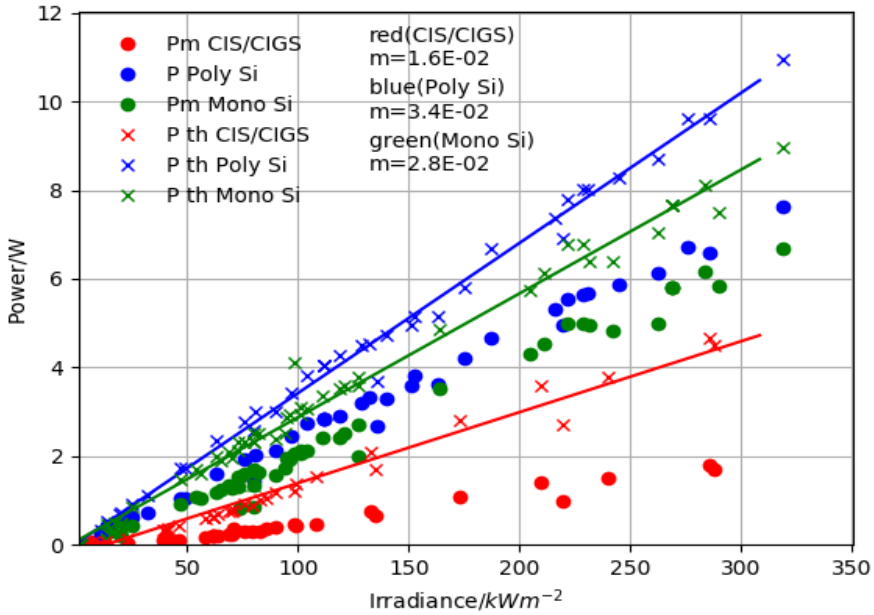

Figure 4.59: Current irradiance graph at T=25 $°C$

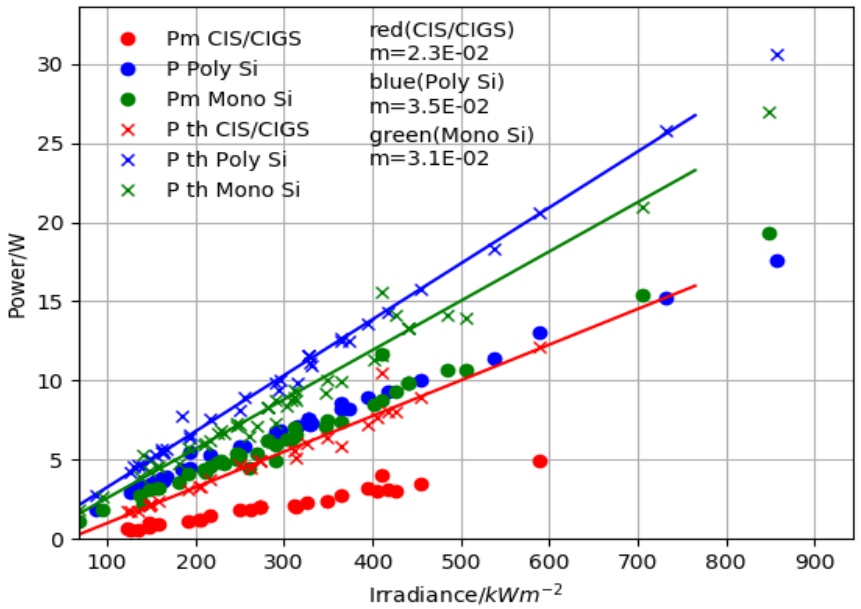

Figure 4.60: Current irradiance graph at T=30 $°C$

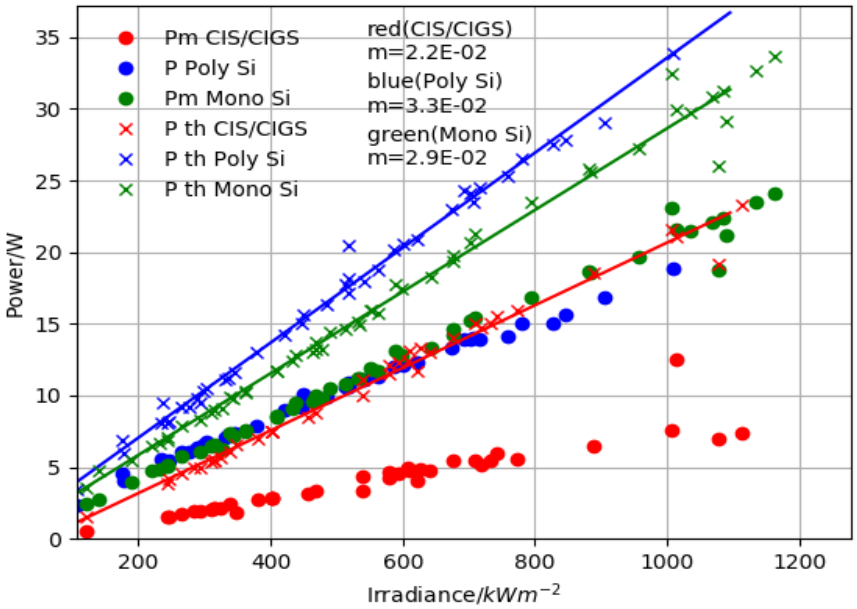

Figure 4.61: Current irradiance graph at T=35 $°C$

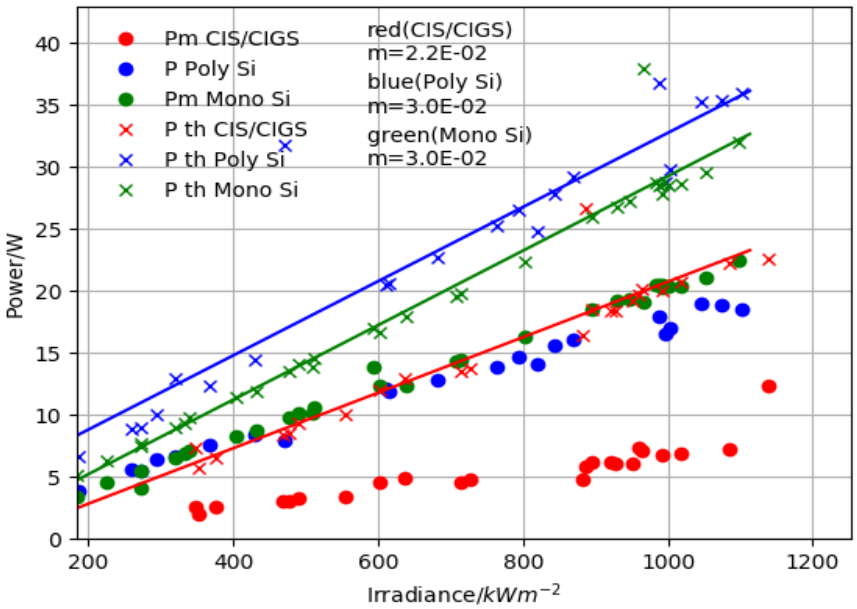

Figure 4.62: Current irradiance graph at T=40 $°C$

4.8 Variation of power with irradiance for fixed temperature

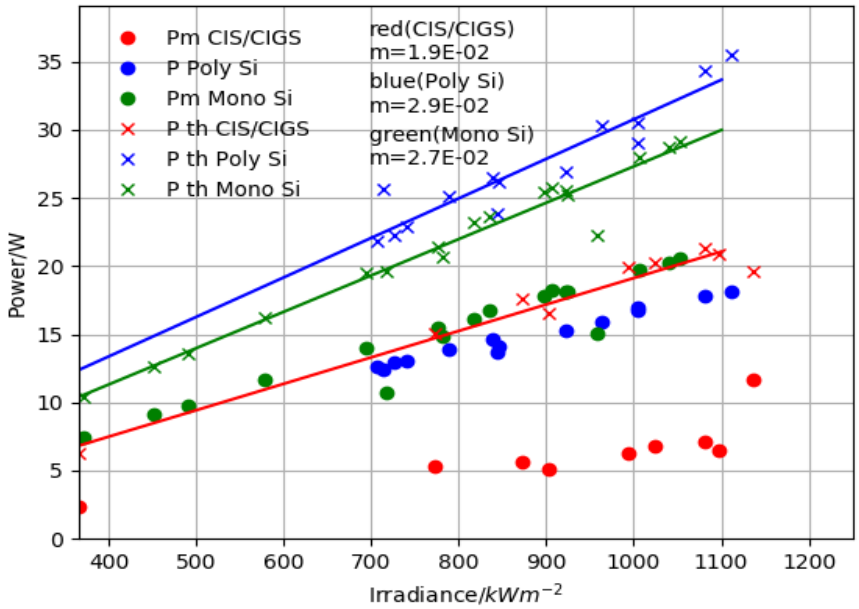

Figure 4.63: Current irradiance graph at T=45 $°C$

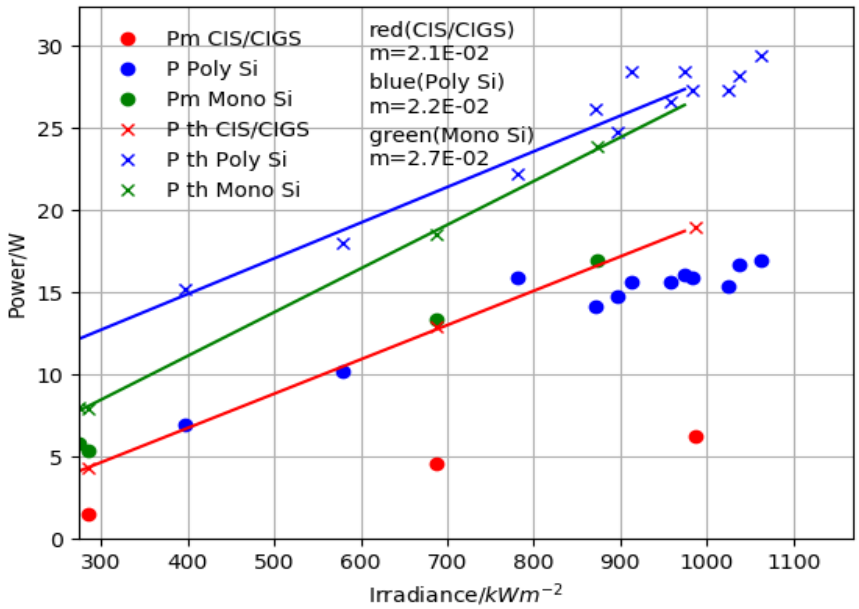

Figure 4.64: Current irradiance graph at T=50 $°C$

There exist a linear relationship between power and temperature. Thus the gradient

of the current temperature graph is defined as the irradiance coefficient of power, $S_k(P)$, at the mentioned irradiance. A graph of irradiance coefficient of current, $S_k(P)$, against temperature was plotted to study its variation. The result is shown below in figure 4.65.

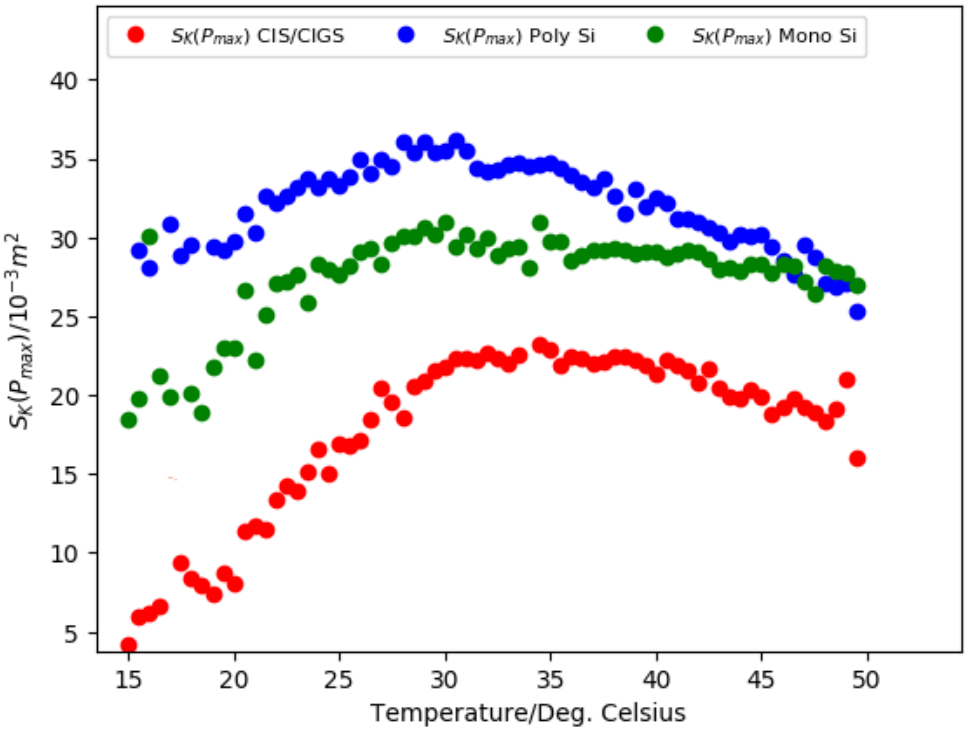

Figure 4.65: Irradiance coefficient of power, $S_k(P)$, temperature graph

The behaviour of the irradiance coefficient of power, $S_k(P)$, is very similar to that of the behaviour of the irradiance coefficient of current, $S_k(I)$.

4.9 Variation of internal parameters of PV cells

From the one diode model used, the various parameters were computed and are shown in the figures below.

4.9.1 Variation of shunt resistance with temperature at fixed irradiance

Considering that higher quality cells have larger shunt resistance, and decrease in shunt resistance leads to a decreased performance. A general trend can be seen that as temperature increases shunt resistance decreases, which can be interpreted in the sense that increase in temperature leads to a decreased performance when analyzing shunt resistance.

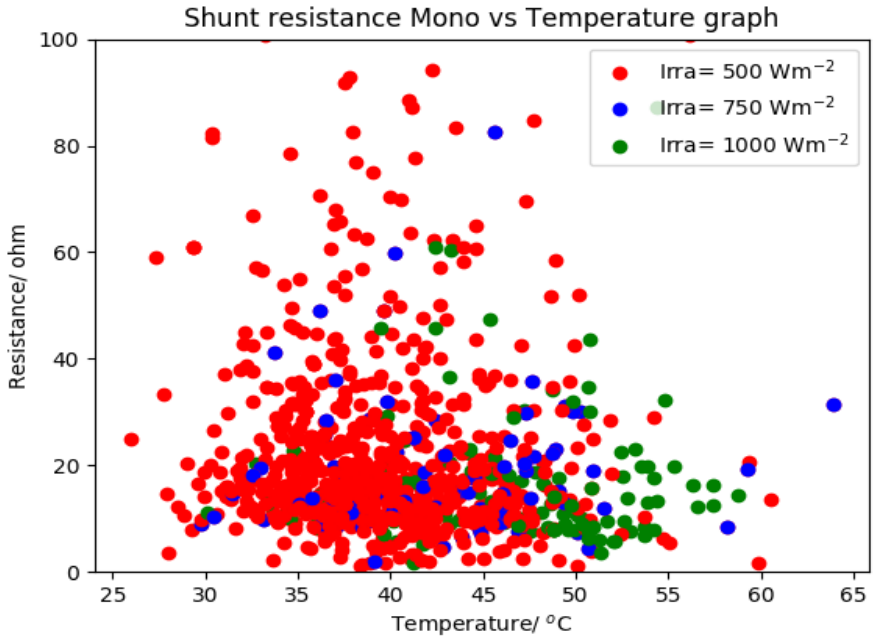

Figure 4.66: Variation of shunt resistance of Mono-Si cell

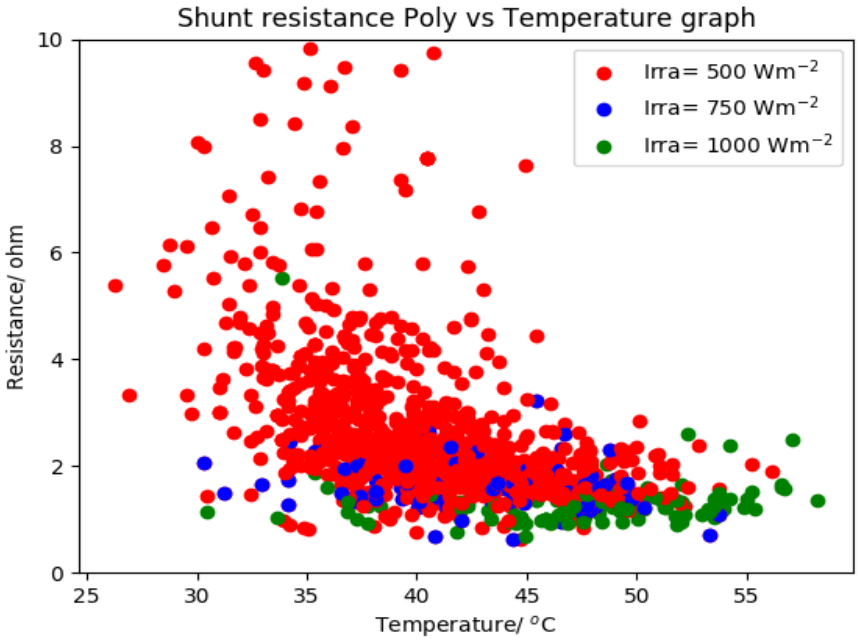

Figure 4.67: Variation of shunt resistance of Poly-Si cell

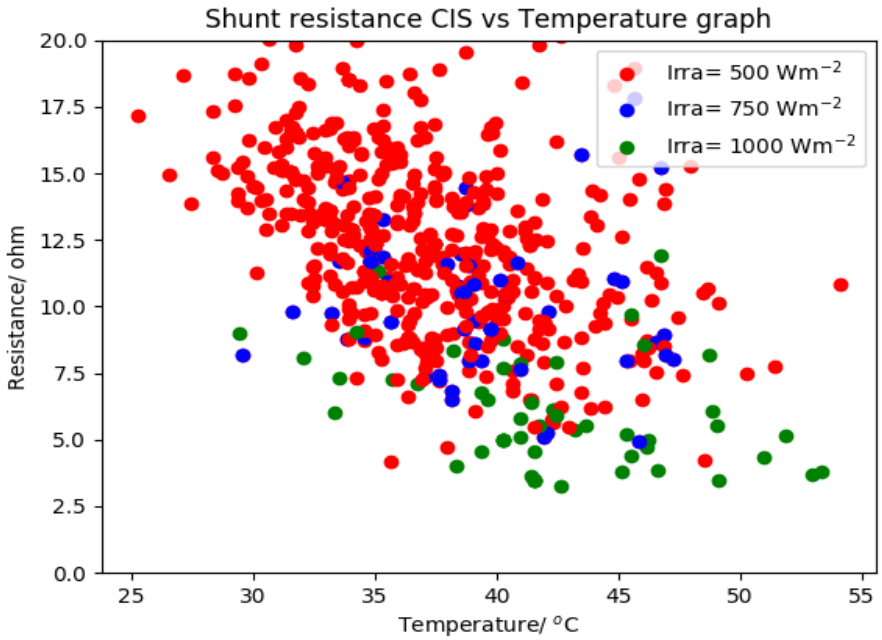

Figure 4.68: Variation of shunt resistance of CIS/CIGS cell

4.9.2 Variation of series resistance with temperature at fixed irradiance

From a performance point of view a decrease in series resistance results in an increased efficiency. On studying the variation of series resistance of Mono-Si, the series resistance may be considered independent of temperature and no general trend can be observed in Poly-Si and CIS/CIGS. Thus only shunt resistance is affected by temperature and thus increase in temperature results in a decrease in efficiency.

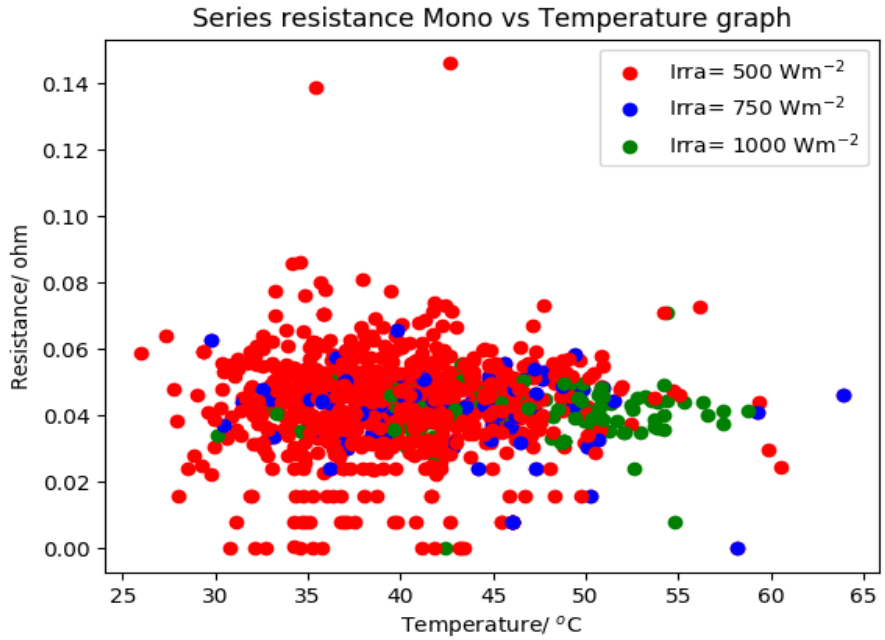

Figure 4.69: Variation of series resistance of Mono-Si cell

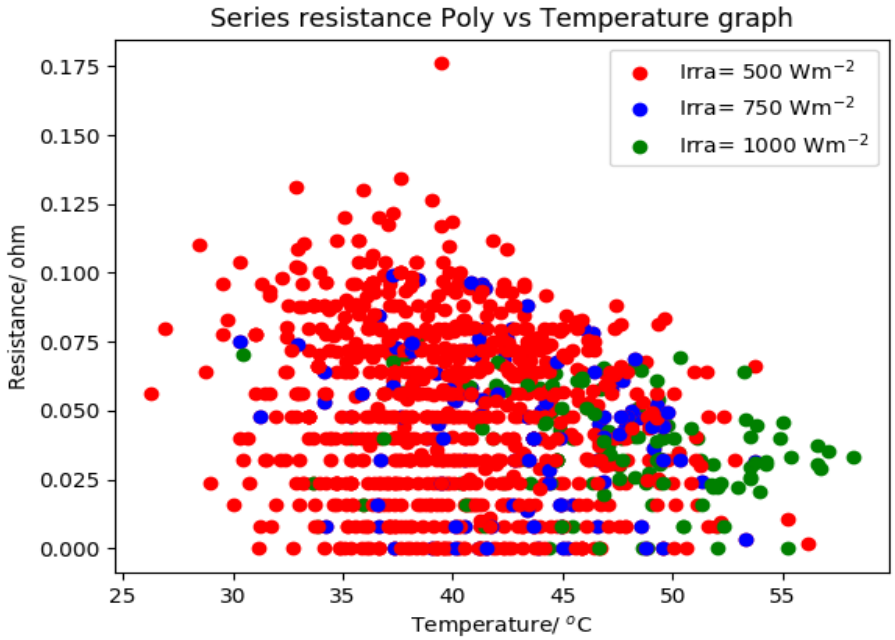

Figure 4.70: Variation of series resistance of Poly-Si cell

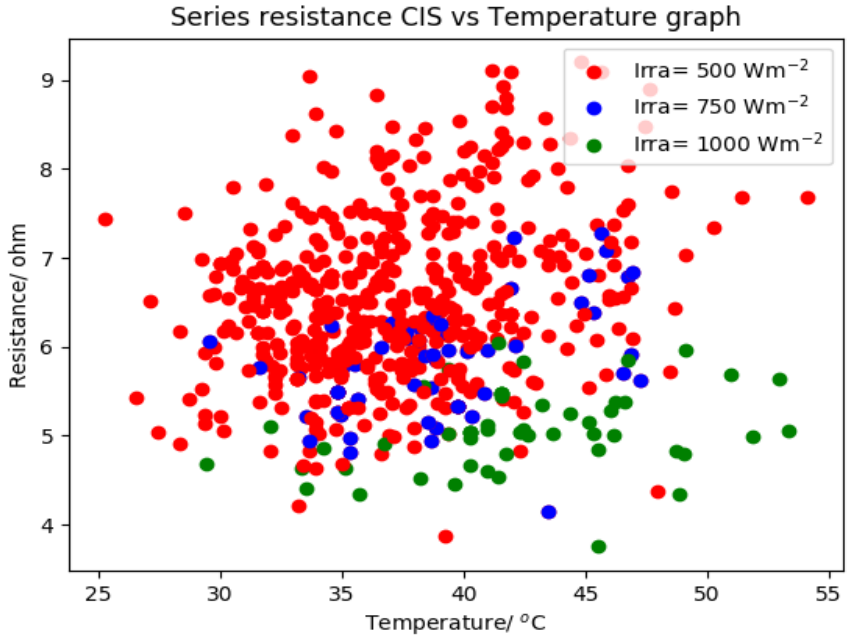

Figure 4.71: Variation of series resistance of CIS/CIGS cell

4.9.3 Variation of shunt resistance with irradiance at fixed temperature

From figure 4.72 to 4.74, it may be observed that the shunt resistance decreases with an increase in irradiance. As for all three temperature the points are scattered within the same range this supports the hypothesis that temperature has little impact in shunt resistance. Also regarding efficiency, an increase in irradiance causes a decrease in shunt resistance which in turn contribute to decrease efficiency.

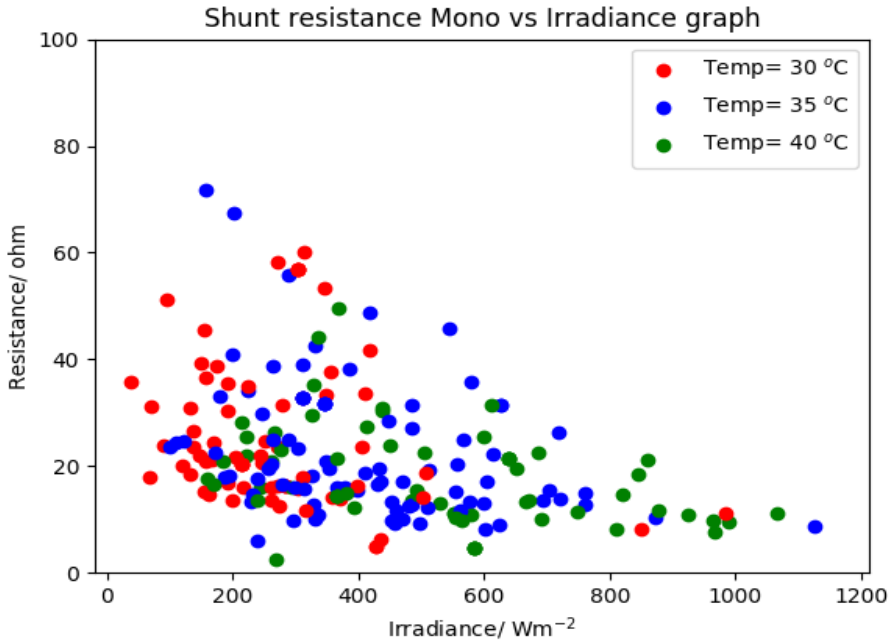

Figure 4.72: Variation of shunt resistance of Mono-Si cell

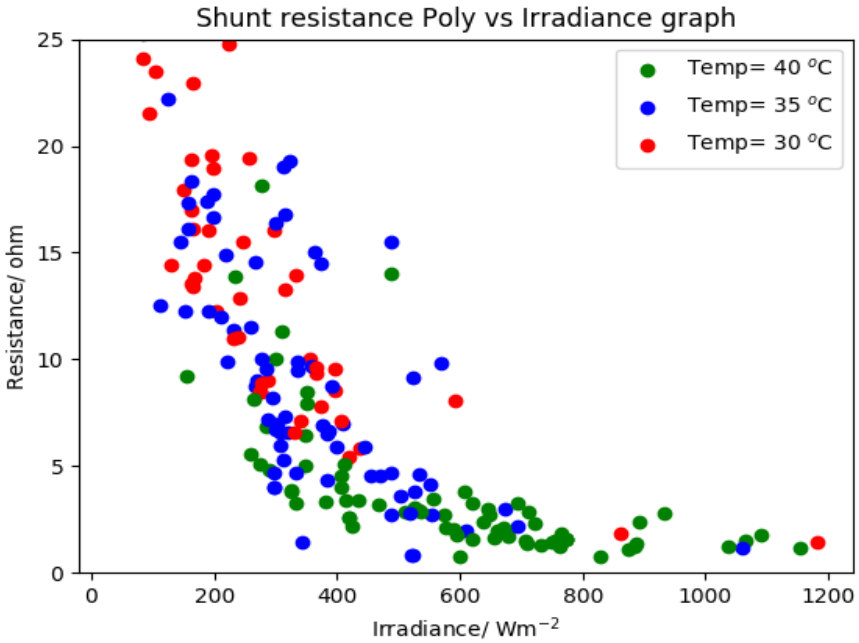

Figure 4.73: Variation of shunt resistance of Poly-Si cell

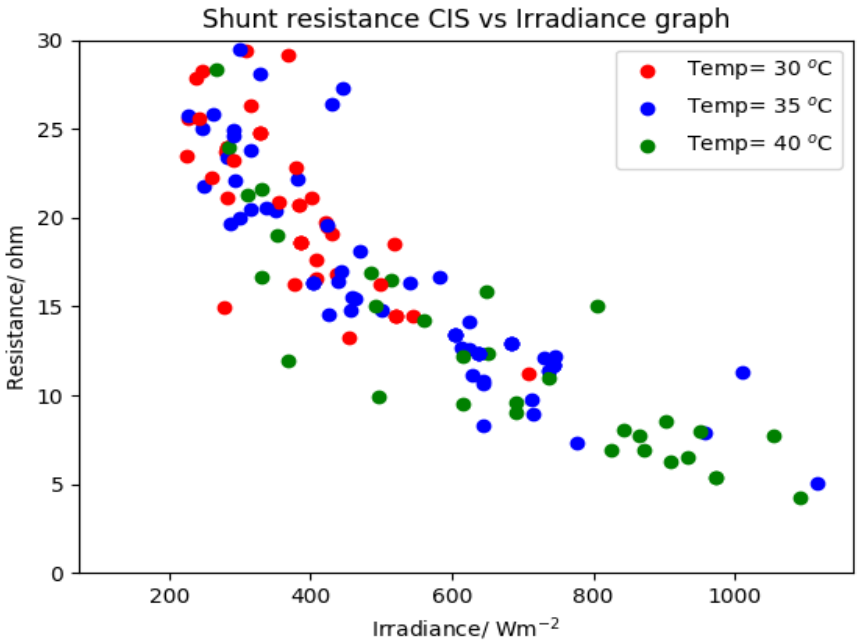

Figure 4.74: Variation of shunt resistance of CIS/CIGS cell

4.9.4 Variation of series resistance with irradiance at fixed temperature

Variation of series resistance exhibit the same behaviour as the shunt resistance with respect to variation of irradiance. Thus the general trend would suggest that the efficiency of the PV cell decreases with increase in irradiance.

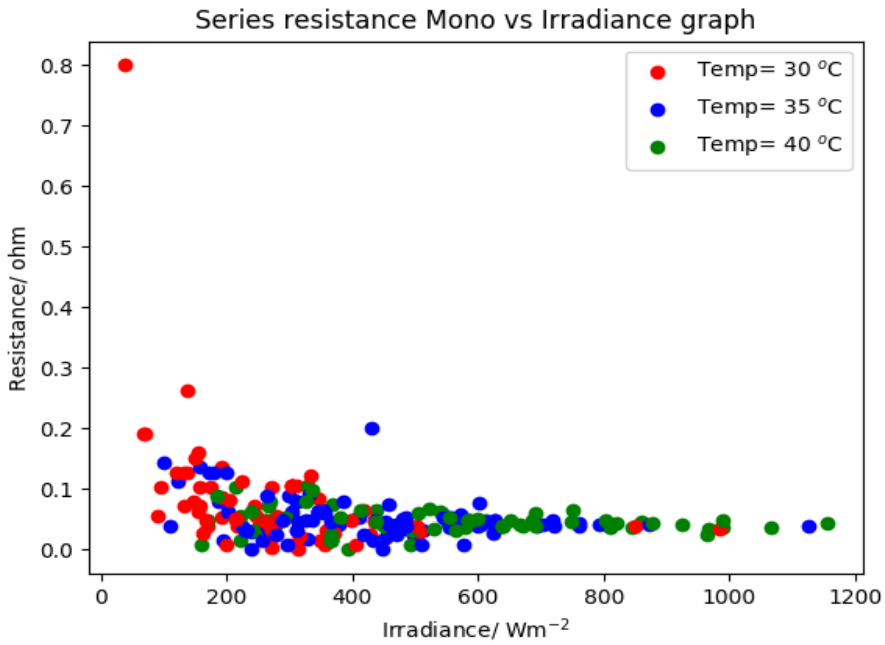

Figure 4.75: Variation of series resistance of Mono-Si cell

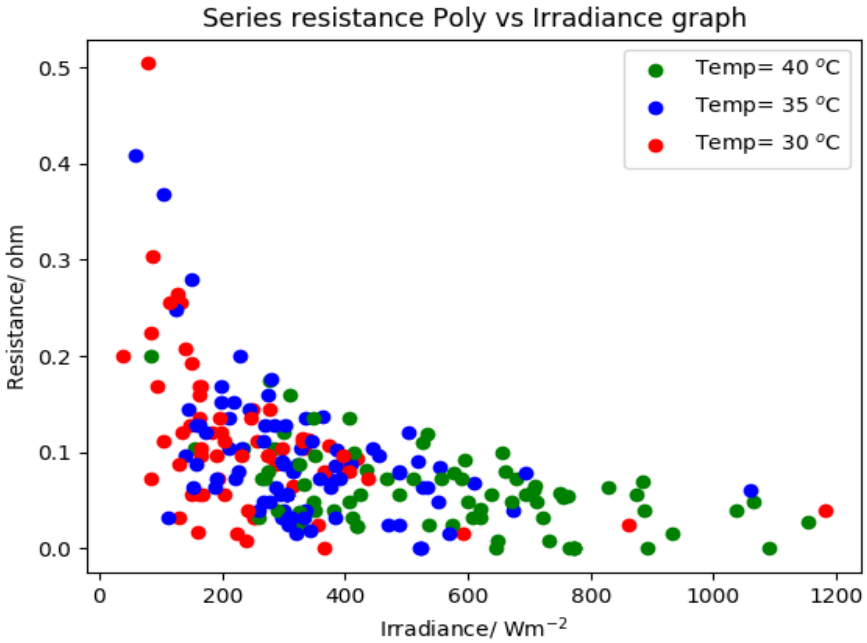

Figure 4.76: Variation of series resistance of Poly-Si cell

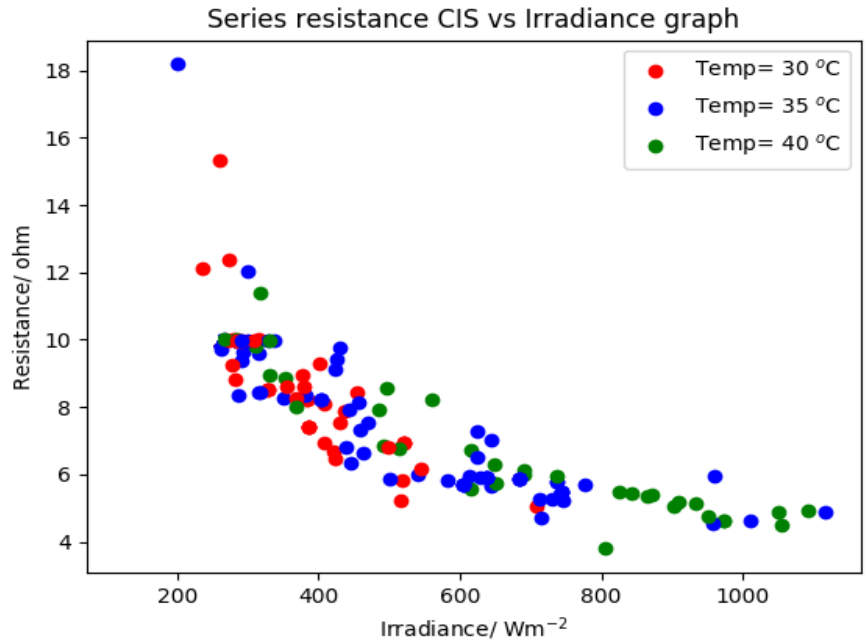

Figure 4.77: Variation of series resistance of CIS/CIGS cell

4.10 Normalised energy received and converted daily

Using equation 2.4 the amount of energy incident on the location under study was computed and is displayed on figure 4.78 below. It can be seen that the insolation peaks at around 6.5 $kWhm^{-2}$ and has a minimum of around 1.2 $kWhm^{-2}$. From such graph it can be concluded that the location has a good solar potential but also the intermittent nature of solar energy is clearly visible.

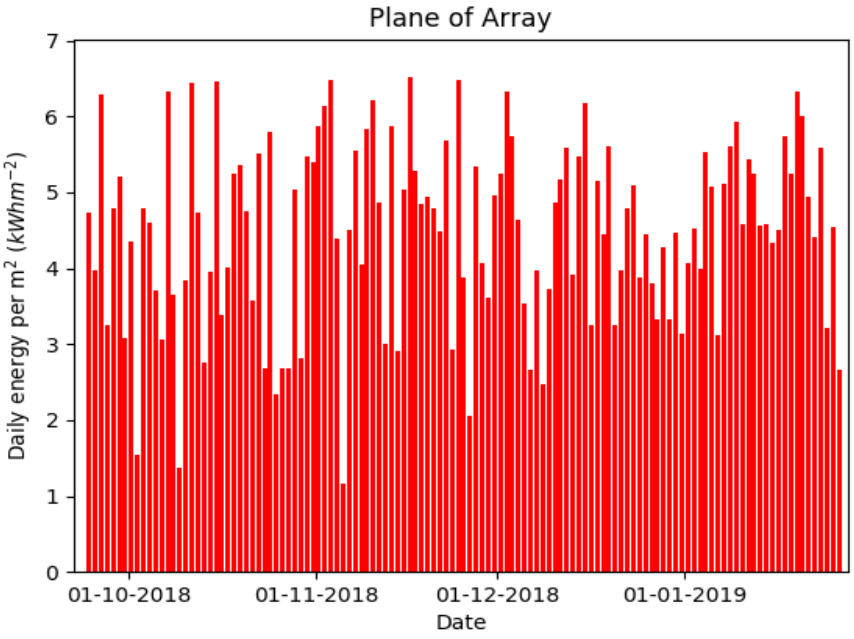

Figure 4.78: Amount of energy received in a day per m^2 on site of study

The energy converted from the PV panels was computed and plotted against energy incident on them. The result is shown in figure 4.79.

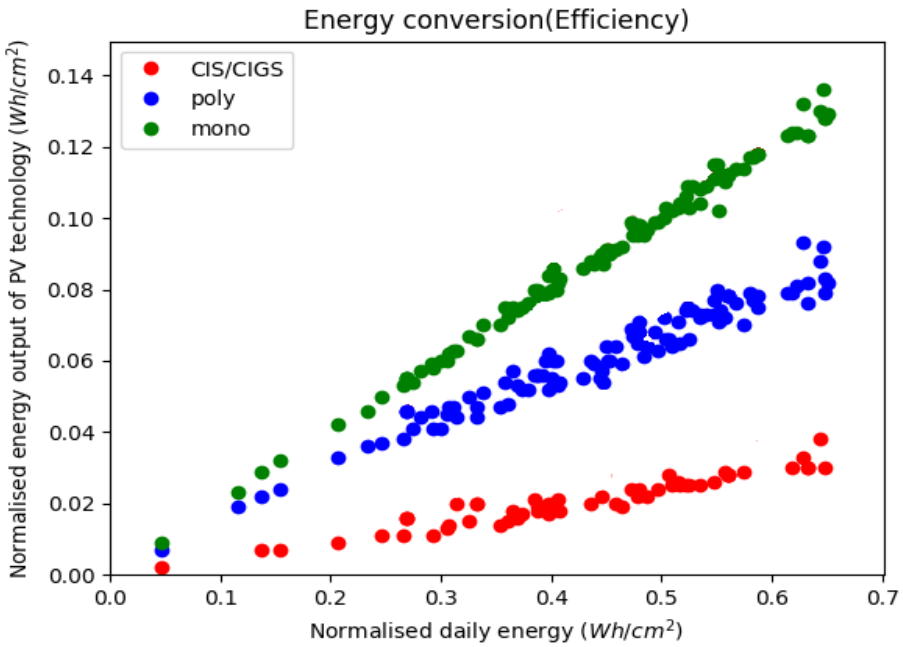

Figure 4.79: Energy conversion of the various PV technologies from sunlight to electrical energy

From that graph the average efficiency for each of the technologies can be obtained by calculating the gradient of best fit line through the points. The efficiency is shown in table 4.1 below.

Technology	Efficiency(%)
CIS/CIGS	6.1
polycrystalline	12.4
monocrystalline	19.1

Table 4.1: Average efficiency

figures 4.80 and 4.81 show the variation of the fill factor of the three technologies. Fill factor is obtained from the equation 4.1 and is an indicator of the quality of the panel. A value of one implies high quality panel and as if decreases so does the quality. Upon analysing the variation of fill factor, monocrystalline silicon technology has the highest and most stable one making it more appropriate for grid tied PV systems and CIS/CIGS is the

least appropriate.

$$\text{Fill factor} = \frac{V_m I_m}{V_{oc} I_{sc}} \tag{4.1}$$

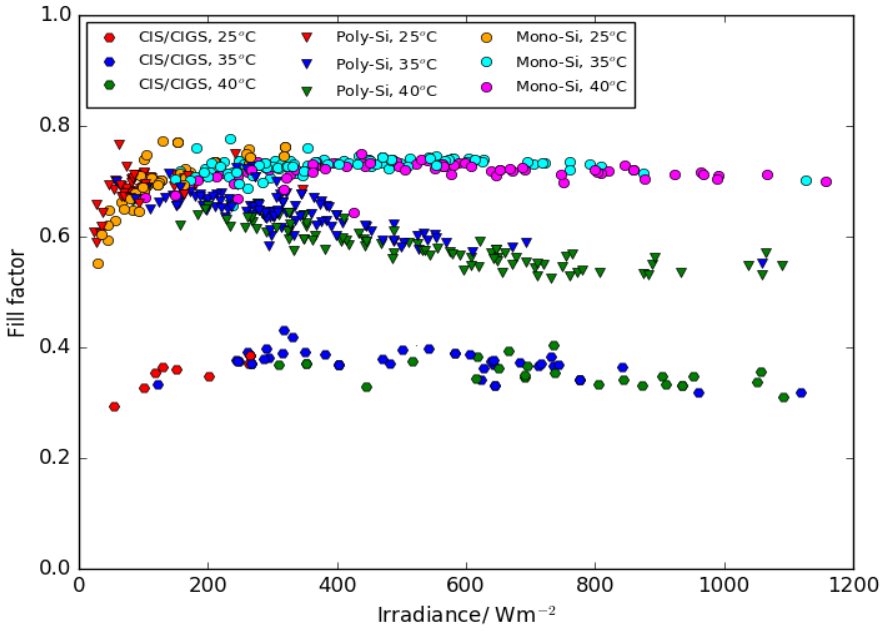

Figure 4.80: Variation of fill factor with irradiance

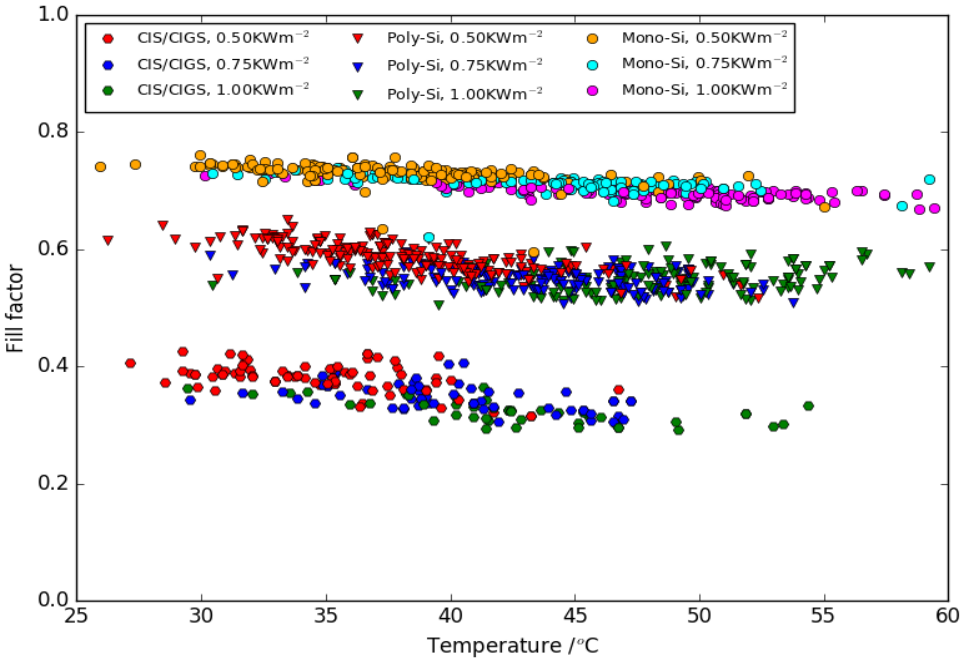

Figure 4.81: Variation of fill factor with temperature

Soiling on the site was also calculated using equation 2.1 and figure 4.82 shows the variation of soiling with time. For the studied site, a weekly cleaning of the panels will result in a 4% increase in output on a yearly basis.

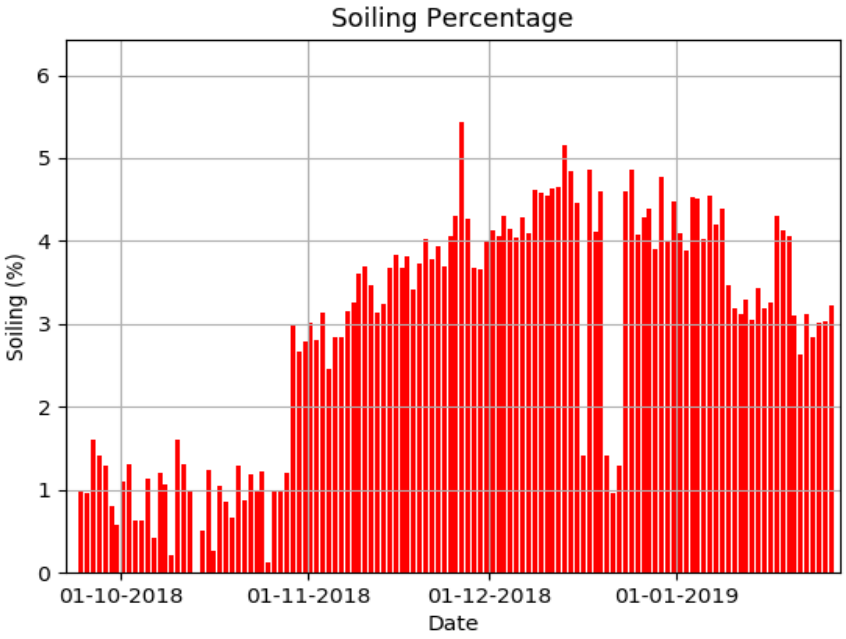

Figure 4.82: Percentage soiling

4.11 Energy yield of various technologies across Mauritius

Using the data from this project along with data from the project "Solar Map of Mauritius, Rodrigues and Agalega", which is freely available online at the following link `http://solarmap.uom.ac.mu/proj.php`, map of energy yield over Mauritius was constructed. The chosen tilt angle was 20 ^{o} as it gives the maximum energy output over a year. Figures 4.83 to 4.85 show the energy output per metre square of each technology over Mauritius.

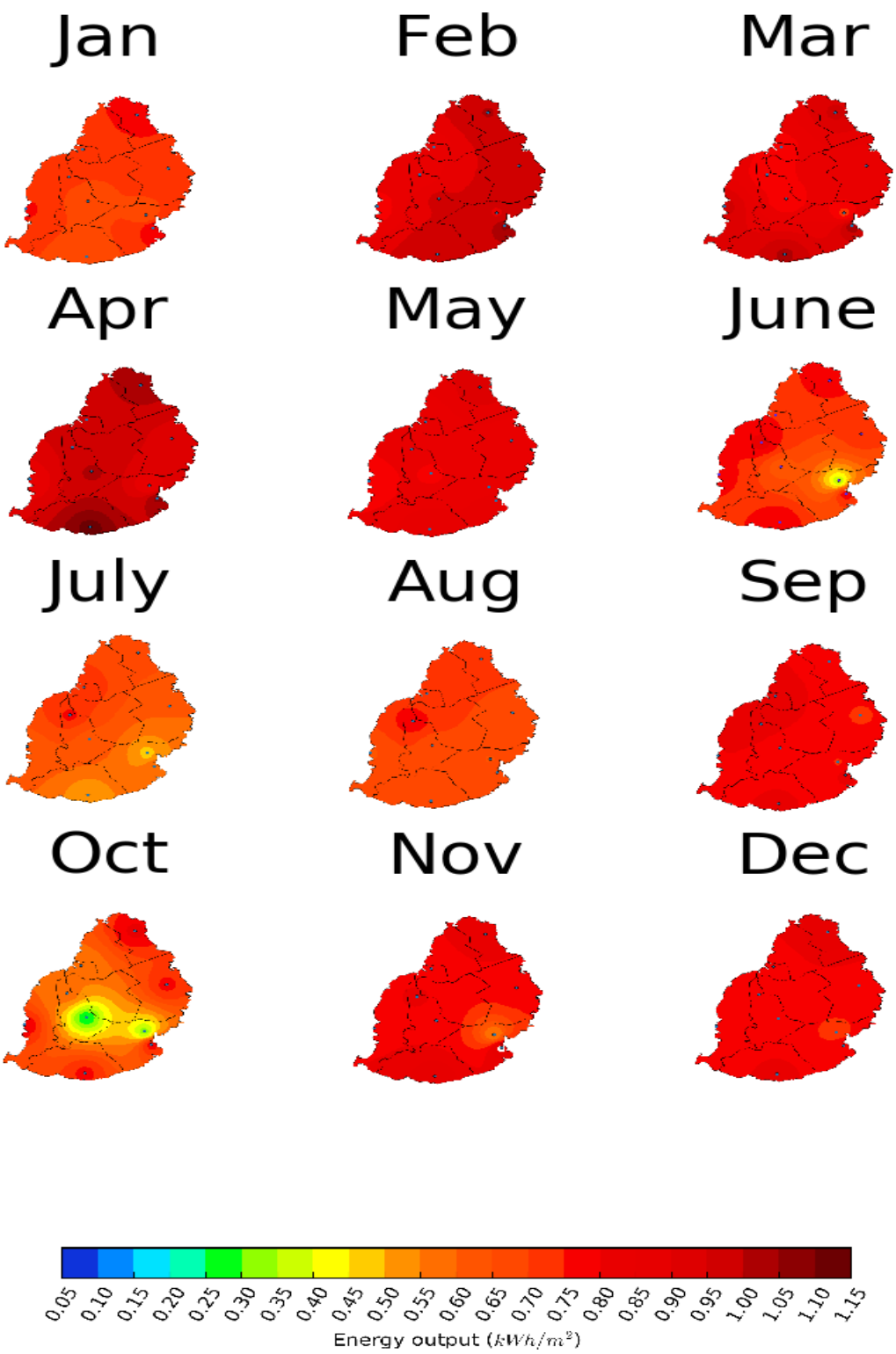

Figure 4.83: Mean monthly energy output per metre square of monocrystalline silicon over Mauritius

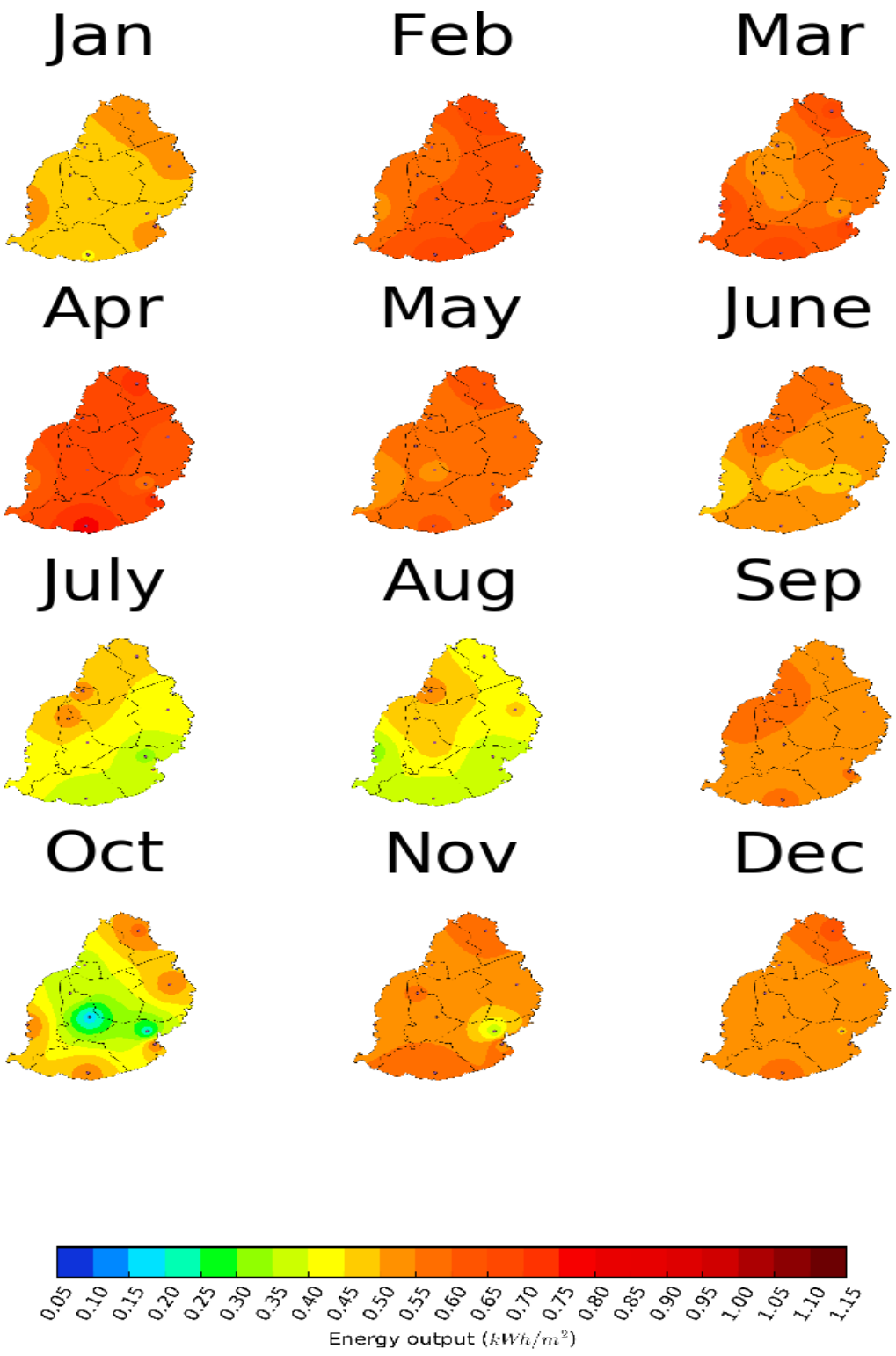

Figure 4.84: Mean monthly energy output per metre square of polycrystalline silicon over Mauritius

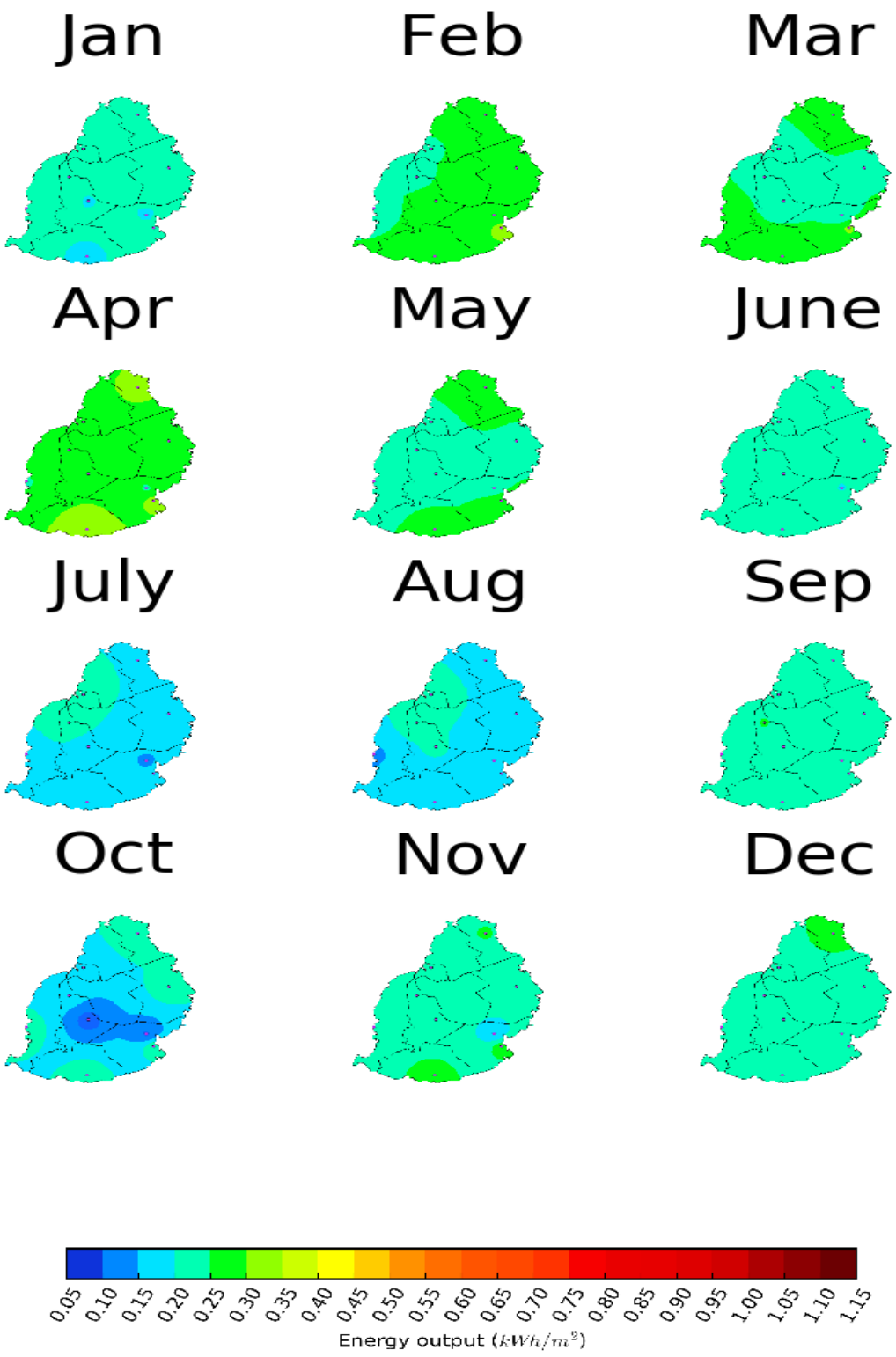

Figure 4.85: Mean monthly energy output per metre square of CIS/CIGS over Mauritius

4.11 Energy yield of various technologies across Mauritius

The mean yearly energy output over Mauritius was calculated for each technology and are displayed in figures 4.86 to 4.88. It can be seen that the monocrystalline technology yields the greatest output with maximum of 1 kWh/m^2 on the northern side of the island. Thus the use of pv for energy production over Mauritius is adequate as it has a good yield.

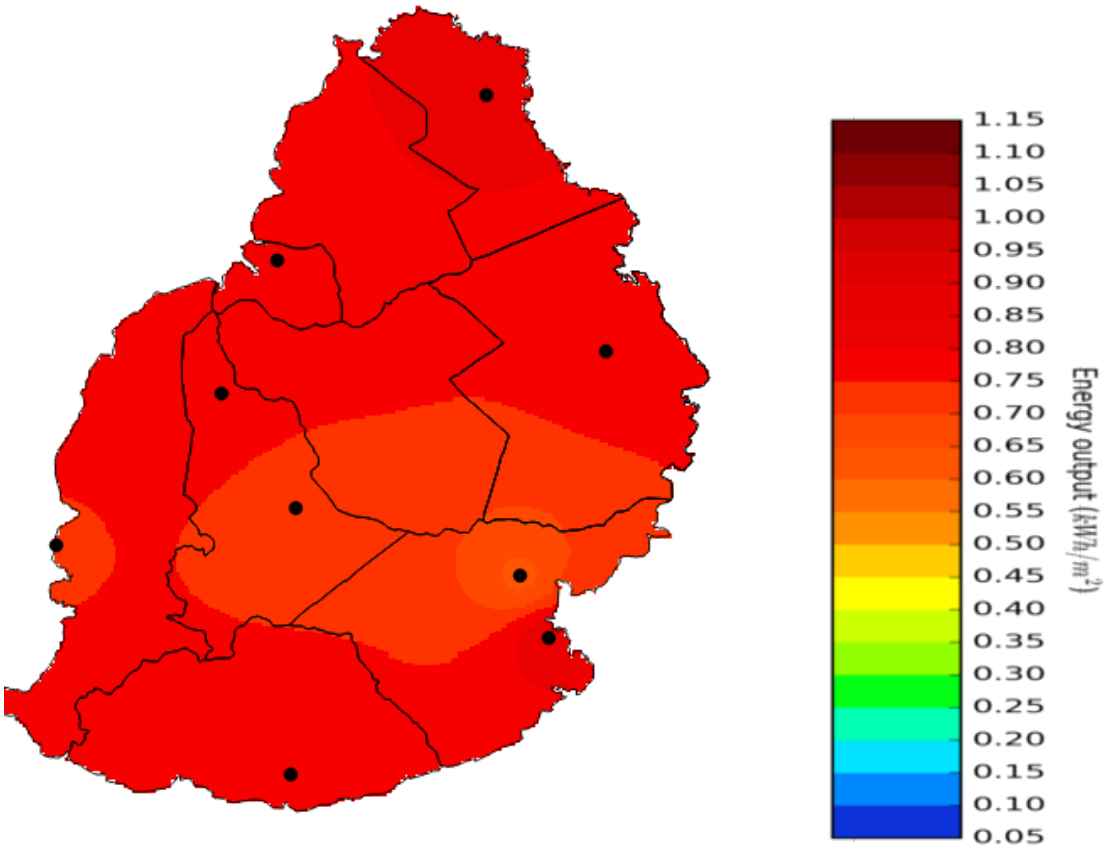

Figure 4.86: Mean yearly energy output per metre square of monocrystalline silicon over Mauritius

4.11 Energy yield of various technologies across Mauritius

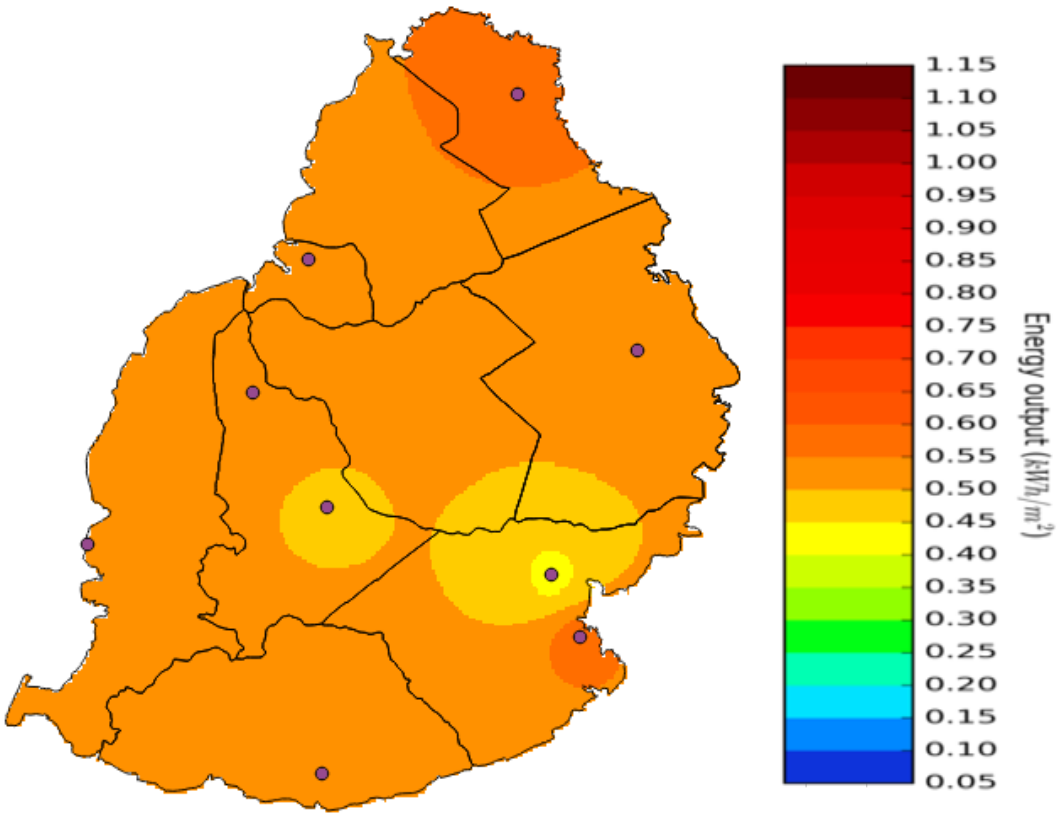

Figure 4.87: Mean yearly energy output per metre square of polycrystalline silicon over Mauritius

4.11 Energy yield of various technologies across Mauritius

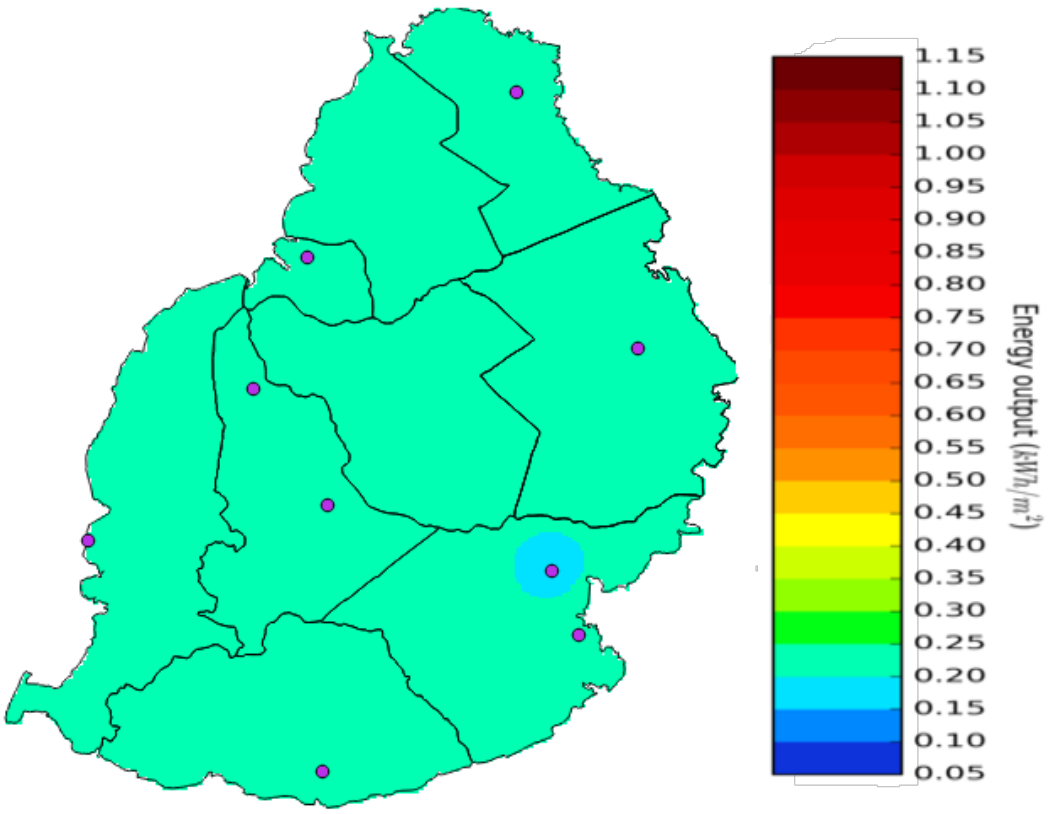

Figure 4.88: Mean yearly energy output per metre square of CIS/CIGS over Mauritius

Chapter 5

Conclusions and recommendations

The outdoor performance of the three different PV technologies, namely monocrystalline silicon, polycrystalline silicon and CIS/CIGS, has been studied in detail in this work. A state of the art outdoor test facility has been developed and implemented at the University of Mauritius. With the aid of sophisticated measurement techniques, simultaneous measurement of electrical parameters of three PV technologies and weather related data were logged. The experimental setup enabled high resolution measurements of the current and voltage produced from the PV panels under outdoor conditions. Moreover the temperature of the PV modules and the ambient temperature were recorded. Two reference cells were used to measured on-site plane of array irradiance. All sensors were connected to an NI chassis which transmitted measurement data to a local server. A sophisticated platform was developed on NI Labview to demonstrate realtime measurement results as well as processed data.

The IV curve data were processed and used to compute the maximum power point characteristics. During the research, all the extracted electrical parameters were analysed and effect of environment on the latter quantities was assessed. Key performance indicators were introduced to assess impact of irradiance on current and voltage quantities. A novel method of quantifying the temperature coefficient of current and voltage has been presented. It should be highlighted that, through this research, dependance of temperature coefficient of the three PV technologies on irradiance was presented for the first time.

It has been found that the performance of PV technologies is strongly dependent on geographical location. Moreover, changes in weather conditions affect different technologies

by different amounts. For instance it has been observed that better quality panels, which may be inferred from the fill factor, show less dependencies on outdoor variables such as temperature and irradiance. The most stable one was found to be the mono-crystalline silicon technology followed by the poly-crystalline silicon technology and last the CIS/CIGS technology.

With the aid of one diode model, the internal characteristics of the solar cells were defined. Hence dependence of the quality of the cell on temperature and irradiance was presented. These results are also new to the research community.

The data obtained can be used to obtain the behaviour of a single cell per unit area thus can then be extrapolated to any size of system. The data allows to select the most appropriate PV technology with regards to factors such as their output voltage and current. Grid tied inverters can only work in a specific range of input voltage supplied by the PV panels, outside this range the system will not provide any useful output. Thus the study provides a good database and knowledge about which type of PV is more appropriate for a given inverter after knowing the number of cells in series and parallel in the PV system. Moreover, based on the results, the performance of the three technologies n be predicted for various outdoor conditions in which it will be exposed around the island of Mauritius.

Also the study shows that, Mauritius being a tropical island, high temperatures and irradiance are observed. Thus an appropriate PV technology for Mauritius is one which has small efficiency drop at high temperatures thus providing maximum power at high temperatures and irradiances. The study showed that the more appropriate one, from the tested sample, is the monocrystalline silicon type which shows small decrease in efficiency as temperature increases. Also the best region for solar farming in Mauritius is the northern part of the region due to the large amount of energy incident daily and also that there is less cloud coverage in the region. Mauritius being a tropical Island, it is recommended that mono-crystalline technology be considered, considering the advantages reported in this work.

References

A. Willoughby, A. and O. Osinowo, M. (2018), 'Development of an electronic load i-v curve tracer to investigate the impact of harmattan aerosol loading on pv module pern2tkformance in southwest nigeria', *Solar Energy* **166**, 171–180.

Al-Chalabi, M. (2015), 'Vertical farming: Skyscraper sustainability?', *Sustainable Cities and Society* **18**, 74 – 77.
URL: *http://www.sciencedirect.com/science/article/pii/S2210670715000700*

Amiry, H., Benhmida, M., Bendaoud, R., Hajjaj, C., Bounouar, S., Said, Y., Raïs, K. and Mouncif, S. (2018), 'Design and implementation of a photovoltaic i-v curve tracer: Solar modules characterization under real operating conditions', *Energy Conversion and Management* **169**.

Appels, R., Lefevre, B., Herteleer, B., Goverde, H., Beerten, A., Paesen, R., Medts, K. D., Driesen, J. and Poortmans, J. (2013), 'Effect of soiling on photovoltaic modules', *Solar Energy* **96**, 283 – 291.
URL: *http://www.sciencedirect.com/science/article/pii/S0038092X1300282X*

Arjyadhara, P., Ali, S. and Chitralekha, J. (2013), 'Analysis of solar pv cell performance with changing irradiance and temperature', *Int. J. Eng. Comput. Sci.* **2**, 214–220.

Australian Space Academy (2018), 'The earth's orbit around the sun', `https://www.spaceacademy.net.au/library/notes/eorbit.htm`. [Accessed on November 2018].

Baka, M., Manganiello, P., Soudris, D. and Catthoor, F. (2019), 'A cost-benefit analysis for reconfigurable pv modules under shading', *Solar Energy* **178**, 69 – 78.
URL: *http://www.sciencedirect.com/science/article/pii/S0038092X18311708*

Boutana, N., Mellit, A., Haddad, S., Rabhi, A. and Pavan, A. M. (2018), 'An explicit i-v model for photovoltaic module technologies', *Energy conversion and Management* **138**, 400–412.

CEB (2015), 'Renewable nergy projects', http://ceb.intnet.mu/grid_code/ssdg.asp. [Accessed on November 2018].

Doorga, J. R., Rughooputh, S. D. and Boojhawon, R. (2018), 'Multi-criteria gis-based modelling technique for identifying potential solar farm sites: A case study in mauritius', *Renewable Energy* .
URL: *http://www.sciencedirect.com/science/article/pii/S0960148118310553*

Drouiche, I., Harrouni, S. and Arab, A. H. (2018), 'A new approach for modelling the aging pv module upon experimental i?v curves by combining translation method and five-parameters model', *Electric Power Systems Research* **163**, 231 – 241.
URL: *http://www.sciencedirect.com/science/article/pii/S0378779618301871*

Duran, E., Piliougine, M., de Cardona, M. S., Galán, J. and Andujar, J. (2008), 'Different methods to obtain i-v curve of pv modules: A review', *IEEE photovoltaic specialist conference* .

ElectronicsTutorials (2018), 'Pn junction theory', https://www.electronics-tutorials.ws/diode/diode_2.html. [Accessed on November 2018].

Fadhel, S., Delpha, C., Diallo, D., Bahri, I., Migan, A., Trabelsi, M. and Mimouni, M. (2019), 'Pv shading fault detection and classification based on i-v curve using principal component analysis: Application to isolated pv system', *Solar Energy* **179**, 1 – 10.
URL: *http://www.sciencedirect.com/science/article/pii/S0038092X18312234*

Firdaus, M. and Daniyal, H. (2013), Modeling and simulation of photovoltaic module with mppt.

Ford, D. (2011), 'Equation of time', https://in-the-sky.org/article.php?term=equation_of_time. [Accessed on November 2018].

gang Wang, Zhao, K., Shi, J., Chen, W., Zhang, H., Yang, X. and yong Zhao (2017), 'An iterative approach for modeling photovoltaic modules without implicit equations', *Applied energy* **202**, 189–198.

Goody, R. and Walker, J. (1972), *Atmospheres*, Prentice Hall.

Government Information Service, (2018), 'Deputy prime minister launches home solar project', http://www.govmu.org/English/News/Pages/

Deputy-Prime-Minister-launches-Home-Solar-Project.aspx. [Accessed on November 2018].

Hathawat, D. H. (2015), 'The solar interior', https://solarscience.msfc.nasa.gov/interior.shtml. [Accessed on November 2018].

Hosseini, S., Taheri, S., Farzaneh, M., Taheri, H. and Narimani, M. (2018), 'Determination of photovoltaic characteristics in real field conditions', *IEEE Journal of Photovoltaics* **8**(2), 572–580.

Hüttl, B., Gottschalk, L., Schneider, S., Pflaum, D. and Schulze, A. (2019), 'Accurate performance rating of photovoltaic modules under outdoor test conditions', *Solar Energy* **177**, 737 – 745.
URL: *http://www.sciencedirect.com/science/article/pii/S0038092X18311782*

Iqbal, M. (1983), *An introduction to solar radiation*, Academic press.

ITACA (2018), 'A guide to photovoltaic cells', https://www.itacanet.org/a-guide-to-photovoltaic-panels/photovoltaic-pv-cells/. [Accessed on November 2018].

Kalogirou, S. A. (2009), *Solar Energy Engineering*, 1 edn.

Kashif Ishaque, Zainal Salam, H. T. (2011), 'Simple, fast and accurate two-diode model for photovoltaic modules', *Solar energy materials solar cells* **95**, 586–594.

Kimber, A. (2013), *The effect of soiling on photovoltaic systems located in arid climates.*

Maghami, M. R., Hizam, H., Gomes, C., Radzi, M. A., Rezadad, M. I. and Hajighorbani, S. (2016), 'Power loss due to soiling on solar panel: A review', *Renewable and Sustainable Energy Reviews* **59**, 1307 – 1316.
URL: *http://www.sciencedirect.com/science/article/pii/S1364032116000745*

Mbogo, M. (2018), 'Mauritius kicks off henrietta solar pv farm project', https://constructionreviewonline.com/2018/06/mauritius-kicks-off-henrietta-solar-pv-farm-project/. [Accessed on November 2018].

McCormick, P. and Suehrcke, H. (2018), 'The effect of intermittent solar radiation on the performance of pv systems', *Solar Energy* **171**, 667 – 674.
URL: *http://www.sciencedirect.com/science/article/pii/S0038092X18305942*

Medine and Akuo Energy (2018), 'Renewable energy: Medine and akuo energy jointly develop a solar farm project at henrietta', https://www.medine.com/newsmedine/item/renewable-energy-medine-and-akuo-energy-jointly-develop-a-solar-farm-project-at-henri [Accessed on November 2018].

Mejia, F. A. and Kleissl, J. (2013), 'Soiling losses for solar photovoltaic systems in california', *Solar energy* **95**, 357–363.

Miller, J. T. A. and Jackson, J. (2009), 'Impact of soiling and pollution on pv generation performance', https://www.energy.gov/sites/prod/files/2014/11/f19/san_jose_pv_module_soiling_impact.pdf. [Accessed on November 2018].

Ministry of Energy and Public Utilities (2009), 'Long teerm energy stratey 2009-2025', https://sustainabledevelopment.un.org/content/documents/1245mauritiusEnergy%20Strategy.pdf. [Accessed on November 2018].

Ministry of Social Security, National Solidarity, and Environment and Sustainable Development (2012), 'construction of a 15mw solar farm at la ferme bambou', http://environment.govmu.org/English/eia/Documents/Reports/bonnelaferma/nts.pdf. [Accessed on November 2018].

Ministry of Social Security, National Solidarity, and Environment and Sustainable Development (2016), 'photovoltaic petite retraite', http://environment.govmu.org/English/eia/Documents/Reports/2017/1804-photovoltaic%20petiteretraite/chap1.pdf. [Accessed on November 2018].

Morton, O. (2006), 'A new day dawning?: Silicon valley sunrise', *Nature* **443**.

NATIONAL INSTRUMENTS (2016), 'Networking two pcs for remote data acquisition with traditional ni-daq (legacy)', http://www.arcindy.com/cfd-aerodynamics-difference-steady-state-transient-simulation.html. [Accessed on November 2018].

Philips and H, K. J. (1995), *Guide to the Sun*, Cambridge University Press.

Pogosian, D. (2018), 'Lecture 4: Black body radiation', https://sites.ualberta.ca/~pogosyan/teaching/ASTRO_122/lect4/lecture4.html. [Accessed on November 2018].

Premalatha, L. and Rahim, N. (2017), 'The effect of dynamic weather conditions on three types of pv cell technologies ? a comparative analysis', *Energy Procedia* **117**, 275 – 282.

Ramgolam, Y. K. (2017), Performance modeling and evaluation of PV system through holistic resource assessment, PhD thesis, University of Mauritius.

sarako (2012), 'Solar park mauritius, bambous', http://www.sarako.mu/en/chronicle.html. [Accessed on November 2018].

Senturk, A. (2018), 'New method for computing single diode model parameters of photovoltaic modules', *Renewable energy* **128**, 30–36.

Serway, R., Moses, C. and Moyer, C. (2005), *Modern physics*, 3 edn.

Serway, R., Vuille, C. and Faughn, J. (1983), *College physics*, Cengage Learning.

Shenawy, E. T. E., Elbaset, A. A., Esmail, O. N. A. and Hamed, H. F. A. (2014), 'Simple and accurate i-v measuring circuit for photovoltaic applications', *International Journal of Engineering Research Technology* **3**.

Smil, V. (1991), *General energetics : energy in the biosphere and civilization*, New York:Willey.

Sshekhtman, L. and Thompson, J. (2018), 'Solar system exploration', https://solarsystem.nasa.gov/. [Accessed on November 2018].

Statistic Mauritius (2018), 'Energy and water statistics - year 2017', http://statsmauritius.govmu.org/English/Publications/Pages/Energy_Yr17.aspx. [Accessed on November 2018].

Stine, W. and Geyer, M. (2018), 'Power from the sun', http://www.powerfromthesun.net/. [Accessed on November 2018].

The Nobel Foundation (2018), 'The nobel prize in physics 1921', https://www.nobelprize.org/prizes/physics/1921/summary/. [Accessed on November 2018].

Tsuno, Y., Hishikawa, Y. and Kurokawa, K. (2005), 'Temperature and irradiance dependence of the i-v curves of various kinds of solar cells', *15^{th} International Photovoltaic Science Engineering Conference* pp. 422–3.

Wikipedia (2018), 'Sun', https://en.wikipedia.org/wiki/Sun#Structure_and_energy_production. [Accessed on November 2018].

Woolfson, M. (2000), 'The origin and evolution of the solar system', *Astronomy and Geophysics* **41**, 1.12–1.19.